FINAL REPORT

A Synergistic Platform for Defluorination of Perfluoroalkyl Acids (PFAAs) through Catalytic Reduction Followed by Microbial Oxidation

February 2022

Dr. Bruce E Rittmann
Yen- Jung Sean Lai
Chen Zhou
Arizona State University

David Friese
APTwater

SERDP Project ER20-1286

REPORT DOCUMENTATION PAGE

Form Approved
OMB No. 0704-0188

1. REPORT DATE *(DD-MM-YYYY)*	**2. REPORT TYPE**	**3. DATES COVERED** *(From - To)*
02-05-2022	SERDP Final Report	03-04-2020 – 02-04-2022

4. TITLE AND SUBTITLE

A Synergistic Platform for Defluorination of Perfluoroalkyl Acids (PFAAs) through Catalytic Reduction Followed by Microbial Oxidation

5a. CONTRACT NUMBER
W912HQ20P0006

5b. GRANT NUMBER
ER20-C1-1286

5c. PROGRAM ELEMENT NUMBER
ERSON-20-C1

6. AUTHOR(S)
Long, Min; Luo, Yihao; Zhou, Chen; and Rittmann, Bruce E.

5d. PROJECT NUMBER
ER20-C1-1286

5e. TASK NUMBER
NA

5f. WORK UNIT NUMBER
NA

7. PERFORMING ORGANIZATION NAME(S) AND ADDRESS(ES)

Arizona State University
660 S MILL AVE STE 312 TEMPE AZ 85281-3670

8. PERFORMING ORGANIZATION REPORT NUMBER

ER20-1286

9. SPONSORING / MONITORING AGENCY NAME(S) AND ADDRESS(ES)
SERDP PROGRAM OFFICE
4800 MARK CENTER DRIVE
SUITE 16F16
ALEXANDRIA VA 22350-3600

10. SPONSOR/MONITOR'S ACRONYM(S)
SERDP

11. SPONSOR/MONITOR'S REPORT NUMBER(S) ER20 - 1286

12. DISTRIBUTION / AVAILABILITY STATEMENT
DISTRIBUTION STATEMENT A. Approved for public release: distribution unlimited.

13. SUPPLEMENTARY NOTES

14. ABSTRACT

Background: Perfluorodoctanoic acid (PFOA) and perfluorooctanesulfonic acid (PFOS) are widespread and persistent water contaminants of great concern today. In our synergistic platform, two membrane-film reactors are linked by sending the effluent of an H_2-based membrane catalyst-film reactor (MCfR) to be the influent of an O_2-based membrane biofilm reactor (MBfR). PFOA/S is reductively defluorinated in the H_2-MCfR to less-fluorinated or non-fluorinated species. The less-fluorinated species are transferred to the O_2-MBfR, where they are further defluorinated and ultimately mineralized.

Results: Fast adsorption of PFOA/S to the Pd^0 filAm in the H_2-MCfR, the release of F^-, and formation of partially to fully defluorinated products verified that the H_2-MCfR catalytically defluorinated both compounds. The MCfR sustained removal of PFOA at environmentally relevant concentrations, averaging 97% removal, to well below 70 ng/L, for continuous flow for more than two months. Continuous oxidative biomineralization of partially defluorinated PFOA/S in the O_2-MBfR proved the capability of MBfR biofilms for biodegradation and mineralization of PFOA/S-hydrodefluorination products. Continuous treatment with the synergistic platform worked as expected: Partially defluorinated products from the MCfR were further defluorinated in the MBfR. Combining catalytic reductive defluorination and biodegradation in the synergistic platform lays the foundation for a reliable and cost-effective treatment of perfluorinated contaminants.

15. SUBJECT TERMS
PFAS, Hydrodefluorination, Oxidative Defluorination, Mineralization, Membrane Catalyst-film Reactor, Membrane Biofilm Reactor

16. SECURITY CLASSIFICATION OF:			**17. LIMITATION OF ABSTRACT**	**18. NUMBER OF PAGES**	**19a. NAME OF RESPONSIBLE PERSON**
a. REPORT	**b. ABSTRACT**	**c. THIS PAGE**			Bruce Rittmann
U	U	U	UU	124	**19b. TELEPHONE NUMBER** *(include area code)* 480-727-0434

Abstract

Introduction: The per- and polyfluoroalkyl substances (PFASs, $C_nF_{2n+1}-R$) refer to a family of chemicals that have been produced since the late 1940s. Perfluorodoctanoic acid (PFOA) and perfluorooctanesulfonic acid (PFOS) are widespread and persistent water contaminants. The presence of PFCs in food, human serum, ground water, and various animal species is of great concern due to their deleterious impacts on environmental and human health. The primary producers of PFOA and PFOS are fluoropolymer and ammonium salt of perfluorooctanoic acid manufacturers, who are responsible for the release of ~85% of all PFAS.

Technical Approach: In our synergistic platform, two membrane-film reactors are connected by sending the effluent of an H_2-based membrane catalyst-film reactor (MCfR) to be the influent of an O_2-based membrane biofilm reactor (MBfR). PFOA/PFOS is first reductively defluorinated in the H_2-MCfR and converted to less-fluorinated or non-fluorinated OA/OS. Then, these OA/OS are transferred to the O_2-MBfR to be biodegraded by the biofilm. In the O_2-MBfR, the OA/OS can be the primary substrates for the co-oxidation of defluorinated PFOA/PFOS. The tasks of our project are designed to demonstrate proof-of-concept of our novel synergistic platform for the removal and mineralization of PFAS, as well as to explore strategies to optimize the catalytic-biological synergy.

Results: Fast adsorption of PFOA and PFOS and the release of F^- and partially and fully defluorinated compounds verified that the H_2-MCfR catalytically removed and destroyed PFAS. Defluorination, preceded by PFOA adsorption in an orientation parallel to the Pd^0 surface, enabled a fast reaction between F substituents on PFOA/S and activated H on the Pd^0 surface. The addition of a promoter metal enabled Pd-based bimetallic catalysts to defluorinate PFOA and PFOS at neutral pH. The MCfR was capable of sustained removal of PFOA at environmentally relevant concentrations, averaging 97% removal, to well below 70 ng/L, for continuous flow for more than two months. The continuous oxidative biomineralization of partially defluorinated PFOA/S in the O_2-MBfR proved the capability of MBfR biofilms for further biodegradation and mineralization of PFOA/S-hydrodefluorination products from the H_2-MCfR. Continuous experiments with the synergistic platform proved that the H_2-MCfR and O_2-MBfR worked as expected when linked together in the synergistic platform: partially defluorinated products from the MCfR were further defluorinated in the MBfR. The defluorinated ratio in H_2-MCfR affected the biodegradation in O_2-MBfR, with more hydrodefluorination in the MCfR allowing more oxidative biodefluorination in the MBfR.

Benefits: This research contributes to fundamental understanding of the factors controlling reductive defluorination of PFAAs using MCfR with Pd^0 and other precious metal catalysts. The cooperation of catalytic reductive defluorination and biodegradation achieved in the synergistic platform reveals a novel strategy for the treatment of persistent PFAAs. It also lays the foundation for developing a reliable and cost-effective synergistic platform for treating PFAAs which is of intense interest to the Department of Defense.

Table of Contents

List of Tables

List of Figures

List of Acronyms

PFAS	Per- and polyfluoroalkyl substances
PFOA	Perfluorooctanoic acidP
OA	Octanoic acid
2-FOA	2-fluorooctanoic acid
2H-PFOA	2H,2H-perfluorooctanoic acid
PFOS	Perfluorooctanesulfonic acid
OS	Octanesulfonic acid
4H-PFOS	1H,1H,2H,2H-perfluorooctanesulfonic acid
C2PFA	Trifluoroacetic acid
C3PFA	Pentafluoropropionic acid
C4PFA	Heptafluorobutyric acid
C5PFA	Perfluoropentanoic acid
C6PFA	Perfluorohexanoic acid
C7PFA	Perfluoroheptanoic acid
H_2-MCfR	Hydrogen based membrane catalytic-film reactor
O_2-MBfR	Oxygen based membrane bio-film reactor

Keywords

PFAAs, palladium, nanoparticle, catalyst-film, biofilm.

Acknowledgements

The authors gratefully thank the U.S. Department of Defense's Strategic Environmental Research and Development Program (SERDP) for funding the research through Project ER20-1286.

Executive Summary

Introduction

Contamination. The per- and polyfluoroalkyl substances (PFASs, C_nF_{2n+1}−R) refer to a family of chemicals that have been produced since the late 1940s.[1] Perfluorodoctanoic acid (PFOA) and perfluorooctanesulfonic acid (PFOS) are widespread and persistent water contaminants[2,3]. The presence of PFCs in food,[4,5] human serum,[6] ground water,[2] and various animal species[7] is of great concern due to their deleterious impacts on environmental and human health.[8–10] The primary producers of PFOA and PFOS are fluoropolymer and ammonium salt of perfluorooctanoic acid manufacturers, who are responsible for the release of ~85% of all PFAS.[11] PFAS were developed in the early 1940s to be used as refrigerants and flame retardants[12,13] and in materials such as fabrics and food packaging, resulting in large quantities being introduced into the environment.

Treatment Methods. The strong carbon-fluorine (C-F) bond energy (~485 kJ mol^{-1}) makes PFASs persistent[14] to oxidation, and complete biodegradation has not been documented up to now. Although advanced oxidation/reduction processes,[15,16] photocatalysis,[17,18] and thermal destruction[19] can convert the PFAS into less-fluorinated and/or shorter-chained compounds, these approaches add or generate hazardous materials, are very energy-consuming, or both.[20,21] Innovative technologies that overcome these crucial roadblocks would be major benefits for the ammunition-related water/wastewater-treatment industry.

Synergistic Platform. In our synergistic platform, two membrane-film reactors are connected by sending the effluent of an H_2-MCfR to be the influent of an O_2-MBfR, as shown in Fig. E1. In our previous SERDP project (ER-2721), the groundwater co-contaminated by TCE, 1,1,1-trichloroethane (TCA), and 1,4-dioxane were successfully treated by a similar synergistic platform. TCE and TCA were first reductively dechlorinated in the H_2-MCfR and converted to ethane. In the subsequent O_2-MBfR, the produced ethane was used as primary substrate to support the removal of 1,4-dioxane through co-oxidation. In this project, POFA/PFOS is first reductively defluorinated in the H_2-MCfR and converted to less-fluorinated or non-fluorinated OA/OS. Then, these OA/OS (perhaps with a small concentration of residual PFOA/PFOS) are transferred to the O_2-MBfR to be biodegraded by the biofilm. In the O_2-MBfR, the OA/OS can be the primary substrates for the co-oxidation of defluorinated PFOA/PFOS.

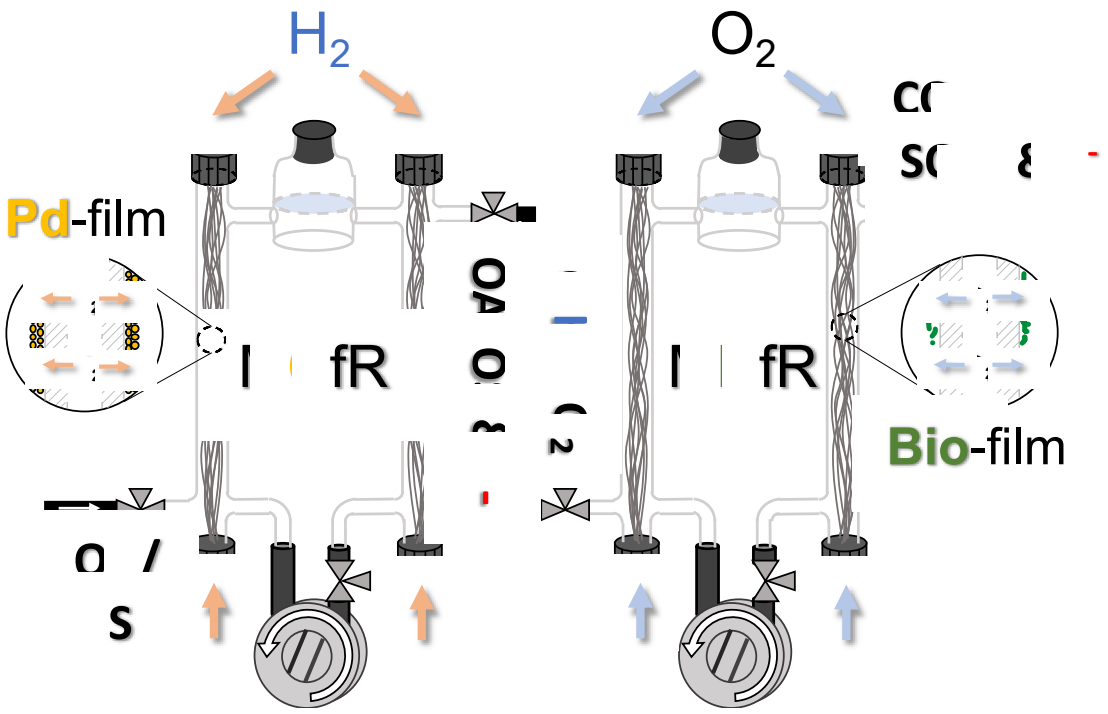

Figure E1: Schematic of the synergistic platform.

Objectives

Four tasks are designed to demonstrate proof-of-concept of the novel synergistic platform and to explore strategies to optimize the catalytic-biological synergy. Specific tasks are:

1. Reductive defluorination of PFOA and PFOS in the H_2-MCfR
2. Oxidative defluorination and mineralization of partially fluorinated OA/OS in the O_2-MBfR
3. Synergistic defluorination of PFOA/PFOS
4. Cost analysis

Technical Approach

This project had three tasks of experimental work. In Task 1, we determined the optimal catalyst synthesis method and catalytic conditions that yielded fast PFOA/PFOS removal with least-fluorinated products. The intermediates and products of PFOA/PFOS reductive defluorination were determined to investigate the reaction mechanisms.

In Task 2, we conducted continuous operation of the O_2-MBfR for partially fluorinated OA/OS for oxidative defluorination and mineralization using non-fluorinated counterpart as the primary substrate. The functional microbial community and genes was identified by analyzing the shallow-metagenomic sequencing results of biofilms.

In Task 3, we operated a complete synergistic system with the two membrane-film reactors in series and successfully achieved PFOA/PFOS continuous removal.

In the Task 4, we estimated capital and annual operating costs of a 100-gpm system treating low or high concentrations of PFOA/S.

Results and Discussion

Interpretations from the MCfR experiments (Task 1)

We first documented that *in situ* reduction and deposition of Pd^0NPs was simple and reliable. *In situ* deposition yielded a Pd^0 film that was reactive and robust.

Fast adsorption of PFOA and PFOS and the release of F^- and partially and fully defluorinated compounds verified that the H_2-MCfR catalytically removed and destroyed PFAS. Defluorination preceded by PFOA adsorption in a parallel orientation enabled a fast reaction between F substituents on PFOA/S and activated H on the Pd^0 surface. The addition of a promoter metal enabled Pd-based bimetallic catalysts to defluorinate PFOA and PFOS at neutral pH. Fig. E2 (A-C) shows that the MCfR was capable of sustained removal of PFOA at environmentally relevant concentrations, averaging 97% removal, to well below 70 ng/L, under continuous flow for more than two months.

The success of the H_2-MCfR is based on its efficient H_2 delivery to the nanoparticle catalysts in the MCfR's film. In conventional heterogeneous catalysis, Pd^0 is supported on solid carriers, but H_2 is delivered from the headspace or by sparging. In that setting, non-reactive adsorption of PFOA/S occurs quickly due to slow H_2 mass transfer from the liquid phase to the catalyst surface; this leads to slow defluorination kinetics and accentuated deactivation, leading to no defluorination. In contrast, the nonporous membrane in the MCfR circumvents mass-transfer limitation delivering bubble-free H_2 directly to the Pd^0 film. Consequently, H* can be amply available at the Pd^0 surface of Pd^0, which blocks vertical non-defluorinative adsorption and promotes defluorination via parallel adsorption (Fig. E2 D).

pH effects. PFOA was more strongly adsorbed at higher pHs, but lower pHs promoted defluorination. In all cases, PFOA first was adsorbed to the PdNP surfaces, and then the adsorbed PFOA was catalytically defluorinated for pHs ≤ 6. The rate was gradually slowed due to gradual deactivation of the PdNPs, probably due to adsorption of PFOA-defluorination products.

Different catalyst elements. At acidic pH, Pt^0, Ru^0, and Rh^0 exhibited moderately higher PFOA-removal rates than Pd^0, but Pd^0 had at least 15-fold higher defluorination kinetics (maximally 2.52 mM/hr) and capacity (77% within 50 hours) than the other three PGM catalysts. The advantage of Pd^0 probably was caused by its superior capacity for H_2 adsorption at acidic pH. At neutral pH, the trends were reversed. On the one hand, the PFOA-removal rate for Pd^0 (maximally 1.47 mM/hr) was fastest among the PGMs. On the other hand, Rh^0 yielded a slightly higher defluorination rate (maximally 0.36 mM/hr) and capacity (45% within 50 hours) than other PGMs, which indicates that Rh^0 might have higher catalytic activity at neutral pH. Overall, Pd^0

was superior to the other PGMs in defluorinating PFOA at pH 4 and adsorbing PFOA at pH 7. In the following tests, we used Pd as the default catalyst.

Catalyst surface loading. The PFOA-removal rate was greatest for 0.7 g Pd^0/m^2, but the defluorination rate was greatest for 1.2 g Pd^0/m^2. Both rates declined precipitously for 2.3 g Pd^0/m^2. The peaking of catalytic activity at 1.2 g Pd^0/m^2 probably occurred because the defluorination of PFOA with H_2 occurred mainly at the water-Pd^0 interface. Excessive Pd^0 coverage resulted in aggregation of Pd^0NPs, which decreased accessible specific surface area and led to lower catalytic activity. In addition, a thick and agglomerated Pd-film may have hindered H_2 transfer to Pd^0 sites near the bulk liquid. This hypothesis is bolstered by the result for the catalyst-specific activity, which peaked at 1.2 g Pd^0/m^2. Because 1.2 g Pd^0/m^2 gave the best removal and defluorination performance, it was chosen as optimal for subsequent experiments in this study.

Bimetallic catalysts. Bimetallic catalysts had better defluorination ability for treating PFOA or PFOS (Fig. E2 E&F), and they also had faster defluorination kinetics than Pd alone. Of these bimetallic catalysts, Pd^0/Rh^0 in the mixed method catalyzed defluorination faster than the other four bimetallic catalysts at pH 7. Pd^0/Ir^0 showed the highest capacity in removing PFOA and PFOS (similar to Pd alone), presumably due its greater adsorption capacity.

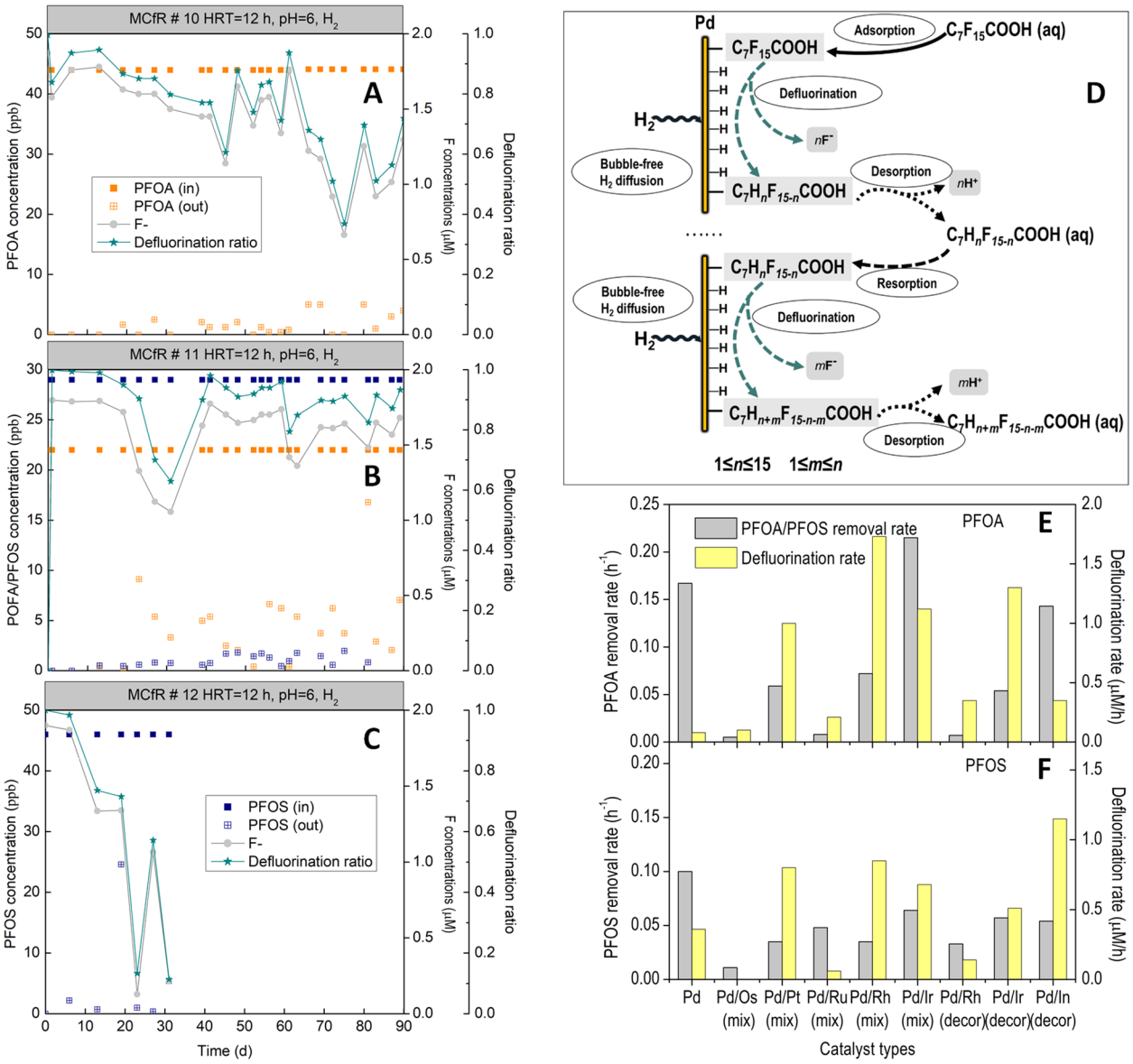

Figure E2. Concentrations of PFOA, PFOS and F^- in continuous operation of MCfRs for PFOA (A), mixed PFOA/PFOS (B), and PFOS removal (C). D: Proposed pathway of PFOA hydrodefluorination by Pd^0NPs in the MCfR. PFOA (E) and PFOS (F) removal first-order rate constant and defluorination zero-order rate constant for the bimetallic catalysts in the batch tests of catalytic reductive defluorination of ~10-μM PFOA or PFOS with about 1 g /m^2 catalyst at 7 with H_2 supplied at 20 psig.

Interpretations from the MBfR experiments (Task 2)

The continuous oxidative biomineralization of partially defluorinated PFOA/S in the O_2-MBfR proved the capability of MBfR biofilms for further biodegradation and mineralization of PFOA/S-hydrodefluorination products from the H_2-MCfR. Fig. E3 A shows that 2-fluorinated octanoic acid (2-FOA) could be completely mineralized with F^- release in continuous operation of O_2-MBfR. Fig. E3 B shows that highly fluorinated OA (2H-PFOA) was less biodegradable compared to less fluorinated OA, but it was biodegraded and defluorinated. Fig. E3 C shows that partially fluorinated OS (4H-PFOS) can also be defluorinated through biodegradation in O_2-MBfR.

We collected biofilm sample and extracted their DNA. Metagenomic sequencing of DNA samples revealed the dominant bacteria in the OA and OS biodegradation biofilm communities, and these bacteria contained the key functional genes for biotransformation of PFOA/S products. For example, the PFOA-biofilms had many genes for β-oxidation: e.g.,β-oxidation of 2H-PFOA released two F^- and shortened the molecular from 8C to 6C. Likewise, the PFAS biofilms had monooxygenases able to release a sulfate from the 4H-PFOS molecule and produce 2H-PFOA. The results document the potential of the O_2-MBfR to biodegrade partially defluorinated PFOA/S.

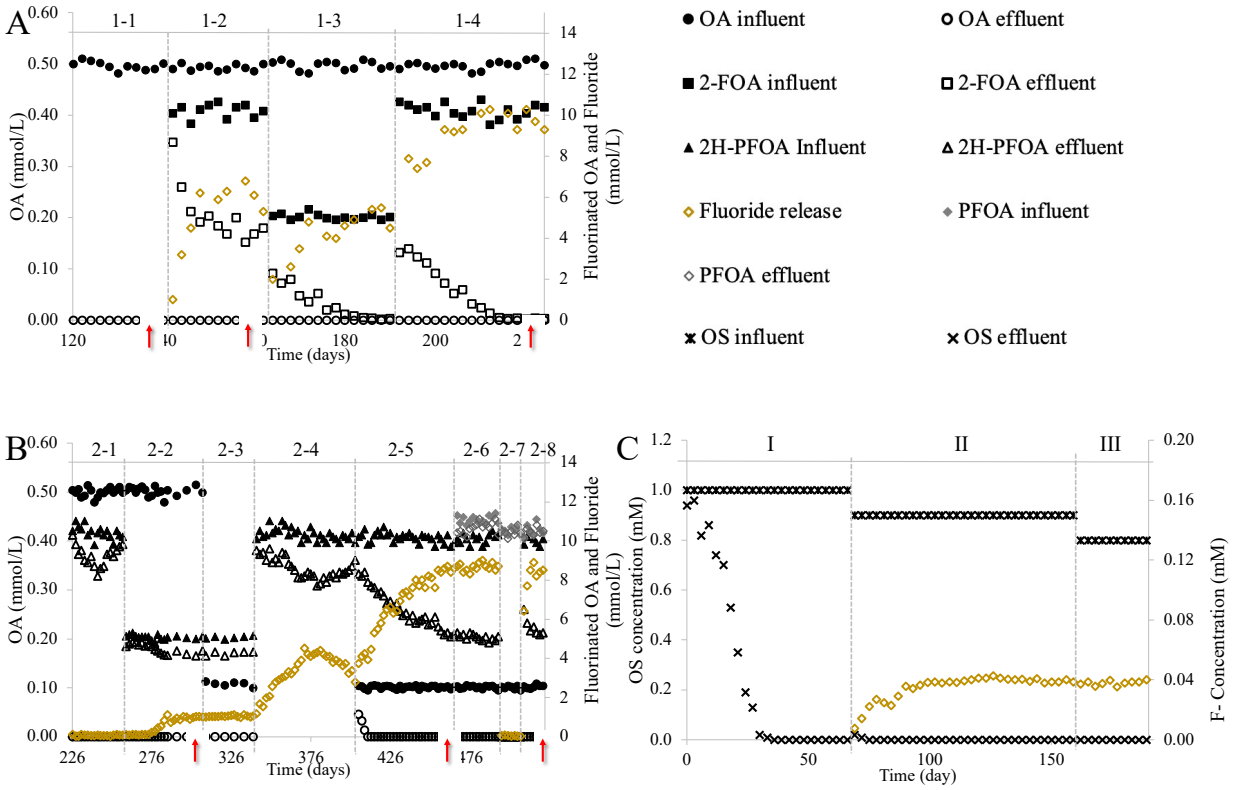

Figure E3. Continuous operation for fluorinated and non-fluorinated OA/OS biodegradation in the O_2-MBfR. A: removal of 2-FOA; B: removal of 2H-PFOA; C: removal of 4H-PFOS.

Interpretations from the synergistic platform experiments (Task 3)

Combining catalytic reductive defluorination and oxidative biodegradation created the synergistic platform. When the influent PFOA concentration was 1 μM (or 414 ppb), Fig. E4 A and B show removal of PFOA and F^- release, although defluorination gradually decreased with deactivation of the catalyst due to the high influent concentration of PFOA. PFOA removal could be recovered by regeneration using HCl. When the influent PFOA concentration was 0.2 μM (or 83 ppb), the released F^- concentrations in MCfR and MBfR were 1.0 μM and 0.7 μM (or 40% and 30% of the total F on removed PFOA), respectively, and deactivation of the catalyst was lessened. In practical use of the MCfR with typically low concentrations, the regeneration of catalysts could have a long repetition period, say over 3 months.

Continuous experiments with the synergistic platform proved that the H_2-MCfR and O_2-MBfR worked as expected when linked together in the synergistic platform: partially defluorinated products from the MCfR were further defluorinated in the MBfR. The defluorinated ratio in H_2-MCfR affected the biodegradation in O_2-MBfR, with more hydrodefluorination in the MCfR allowing more oxidative biodefluorination in the MBfR.

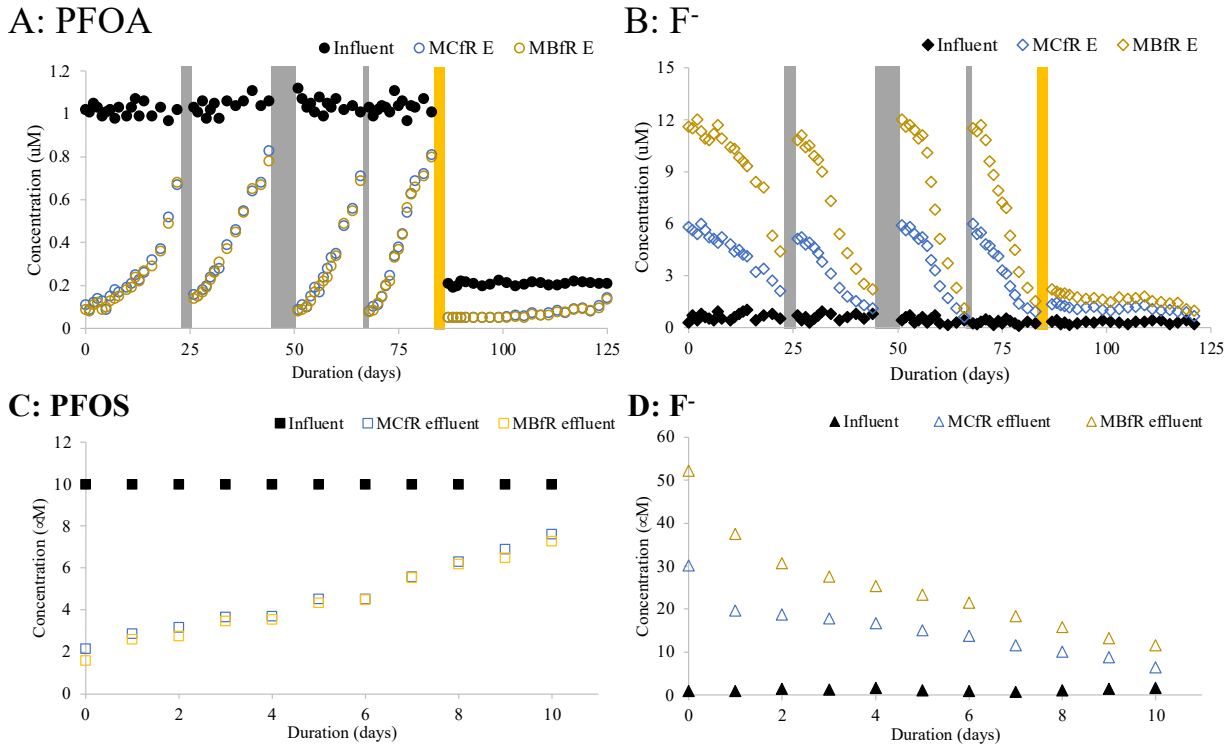

Figure E3. The PFOA (A), PFOS (C) and F^- (B and D) concentrations of influent and MCfR/MBfR effluents for PFOA/PFOS removal in the synergistic platform. Gray columns and yellow columns indicate the period of regeneration and recoating, respectively.

Cost analysis

Using the experimental data along and few interpretations for process optimization, APTwater developed four different cost analyses. Each analysis assumes an influent flow rate 100 gallons per minute with standard APTwater modules. Each module is 6 feet in length with 143 m^2 active surface area. Overall system capital and operating cost depended strongly on the PFOA/S flux and surface loading of the Pd catalyst. Lower the flux led to more costs for all equipment (modules, pumps, tanks, pipelines), which also drives up the operating costs. Table E1 illustrates that reduced catalyst loading and higher PFOA/S fluxes in an optimized synergistic system can have costs as low as ~$2 per gram of PFAS removed.

According to a CH2M-Hill report (summarized in Table E2), ion exchange is least expensive among the processes being used today.[22] For removing the same 615 ng/L PFOS at the same flow rate of 100 GPM, the capital cost of the ion exchange was $29 million (over one order of magnitude higher than the MCfR), and operating cost was $0.6 million (over three times that of the MCfR). Furthermore, all the processes tested in the CH2M-Hill project are non-destructive. This means that PFAS was transferred and concentrated from contaminated water, but not converted to less- or non-toxic compounds. Downstream treatment of the disposed materials containing concentrated PFAS is required and even more costly and energy-consuming. Overall, cost estimation and comparison confirm that destructive removal of PFAS using MCfR could be remarkably more efficient and economical than non-destructive approaches like GAC, ion exchange, and reversed osmosis.

Future Research

- Achieve complete mineralization of PFOA and PFOS using the synergistic MCfR-MBfR with recycling
- Understand and attenuate catalyst deactivation caused by other water-born components (e.g., S)
- Test the capability of MCfR/MBfR in removing PFOA and PFOS from real contaminated waters
- Test the capability of MCfR/MBfR in removing shorter-chain per-fluorinated carboxylic acids (C2 – C7)
- Submit a proposal for an ESTCP project including Industry Partners

Table E1. Summary of the budgetary capital costs and annual operating cost

Budgetary Capital costs	H_2-MCfR only		Synergistic platform	
	Low PFAS concentration/high Pd loading	**Low PFAS concentration/Low Pd loading**	**High concentration/high Pd loading**	**High concentration/low Pd loading**
Equipment (no modules)	$6,306,683	$863,000	$20,463,310	$841,400
Aronite modules	$5,370,825	$531,525	$18,176,425	$374,850
Module Quantity	3769	373	12,743	263
Catalyst Cost	$42,039	$4,160	$23,431,208	$18,895
System fabrication	$695,000	$95,000	$2,265,000	$115,000
Site improvement and design	$1,225,000	$293,000	$3,337,000	$292,421
Start-up costs	$52,800	$52,800	$105,600	$105,600
Contingency	$2,738,469	$367,897	$13,555,709	$349,633
Total installed cost	$16,430,817	$2,207,383	$81,334,251	$2,097,799
Installed cost per g of PFOA and PFOS over 10-year period	$7,400	$990	$45	$1.20
Annual Operating Cost				
Labor	$20,000	$20,000	$30,000	$36,667
Consumables	$0	$0	$2,000	$2,000
Parts and maintenance	$164,308	$22,074	$813,343	$20,978
Module Replacement	$773,266	$76,526	$5,943,948	$56,249
Power	$672,000	$69,600	$2,267,000	$54,200
Total annual costs	$1,629,575	$188,200	$9,056,290	$170,094
Total operating cost per g of PFOA and PFOS	$7,300	$850	$50	$0.95

Note: Low PFAS concentration means 500 ng PFOA /L or 600 ng PFOS/L; High PFAS concentration means 0.4 mg PFOA /L or 0.5 mg PFOS/L; low Pd loading means 1.2 mg-Pd/m^2; high Pd loading means 1.2 g-Pd/m^2.

Table E2. Summary of costs from the CH2M-Hill report made for NAVFAC

Background NAS Oceana report		
influent	1115	ng/L PFOS and PFOA
Flow rate	7000	gal/month
resin cost	350	$/ft^3
resin amount	3	ft^3
exchange frequency	1	every two years
Exchange cost	525	$/yr
Capital Cost	47,810	$
Disposal costs		
$200 per disposal event		
$175 for profiling		
$49/ft^3 of material disposed		
Disposal cost	448.5	$/yr
Cost conversion for 100-gpm system		
Capital Cost	29,000,000	$
Exchange cost	324,000	$/yr
Disposal cost	277,000	$/yr

1. Objectives

From 2020 to 2021, our research team completed the limited-scope project (ER20-1286) in response to Strategic Environmental Research and Development Program (SERDP)'s 2017 Statement of Need (SON): "Proposals focused on the common DoD contaminants of concern (COCs) are of most interest. These include: chlorinated and non-chlorinated volatile organic compounds (VOCs), polychlorinated biphenyls (PCBs), metals, perchlorate, 1,4-dioxane (1,4-D), perfluorinated chemicals (PFCs), N-nitrosodimethylamine (NDMA) and munitions constituents."

In a synergistic platform, the two membrane reactors are connected by sending the effluent of the H_2-MCfR to be the influent of the O_2-MBfR. In our previous SERDP project (ER-2721), tgroundwater co-contaminated by TCE, 1,1,1-trichloroethane (TCA), and 1,4-dioxane were successfully treated by the synergistic platform. TCE and TCA were first reductively dechlorinated in the H_2-MCfR and converted to ethane. In the subsequent O_2-MBfR, the produced ethane was used as primary substrate to support the removal of 1,4-dioxane through co-oxidation. In this project, POFA/PFOS is first reductively defluorinated in the H_2-MCfR and converted to less-fluorinated or non-fluorinated OA/OS. Then, these OA/OS (perhaps with a small concentration of residual PFOA/PFOS) are transferred to the O_2-MBfR to be biodegraded by the biofilm. In the O_2-MBfR, the OA/OS can be the primary substrates for the co-oxidation of defluorinated PFOA/PFOS.

The tasks of our project are designed to demonstrate proof-of-concept of our novel synergistic platform for the removal and mineralization of PFAS, as well as to explore strategies to optimize the catalytic-biological synergy. Specific tasks are:

1. Reductive defluorination of PFOA and PFOS in the H_2-MCfR: determine the optimal catalyst synthesis method and catalytic conditions that yield fast PFOA/PFOS removal with less-fluorinated products.
2. Oxidative defluorination and mineralization of partially fluorinated OA/OS in the O_2-MBfR: continuously operate O_2-MBfRs for partially fluorinated OA/OS for oxidative defluorination and mineralization using non-fluorinated counterpart as the primary substrate and identify the microbial community and its key genes.
3. Synergistic defluorination of PFOA/PFOS: operate a complete synergistic system with the two reactors in series to achieve PFOA/PFOS continuous removal.
4. Cost analysis: conduct a preliminary cost analysis for PFOA/PFOS removal.

2. Background

2.1. PFAS contamination

The per- and polyfluoroalkyl substances (PFASs, C_nF_{2n+1}−R) refer to a family of chemicals that have been produced since the late 1940s.[1] The presence of PFCs in food,[4,5] human serum,[6] groundwater,[2] and various animal species[7] is of great concern due to their deleterious impacts on environmental and human health.[8–10] PFAS were developed in the early 1940s to be used as refrigerants and flame retardants[12,13] and in materials such as fabrics and food packaging, resulting in large quantities being introduced into the environment. In 1969, they became the dominant agent for fighting fires at airports and military installations to meet MIL-F-24385 specifications.[13,23]

Prominent among the PFAS are perfluorodoctanoic acid (PFOA) and perfluorooctanesulfonic acid (PFOS).[2,3] The primary producers of PFOA and PFOS are manufacturers of fluoropolymers and ammonium salt of perfluorooctanoic acid, who are responsible for the release of ~85% of all PFAS.[11]

2.2. PFAS treatment methods

The strong carbon-fluorine (C-F) bond energy (~485 kJ mol^{-1}) makes PFASs persistent[14] to oxidation, and no successful biodegradation has been documented up to now. Although advanced oxidation/reduction processes,[15,16] photocatalysis,[17,18] and thermal destruction[19] can convert the PFAS into less-fluorinated and/or shorter-chained compounds, these approaches add or generate hazardous materials, are very energy-consuming, or both.[20,21] Innovative technologies that overcome these crucial roadblocks would be major benefits for the ammunition-related water/wastewater-treatment industry.

Removing fluorine (F) substituents can make PFOA and PFOS products biodegradable, but the first step, reductive defluorination using hydrogen gas (H_2) as the reductant, requires the use of an efficient catalyst. Elemental palladium (Pd^0) is widely applied as a catalyst in industry,[24,25] but catalysts composed of Pd^0 normally are expensive, making them cost prohibitive at large scale. However, sources for Pd^0 recovery from industrial wastes are diverse and plentiful. Efficient recovery of Pd^0 from its major waste streams -- mining, metal refining, waste electrical and electronic equipment (WEEE), and catalytic-converter industries – enables its capture, which helps to meet market demand, maintain an affordable market price, and reduce their environmental impacts.[26]

2.3. The Membrane Catalyst-film Reactor (MCfR)

To overcome the challenge of H_2's low water solubility and to increase the H_2 mass-transfer rate to the Pd^0 catalysts, we developed the H_2-based membrane catalyst-film reactor (MCfR), which has a film of Pd^0 nanoparticles (Pd^0NPs) deposited on the outer surface of hollow fiber membranes that deliver the H_2 directly to the Pd^0 film.[27,28] The MCfR is an adaptation of its biological counterpart, the membrane biofilm reactor, or MBfR: The microbial biofilm of the MBfR is replaced by an abiotic catalyst film. In the MCfR, H_2 that diffuses from the lumen can directly adsorb onto the Pd^0NPs, which avoids having to dissolve the H_2 in aqueous phase. The distinctive feature of the H_2-MCfR lies in the versatile functions of the membrane: a substratum that produces and retains a robust catalyst and also delivers the H_2 in a bubble-free manner that allows efficient and accurate on-demand delivery of H_2 to the catalysts. A schematic of the MCfR is shown in Figure 1.

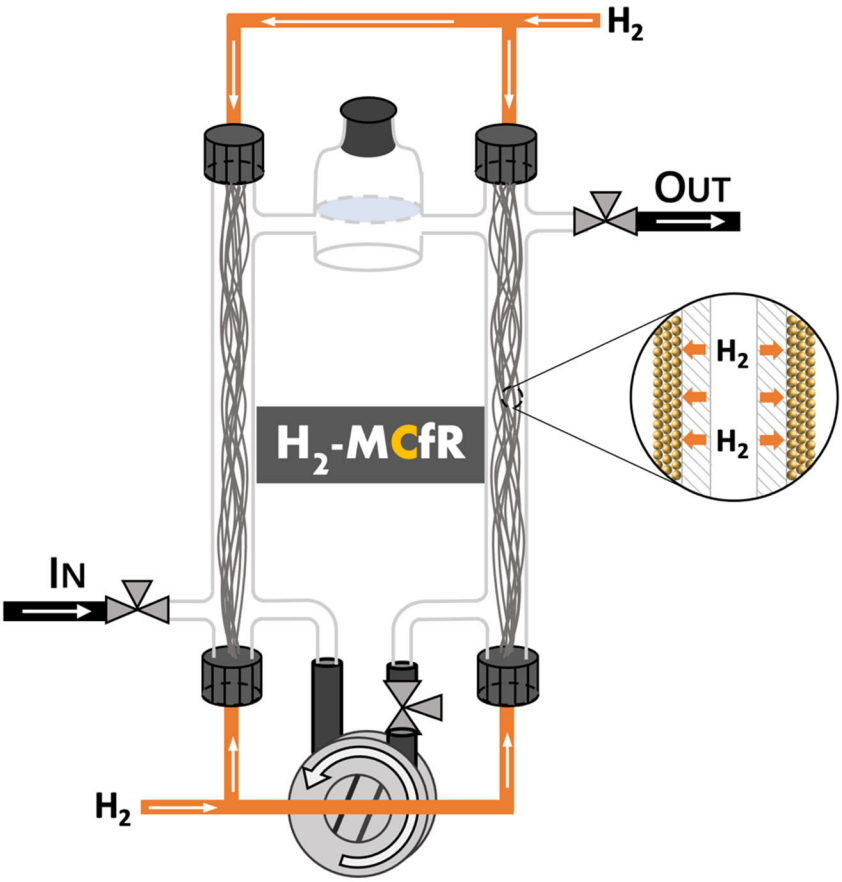

Figure 1. Schematic of the H_2-MCfR (from Luo et al. (2021))

2.4. The Membrane Biofilm Reactor (MBfR)

The membrane biofilm reactor (MBfR) uses hollow-fiber membranes as an active substratum for biofilm growth and biodegradation of water pollutants. The hollow fibers deliver a gaseous substrate (e.g., H_2, O_2, CH_4, CO, or CO_2) from its lumen to the outer surface of the membrane by the gas's diffusion through the membrane wall; it does this without forming bubbles.[29,30] Figure 2 provides schematics of O_2-based and H_2-based MBfRs. In Fig. 2.A, the H_2-MBfR supplies H_2 gas as an inorganic electron donor for reductively removing various oxyanions by enriching a biofilm of hydrogenotrophic microorganisms in its biofilm (Zhou et al. 2020). Fig. 2.B presents the O_2-MBfR, which is what we use in this work. In the O_2-MBfR, O_2 gas is supplied as the electron acceptor, and organic compounds in the water can be aerobically biodegraded. A previous SERDP-supported project documented removal of 1,4-dioxane in O_2-MBfR in which ethane was the primary substrate.[31]

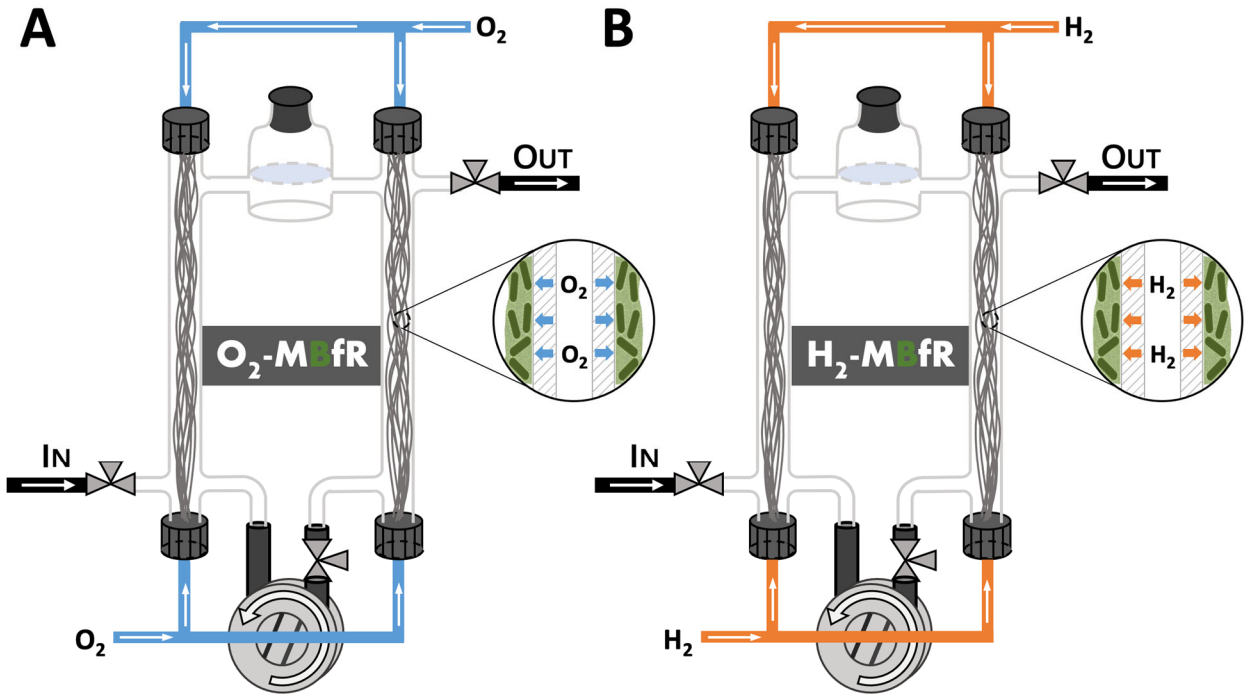

Figure 2. Schematic of the O_2-MBfR (A) and H_2-MBfR (B) (from Luo et al. (2021))

2.5. Synergistic platform

In the synergistic platform, the two membrane-film reactors are connected by sending the effluent of the H_2-MCfR to be the influent of the O_2-MBfR, as shown in Fig 3. In our previous SERDP project (ER-2721), the groundwater co-contaminated by TCE, 1,1,1-trichloroethane (TCA), and 1,4-dioxane were successfully treated by the synergistic platform. TCE and TCA were

first reductively dechlorinated in the H_2-MCfR and converted to ethane. In the subsequent O_2-MBfR, the produced ethane was used as primary substrate to support the removal of 1,4-dioxane through co-oxidation. In this project, POFA or PFOS is first reductively defluorinated in the H_2-MCfR and converted to less-fluorinated or non-fluorinated OA or OS. Then, the reduced products are transferred to the O_2-MBfR to be biodegraded by the biofilm.

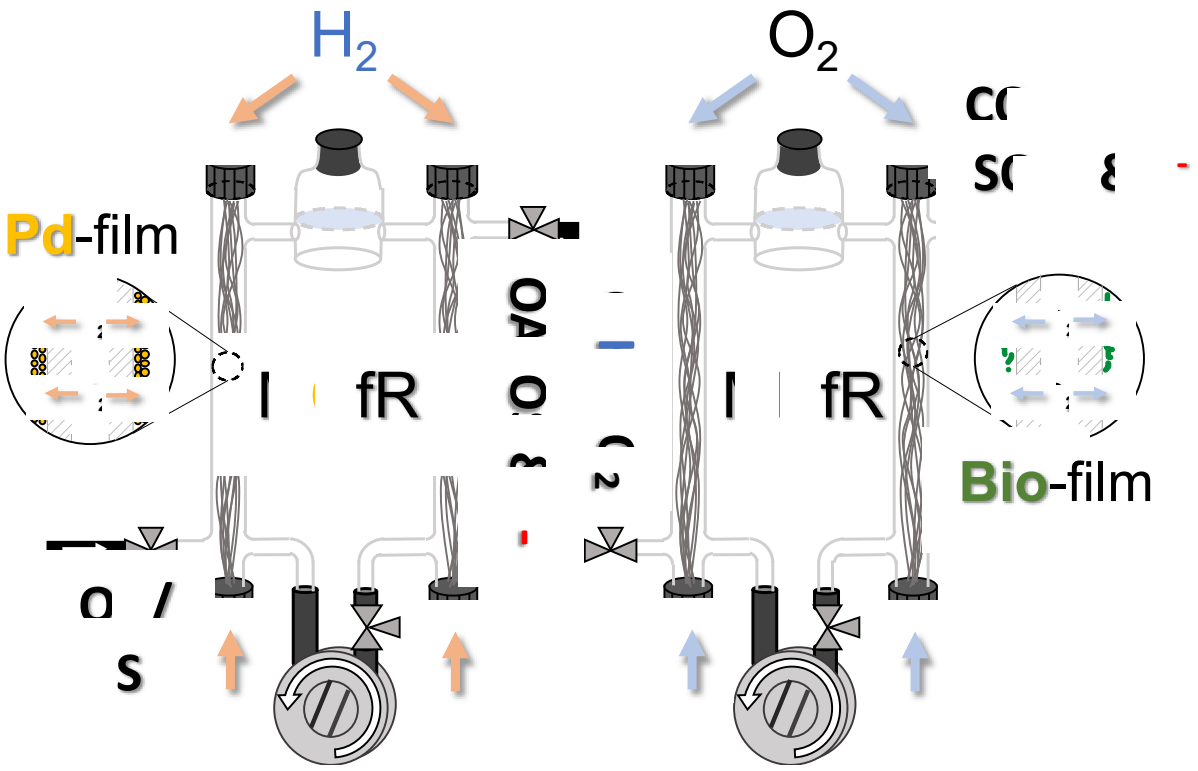

Figure 3. Schematic of the synergetic platform of an H_2-MCfR followed by an O_2-MBfR.

2.6. Overview of the Project

In Tasks 1 and 2 of this project, we conducted catalytic reductive defluorination of PFOA and PFOS and oxidative bio-defluorination of partially fluorinated OA and OS in H_2-MCfRs and O_2-MBfRs, respectively. In Task 3, we operated a complete synergistic system with the two reactors in series to achieve PFOA/PFOS continuous removal. The catalytic reductive defluorination converted PFOA and PFOS into biodegradable partially fluorinated OA and OS in the H_2-MCfR. The partially fluorinated OA and OS were then oxidatively defluorinated and mineralized in the O_2-MBfR. Exploiting the coordination of catalytic and microbial reactions, the synergistic platform could remove and mineralize PFOA and PFOS without needing extreme or hazardous

conditions and without large energy input. The capital and operating costs of a full-scale synergistic platform were estimated based on the bench-scale results and good engineering practice (Task 4).

3. Materials and Methods

3.1. Task 1: Reductive defluorination of PFOA and PFOS in the H_2-MCfR

Reactor setup. Figure 4 shows photographic and schematic images of the bench-scale H_2-MCfR, which was used for batch and continuous experiments of catalytic PFOA/PFOS reductive defluorination. The MCfRs had a total working volume of 40 mL and contained one bundle of 120 identical hollow-fiber membranes (polypropylene, nonporous, 200 μm ID, 300 μm OD, wall thickness 50–55 μm, made by Teijin, Ltd., Japan) in glass tubes (6 mm ID and 27 cm length). H_2 gas (>99.9%) was supplied to both ends of each fiber bundle at a pressure controlled by a pressure regulator. A solute's concentration inside an MCfR was equal to its effluent concentrations due to mixing from a recirculation rate of 150 mL/min created by using a peristaltic pump. Pure palladium nanoparticles (Pd^0NPs) were deposited on the membranes via auto-catalytic reduction.

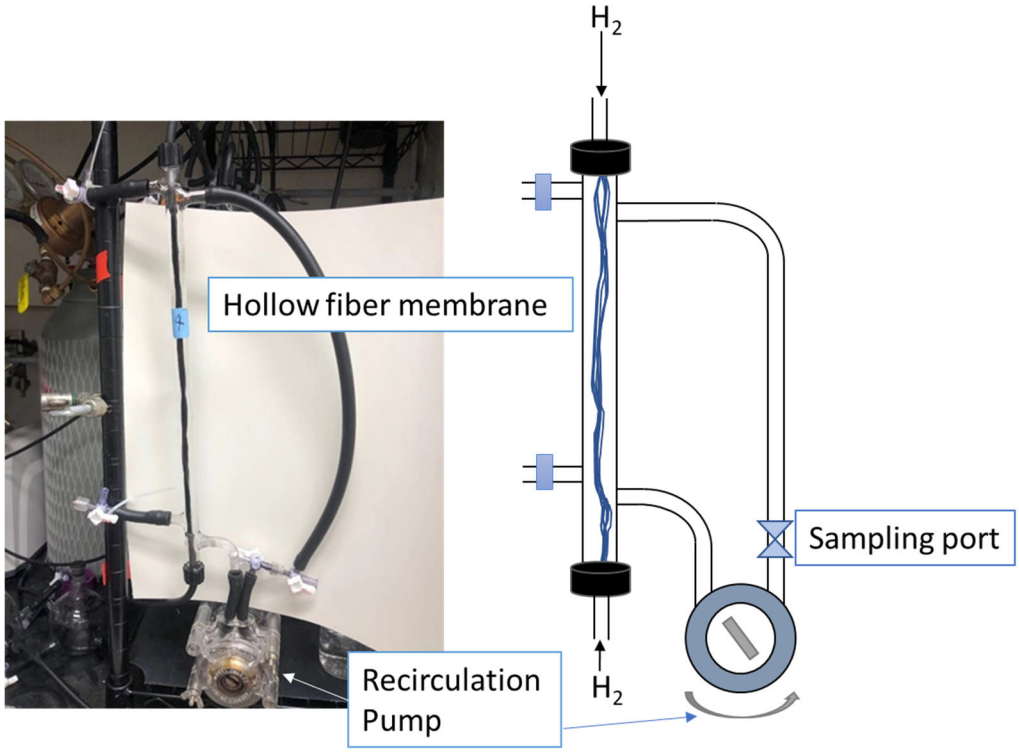

Figure 4. Photographic (left) and schematic (right) images of the bench-scale MCfR system. The black solid arrows indicate the liquid flow and the gas flow.

Catalyst deposition. For depositing mono-catalysts, we chose four types of PGMs (Pt, Pd, Rh, and Ru) that are known to have hydrogenation capability. We prepared the precursor solutions by dissolving each of the PGM salts -- sodium tetrachloropalladate (Na_2PdCl_4), sodium tetrachloroplatinate (Na_2PtCl_4), potassium hexachlororhodate (K_3RhCl_6), or potassium pentachlororuthenate (K_2RuCl_5) -- into deionized water (DI) and adjusting the solution pH to 6.5 by addition of a 10-mM phosphate buffer.

For depositing bimetallic catalysts, we used two methods: mixed and decoration. For the mixed method, we set up ten new H_2-MCfRs equipped with an identical membrane and coated the membranes with 2.5 mM/2.5 mM Pd/Rh, Pd/Ru, Pd/Pt, Pd/Ir, Pd/Os (in duplicate for PFOA and PFOS testing) to simultaneously form bimetallic catalysts on the membrane. For the decoration method, we set up six new H_2-MCfRs equipped with identical membranes and coated the membranes first with 5 mM Pd (II). After the complete formation of PdNPs on the membrane, we added to the MCfRs the decoration solution of 1 mM Rh to form 5:1 (mol/mol) Pd/Rh bimetallic catalyst, 1 mM In to form 5:1 (mol/mol) Pd/In bimetallic catalyst, or 1 mM Ir to form 5:1 (mol/mol) Pd/Ir bimetallic catalyst (in duplicate for PFOA and PFOS testing).

For each batch or continuous test, we used freshly prepared catalysts in which the MCfR was fed with the precursor solution and then kept in batch mode for 24 hours until more than 99% of the precursor cation was reduced and removed from the liquid phase; the MCfRs were then drained and rinsed with DI water 3 times. At this time, the MCfR was ready for experiments with PFOA or PFOS.

Batch tests. We conducted a series of batch tests as a means to find good conditions for defluorination of PFOA or PFOS. To begin each batch experiment, the MCfR was purged with pure N_2 gas for at least 15 minutes, and then the PFOA stock solution was rapidly introduced into the MCfR using the feeding pump.

For the experiments evaluating the different catalysts, we evaluated Pt, Pd, Rh, or Ru for the conditions of ~10 μM PFOA, 20 psi H_2, and pH 4. For the Pd^0-loading tests, we tested different loadings of Pd^0 (0.2, 0.7, 1.2, 2.3, and 4.5 g/m^2) for removing and defluorinating PFOA with the conditions of ~10 μM PFOA, 20 psig H_2, and at pH 4. For the pH tests, we conducted defluorination tests at pH 4, 5, 6, and 7 using a Pd^0NP loading of 1.2 g Pd^0/m^2, 20 psig H_2, and ~ 10 μM PFOA. For the bimetallic catalysts tests, we conducted defluorination tests using the same conditions (pH 7, ~10 μM PFOA, 20 psig H_2). We adjusted pH by using a phosphate buffer.

Continuous tests. To start the continuous tests, we set up three H_2-MCfRs for continuous operation. Immediately after the formation of 1.2 g/m^2 Pd^0NPs, we started feeding the MCfRs with 10 μM PFOA at a pH of 4, 5, or 6 in parallel. Specific parameters were set as follows: HRT = 6 h, flow rate = 0.1 ml/min, and H_2 = 20 psig, the same as for previous experiments.

After we conducted the tests with HRT = 6h, we determined that a good pH was 6, and we set up one H_2-MCfR for continuous operation with 10 μM PFOA and changed HRT to 24 h. Other parameters were flow rate = 0.025 ml/min, and H_2 = 20 psig.

We also set up one H_2-MCfR for continuous operation with more environmentally relevant concentrations. Immediately after the formation of 1.2 g/m^2 Pd^0NPs, we started feeding the MCfR with 500 ppt (or 1.2×10^{-6} mM) PFOA at pH 6. Specific parameters were set as follows: HRT = 24 h, flow rate = 0.025 ml/min, and H_2 = 20 psig.

We also set up one H_2-MCfR for continuous operation at environmental relevant concentration of PFOS. Immediately after the formation of 1.2 g/m^2 Pd^0NPs, we started feeding the MCfR with 500 ppt (or 1×10^{-6} mM) PFOS at pH 6. We also added ~500 ppt PFOA to this H_2-MCfRs on day 70 to make the influent contain PFOS and PFOA.

Analytical methods. We collected liquid samples from the MCfR using 3-mL syringes and immediately filtered the sample through a 0.22-μm PES membrane filters (NEST Scientific). F^- was analyzed using an ion chromatograph (IC-930, Metrohm, USA). PFOA (> 0.1 μM, 0.04 ppm) was determined using ultra-performance liquid chromatography (UPLC) (WATERS LC-20A, United States) with a Waters C18 column and an evaporative light scattering detector (ELSD). PFOA (at the ppt level) was determined using an Agilent 1290 UPLC coupled to 6490 triple quadrupole mass spectrometer system (QQQ-MS) based on the EPA Method 537.[32] Defluorination products from PFOA were analyzed using an Agilent 1290 high performance liquid chromatography coupled to the Agilent 6530 quadrupole/time-of-flight mass spectrometer (HPLC-QTOF-MS). PFOS and its products were analyzed using HPLC-QTOF-MS.

Solid-catalyst characterization. Pieces were cut from MCfR fiber with a scissors and prepared for solid-state analyses following our established protocol.[33] X-ray powder diffraction analysis was conducted using Philips X'Pert Pro equipment ewith a Cu Kα radiation source (1.540598 Angstrom); from 10-90 2theta degrees range with a step size of 0.0050 s^{-1}. We used a FEI Titan environmental transmission electron microscope (ETEM) to characterize the catalysts by imaging and crystallite diffraction. We carried out X-ray photoelectron spectroscopy using a PHI Quantera SXM (ULVAC-PHI. Inc) with an Al source (focused beam of 1.5 kV, 25 W).

Computational Methods. We performed Density Functional Theory (DFT) calculations to determine the PFOA adsorption modes on the most stable Pd (111) surface and to investigate the effect of surface hydrogen coverage on PFOA adsorption. On the Pd (111) surface, we calculated the adsorption energy of the PFOA molecule as

$$\Delta E^{ads}_{Pd/PFOA} = E_{Pd/PFOA} - E_{Pd} - E_{PFOA} \quad (1)$$

where $E_{Pd/PFOA}$ is the energy of PFOA adsorbed on Pd (111), E_{Pd} is the energy of the clean Pd (111) slab, and E_{PFOA} is the energy of the isolated PFOA molecule. DFT calculations were performed with the Vienna *ab initio* simulation package (VASP 5.4.4) in conjunction with the VASPsol implicit solvation model.[34–37] We employed the Perdew−Burke−Ernzerhof (PBE) generalized gradient approximation of the exchange-correlation functional within the projector augmented wave (PAW) formalism. The valence electrons of Pd ($4d^{10}$), C ($2s^2 2p^2$), F ($2s^2 2p^5$), O ($2s^2 2p^4$), and H ($1s^1$) were treated self-consistently, and all the calculations were spin polarized.[38,39] A kinetic energy cutoff of 450 eV was used for the plane-wave basis sets and a Monkhorst-Pack k-point mesh of 2×2×1 was used for sampling the Brillouin zone.[40,41] The Methfessel–Paxton smearing method with a smearing width of 0.2 eV was used to integrate the Brillouin zone. We applied Grimme's DFT-D3 dispersion correction to include the van der Waals interactions.[42–44] All the self-consistent electronic optimizations were converged to within 0.01 meV, and all the geometry optimizations were converged to forces within 0.02 eV $Å^{-1}$.

We employed the most stable Pd (111) surface for the PFOA adsorption calculations. A 6×6 slab model consisted of four layers of Pd atoms, where the bottommost layer was frozen to represent the bulk. Each layer was comprised of 36 Pd atoms, and periodic boundary conditions were applied in all three directions. An implicit electrolyte region of 28 Å was employed in the direction perpendicular to the Pd surface to include the solvation effects and to avoid the spurious interactions between the periodic cell images. Default VASPsol parameters were used for the implicit solvation model, except for the effective surface tension (τ) parameter, which was set to zero to avoid instabilities in the local electrostatic potential in the electrolyte region.[34–37] The cell containing the deprotonated form of PFOA was negatively charged to treat PFOA as an anion, which required the addition of a QV correction term in the potential energy of the system with Q being the charge of the simulation cell and V being the local electrostatic potential in the electrolyte region. The overall cell charge was balanced through implicit counter-ions introduced by the VASPsol solvation model, as described by Hennig and co-workers. [34,35]

3.2. Task 2: Oxidative defluorination and mineralization of partially fluorinated OA and OS in the O_2-MBfR

Reactor setup. Fig. 2.A is a schematic of the bench-scale O_2-MBfR. Continuous-mode biodegradation of OA/OS and partially fluorinated OA/OS was performed in two O_2-MBfRs. The MBfRs had a total working volume of 90 mL (70-mL medium and 20-mL headspace) and contained two bundles of 32 hollow-fiber membranes (composite gas-transfer membrane, 280 μm OD, 180 μm ID, wall thickness 50 μm, length 26 cm, total surface area 0.0146 m^2; Model MHF 200TL Mitsubishi Rayon Co., Ltd, Tokyo, Japan) in two glass tubes (6-mm internal diameter and 27-cm length). O_2 gas (>99.9%) was supplied to the end of fiber bundles at pressures controlled by a pressure regulator set at 3 psig (1.2 atm absolute pressure).

Analytical methods. Aqueous samples from the serum bottles and O_2-MBfR influent and effluent were collected using 3-mL syringes. All samples are filtered through 0.22-μm polyvinylidene difluoride syringe filters (MID Membrane Technologies, Inc., USA) before being stored in the 4°C refrigerator. The OA and OS concentrations in the aqueous samples were measured by using gas chromatography (GC) equipped with flame ionization detection (FID) and a column of "Rt-QSPLOT column 30m×0.53mm×10 mm (Restek®, Bellefonte, PA)." The detection limit of aqueous OA and OS was ~0.1 μM and ~0.3 μM, respectively. The fluoride ion (F^-) and concentrations were quantified using anionic chromatography (IC) (Metrohm 930 Compact IC). The IC was equipped with a Metrosep A supp 5 -250/4.0 column and fed with an eluent of 1 mM sodium bicarbonate ($NaHCO_3$) and 3.2 mM sodium carbonate (Na_2CO_3) with a flow rate of 0.7 mL/min. The detection limit of acetate was 1 μM. The high concentration PFOA (>0.1 mM) was quantified using the same anionic chromatography, but the eluent was 2.5 mM sodium bicarbonate ($NaHCO_3$) and 8.0 mM sodium carbonate (Na_2CO_3) dissolved in 20%/80% (v/v) acetonitrile/water mix solution. The detection limit for PFOA was 0.1 mM.

Medium compounds. A modified nitrate mineral solution (NMS) was used for O_2-MBfRs, as well as for the batch tests in serum bottles. The components of the NMS were: 11.76 KNO_3, 1.28 Na_2SO_4, 0.15 $MgCl_2$, 0.07 $CaCl_2$, 0.08 $FeSO_4$, 3.9 KH_2PO_4, 6.1 K_2HPO_4, 0.002 $ZnCl_2$, 0.002 H_3BO_3, 0.002 $MnCl_2$, 0.004 $CoCl_2$, 0.004 Na_2MoO_4, 0.01 $CuCl_2$, 0.01 $NiCl_2$, and 0.01 Na_2WO_4 (units are mmole/L). The pH of the medium was adjusted to ~7.2 using H_2SO_4 and NaOH.

DNA extraction and sequencing. When the effluent concentrations of all substrates were stable for at least three consecutive sampling dates (standard deviation <5%), O_2-MBfR operation was considered to be at steady state. We collected the biofilm samples of all the O_2-MBfRs at steady state of each stage for the microbial community analysis. We pulled out a bundle of fibers and used sterilized tweezers to grip the biofilm on the fibers. The collected biofilm (about 0.5 mL) was put into sterilized centrifuge tube (two samples for each reactor). After centrifuging the samples at 10,000 rpm for 10 min and removing the supernatant, the biofilm pellet was stored in a -80°C refrigerator. A QIAGEN (USA) DNeasy® PowerBiofilm kit was used to extract the DNA from all biofilm pellets when all the stages were finished. The extracted DNA samples were stored in the -80°C refrigerator before sequencing. All the extracted DNA samples were sent to CosmosID Inc. (MD, US) for shallow metagenomic sequencing. All the samples were quantified using Varioskan and Qubit 4 fluorometer with Qubit™ dsDNA HS Assay Kit (Thermofisher Scientific). DNA libraries were prepared using the Nextera XT DNA Library Preparation Kit.

Genomic DNA was fragmented using a proportional amount of Illumina Nextera XT fragmentation enzyme. Combinatory dual indexes were added to each sample followed by 12 cycles of PCR (polymerase chain reaction) to construct libraries. DNA libraries were purified using AMpure magnetic Beads (Beckman Coulter) and eluted in QIAGEN EB buffer. DNA libraries were prepared using the Illumina Nextera XT library preparation kit. Library quantity was assessed with Qubit (ThermoFisher). Libraries were then sequenced on an Illumina NextSeq 550 2x150bp.

Sequence quality control. After sequencing, all DNA sequencing reads were trimmed to remove low-quality bases (sequence length < 60 bp; quality score < 30) by using the "Trimmomatic" tool.[45] The detailed quality of the DNA sequencing reads before and after quality control (QC) for each sample is listed in the Appendices Table A4.

Taxonomic classification for community structure. In order to relate DNA sequences to a specific genus and species, we aligned our DNA reads to the genome taxonomy database (GTDB) to identify bacteria taxonomy and functions [46,47]. The alignment was accomplished by using the "Kaiju" microbial classification engine [48]. The "Kaiju" system used the BWT (Burrows-Wheeler transform) change to align all samples' DNA-sequence reads to the database of all complete bacterial genomes [49]. The relative abundance (%) of specific taxa was calculated by reads mapped to specific classification category divided by the total reads (after quality control) of each sample.

Functional genes assignment and abundance. To investigate the relative abundance of functional genes, we used the "UProC" toolbox to classify all samples' DNA sequencing reads based on the KEGG (Kyoto Encyclopedia of Genes and Genomes) database [50]. The "UProC" toolbox translated the DNA reads into amino acids sequences. Then, we compared the translated reads with oligopeptides at the protein-level and used the "Mosaic Matching Score" to identity the best-matched protein family [51]. All the relative abundance of functional category is presented as counts per million (CPM). CPM reported here are calculated in a similar way to the transcripts per million calculation method introduced by Wagner et al. (2012).

3.3. Task 3: Synergistic defluorination of PFOA/PFOS

Reactor setup. After achieving stable reductive defluorination of PFOA/PFOS in the H_2-MCfR and biodegradation of OA/OS in the O_2-MBfR, the two parts were connected by linking the effluent tube of H_2-MCfR to the influent tube of O_2-MBfR; this is illustrated in Figure 3. In the synergistic system, PFOA/PFOS was reductively defluorinated in H_2-MCfR and converted to less- or none- fluorinated octanoic acid. The defluorinated products were further oxidize in the O_2-MBfR by the biofilm with or without OA/OS as primary substrate.

3.4. Task 4: Cost analysis

APTwater Inc. developed and launched a commercial scale H_2-based MBfR for nitrate treatment (ARoNite). The hollow fibers used to deliver the hydrogen are woven into a sheet with several of these sheets spiral wound around a water feed tube. This design provides a large surface area in a small footprint. This is referred to as a module. In addition, APTwater has cost estimating tools and models for H_2-based MBfR systems. APTwater modified the design models to develop a cost estimation for a H_2-MCfR along with an O_2-MBfR.

4. Results and Discussion

4.1. Task 1: Reductive defluorination of PFOA and PFOS in the H_2-MCfR

4.1.1. Characteristics of Pd-film in the MCfR

Figure 5 displays characteristics of a Pd-film in the MCfR with a Pd^0 loading of 1.2 g Pd^0/m^2. The XRD pattern in Figure 1A verifies the presence of crystalline Pd^0, with the three characteristic diffraction peaks at 40.3, 46.7, and 68.2 2theta degrees assigned to the (1 1 1), (2 0 0), and (2 2 0) planes, respectively. The crystallite size was calculated applying Scherrer equation, with calculated size of 6.0 nm. XPS analysis on the Pd-fiber (Figure 5B) shows only the presence of one peak at $Pd_{3/2}$ and $Pd_{5/2}$ energy, centered at 340.7 eV and 335.4 eV, which is attributed to Pd^0. TEM images of the cross-section of the Pd-film (Figures 5C and 5D) show that Pd^0NPs were attached onto the membrane fibers, forming a NP-containing layer with the thickness of ~60 nm. The Pd^0NP's size (Fig. 1E) was 2.6±0.5 nm (based on 152 particles in Figure 5D), which is similar to previous MCfR studies.[27,53] The diffraction patterns (Figure 5F) shows three planes of Pd^0: (1 1 1), (2 0 0), and (2 2 0), same planes observed by XRD.

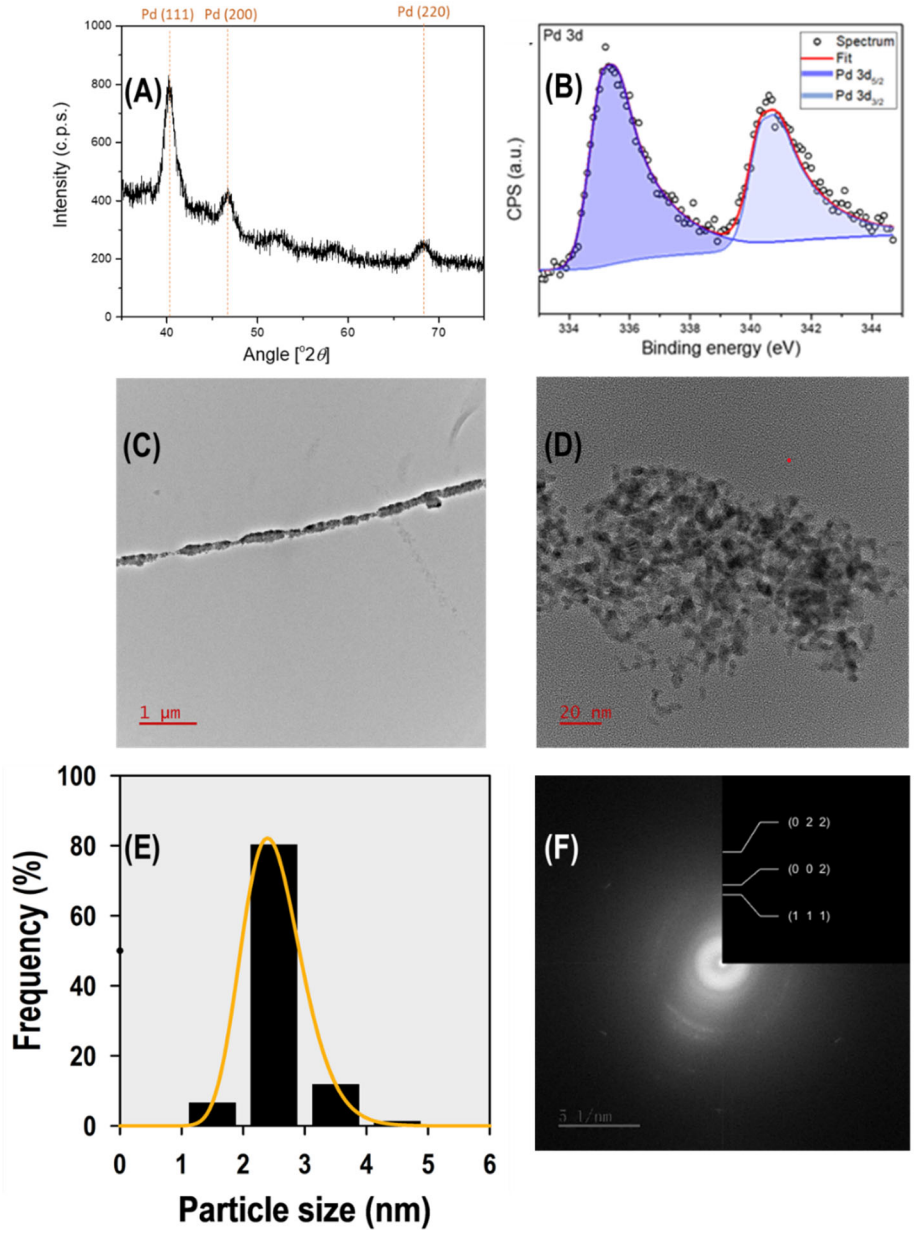

Figure 5. (A) XRD spectra of a Pd-fiber. (B) XPS spectra of a Pd-fiber. (C) TEM image of cross section of a Pd-fiber. (D) TEM image of a Pd-fiber. (E) Size distribution of the nanoparticles of Figure D. (F) Diffraction patterns of Pd^0NPs from Figure D.

4.1.2. Batch tests PFOA removal and defluorination in the H_2-MCfRs

4.1.2.1. Different pHs

We tested defluorination of 10 µM PFOA catalyzed by *freshly synthesized* Pd^0NPs at different pHs. We set up four H_2-MCfRs equipped with similar membranes and coated the membranes with the same 5-mM Pd. Immediately after the formation of PdNPs, we conducted repeated defluorination tests at pHs of 4, 5, 6, and 7 in parallel.

pH 4. The results for pH 4 are in Figure 6. During the first cycle, over 99% of the 10 µM PFOA was depleted, along with accumulation of 0.118 mM F^- (accounting for 77% of the total F in the 10 µM PFOA) within 47 hours. In the following two cycles, the PFOA removal declined gradually: 93.9% PFOA removal along with 0.076-mM F^- accumulation (50.8%) within 47 h (cycle 2) and 82.1% PFOA removal along with 0.068-mM F^- accumulation (45.3%) within 45 hours (cycle 3). We did not observe desorption of PFOA through the three cycles.

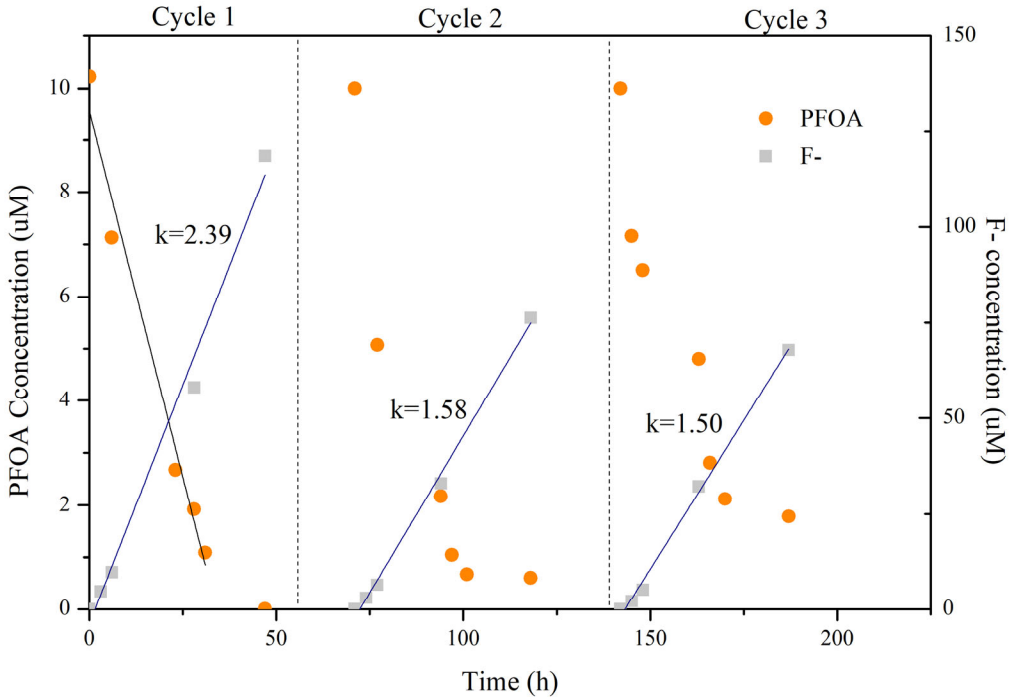

Figure 6. Concentration of PFOA and F-release in series batch tests of catalytic reductive defluorination of ~10-µM PFOA in the MCfR at pH ~ 4 with H_2 of 20 psig. Orange dots: PFOA in the H_2-MCfR; Grey squares: F^- in the H_2-MCfR. Zero-order rate coefficients for F^- release (k) are in units of µM/h.

pH 5. The results for pH 5 are in Figure 7. During the first cycle, over 99% of the 10 µM PFOA was depleted, along with accumulation of 0.103 mM F^- (accounting for 68.7% of the total F in the 10 µM PFOA) within 47 hours. In the following two cycles, the PFOA removal declined gradually: 96.7% PFOA removal along with 0.063-mM F^- accumulation (42.6%) within 47 h (cycle 2) and 95.2% PFOA removal along with 0.055-mM F^- accumulation (36.7%) within 45 hours (cycle 3). We did not observe desorption of PFOA through the three cycles.

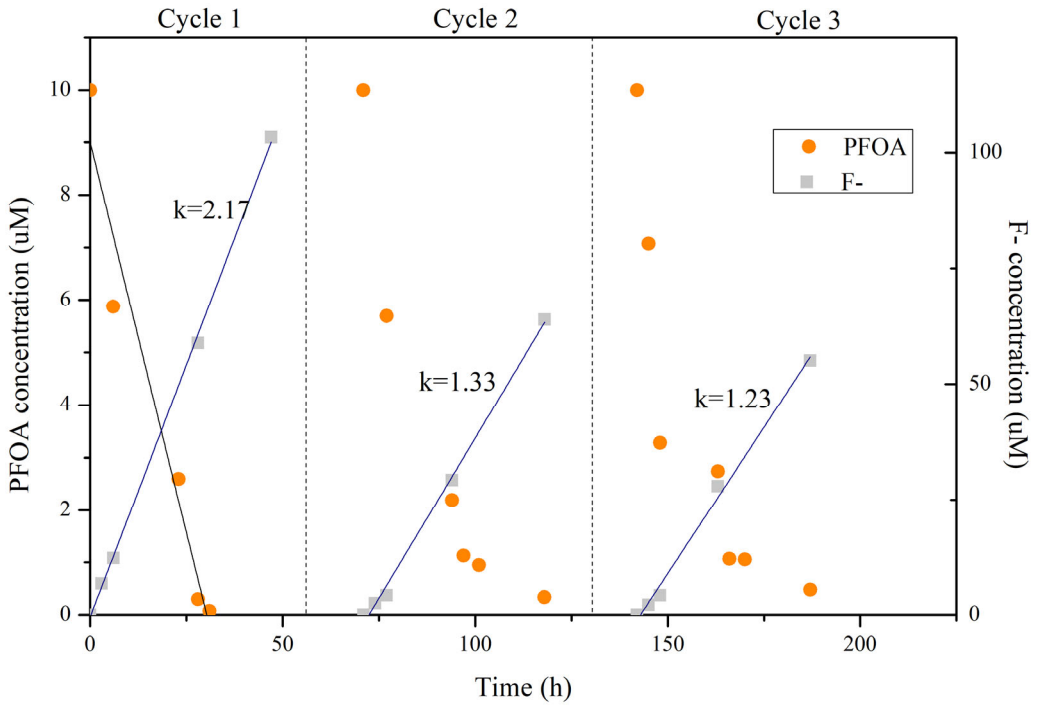

Figure 7. Concentration of PFOA and F-release in series batch tests of catalytic reductive defluorination of ~10-µM PFOA in the MCfR at pH ~ 5 with H_2 of 20 psig. Orange dots: PFOA in the H_2-MCfR; Grey squares: F^- in the H_2-MCfR. Zero-order rate coefficients for F^- release (k) are in units of µM/h.

pH 6. The results for pH 6 are in Figure 8. During the first cycle, we saw over 99% PFOA depletion and substantial reductive defluorination (0.042 mM F^- accumulation, or 28% of the total F in 10 µM PFOA) in the H_2-MCfR during the 47-hour test. In the second cycle, the PFOA removal declined, but was still substantial: 94.5% PFOA removal along with 0.039-mM F^- accumulation (26%) within 47 h (cycle 2). By cycle 3, the concentration of PFOA increased, due to the desorption of the residual PFOA from the first 2 cycles. However, F^- release in this cycle still was 0.034 mM in 45 h in the H_2-MCfR; thus, adsorbed PFOA still was being defluorinated.

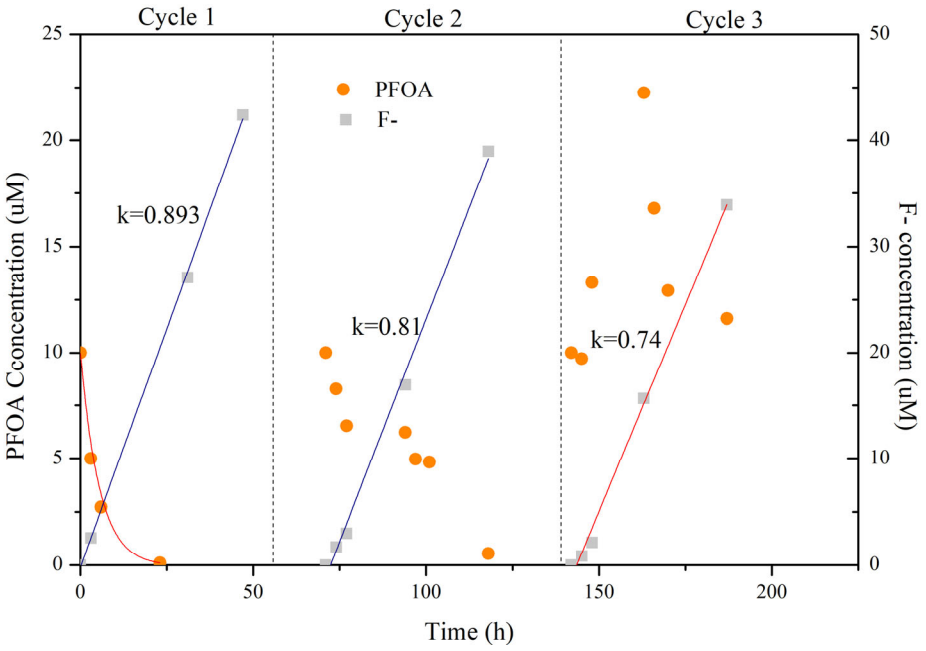

Figure 8. Concentration of PFOA and F-release in series batch tests of catalytic reductive defluorination of ~10-µM PFOA in the MCfR at pH ~ 6 with H_2 of 20 psig. Orange dots: PFOA in the H_2-MCfR; Grey squares: F^- in the H_2-MCfR. Zero-order rate coefficients for F^- release (k) are in units of µM/h.

pH 7. The results for pH 7 are in Figure 9. While all of the 10 µM PFOA was removed in 24 h in the first cycle, F^- release was minimal. This indicates that PdNP catalysis apparently was deactivated at pH 7. Therefore, PdNPs had only adsorption ability for PFOA. With no defluorination in the H_2-MCfR, the adsorption capacity of the PdNPs became saturated, and cycle 3 provides evidence of net desorption.

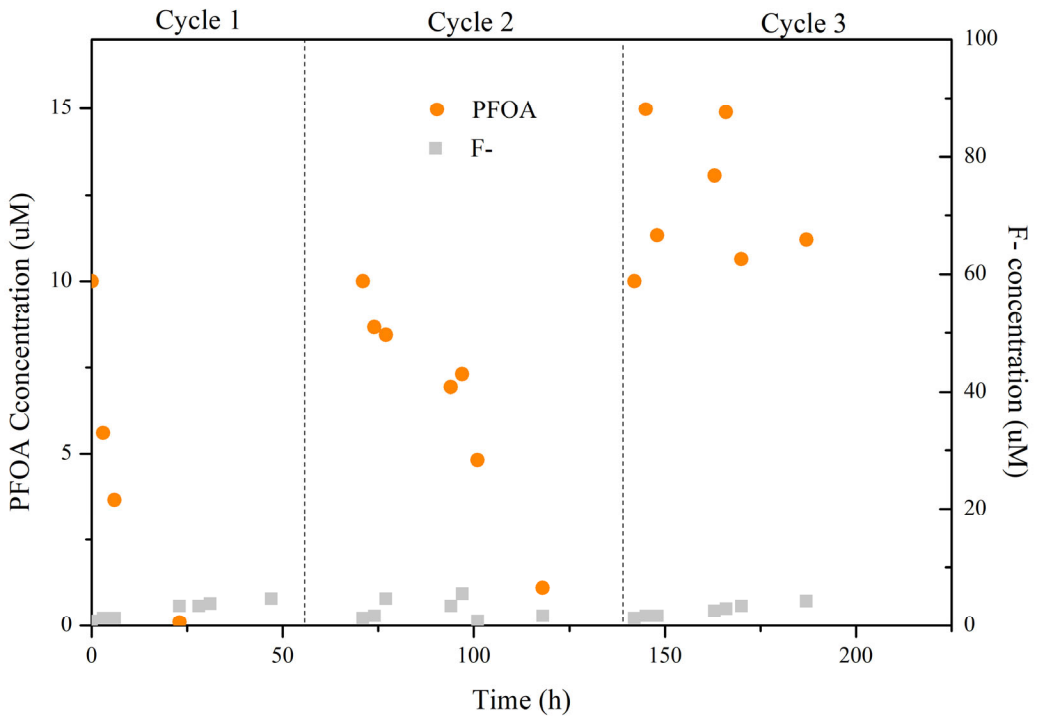

Figure 9. Concentration of PFOA and F-release in series batch tests of catalytic reductive defluorination of ~10-μM PFOA in the MCfR at pH ~ 7 with H_2 of 20 psig. Orange dots: PFOA in the H_2-MCfR; Grey squares: F^- in the H_2-MCfR. Zero-order rate coefficients for F^- release (k) are in units of μM/h.

At pH 4, over 99% of the 10-μM PFOA was depleted, along with the accumulation of 0.118 mM F^- (accounting for 77% of the total F in the 10 μM PFOA) within 47 hours. When the pH was raised from 4 to 7, the removal rate of PFOA increased gradually, and at pH 7 the rate was ~3-fold faster than that at pH 4. However, the defluorination rate decreased monotonically, becoming ~38-fold slower at pH 7 than that at pH 4. Pd^0 has higher capacity for H_2 adsorption at acidic pH, which should promote defluorination at lower pH.[54,55] Also, in the higher-pH condition, more PFOA exists in the deprotonated $PFOA^-$ anion, while lower pH increases the protonated form. Other anions in general also are more prevalent at higher pH and might have competed with $PFOA^-$ for active catalytic sites.[55–57]

The defluorination rate decreased with repeated test cycles, but the defluorination kinetics declined by less than 50% for pHs 4, 5, and 6 from cycle 1 to 3. Thus, deactivation was gradual. In addition, the defluorination-rate decrease was greater between the first and second cycles especially at pH 4 and 5, with the declines being small from cycle 2 to 3. This trend is encouraging for continuous operation.

For pHs of 6 and 7, almost all removal of 10 μM PFOA occurred in 23 h, and it was with a first-order trend that might be explained by adsorption. In contrast, F^- release continued for the duration of the experiment and with zero-order kinetics for pH 6. This supports that adsorption was stronger at higher pH. However, adsorption could become saturated, which led to release of PFOA in cycle 3.

Table 1 summarizes the PFOA first-order removal rates and zero-order defluorination rates. In summary, the rates illuminate different patterns for PFOA adsorption and defluorination by PdNPs in the H_2-MCfRs at different pHs. PFOA was more strongly adsorbed at higher pHs, but lower pHs promoted defluorination. In all cases, PFOA first was adsorbed to the PdNP surfaces, and then the adsorbed PFOA was catalytically defluorinated for pHs ≤ 6. The rate was gradually slowed due to gradual deactivation of the PdNPs, probably due to adsorption of PFOA-defluorination products.

Table 1. Zero-order rates of F^- accumulation (k in unit of μM/h) for the varied pHs for the successive three cycles

Pd/10-μM PFOA	Cycle 1	Cycle 2	Cycle 3
pH = 4	k = 2.39	k = 1.58	k = 1.50
pH = 5	k = 2.17	k = 1.33	k = 1.23
pH = 6	k = 0.89	k = 0.81	k = 0.74
pH = 7	negligible	negligible	negligible

4.1.2.2. Different catalyst types

We tested defluorination of 10 μM PFOA catalyzed by *freshly synthesized* Pd^0NPs, Pt^0NPs, Ru^0NPs, and Rh^0NPs. We set up three H_2-MCfRs equipped with similar membranes and coated the membranes with the 5 mM of Pd, Pt, Ru, or Rh precursors. This yielded the same catalyst loading of 11 mM/m^2. Immediately after the formation of these NPs, we conducted defluorination tests using the same conditions (10 μM PFOA, 20 psi H_2) at two pHs (4 and 7) in parallel and compared them with PdNPs.

Pd: The results of PFOA and F^- concentrations for PdNPs are shown in Figure 10. At pH 4, within 47 hours, over 99% of the 10 μM PFOA was depleted with a pseudo-first-order rate of 0.066 h^{-1}, along with accumulation of 0.118 mM F^- (accounting for 77% of the total F in the 10 μM PFOA) with a pseudo-zero-order rate of 2.4 μM/h. At pH 7, all of the 10 μM PFOA was removed with a pseudo-first-order rate of 0.17 h^{-1} within 24 h, while F^- release was minimal (3.8

μM F^- accumulation, accounting for 2.5% of the total F in the 10 μM PFOA) with a pseudo-zero-order rate of 0.08 μM/h.

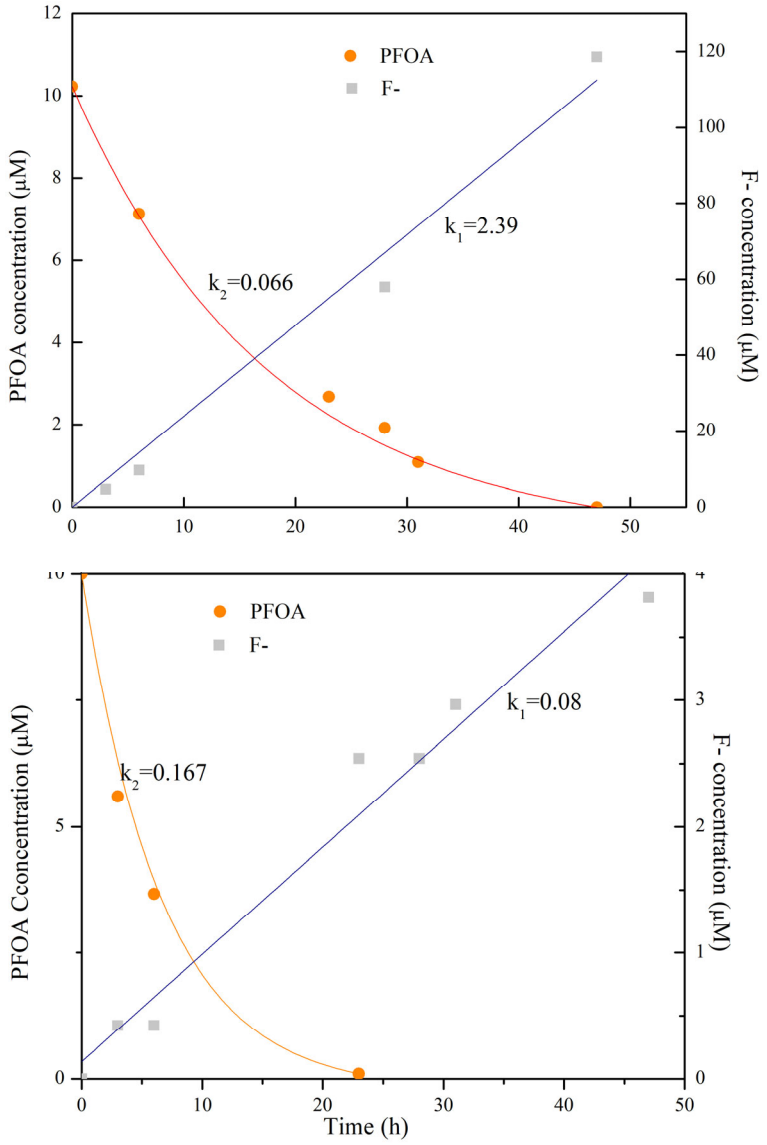

Figure 10. Concentrations of PFOA and F^- released in the batch test of catalytic reductive defluorination of ~10-μM PFOA in the MCfR with 1.2 g/m^2 or 11 mM/m^2 Pd^0 at pH 4 (top) and 7 (bottom) with aH_2 supplied at 20 psig.

Pt: The results of PFOA and F^- concentrations for PtNPs are shown in Figure 11. At pH 4, over 99% PFOA was depleted with a pseudo-first-order rate of 0.14 h^{-1}, but defluorination was slow (5.62 µM F^- accumulation, accounting for 4.4% of the total F in the ~9 µM PFOA) with a pseudo-zero-order rate of 0.13 µM/h during the 44-hour test. At pH 7, over 99% PFOA was depleted with a pseudo-first-order rate of 0.059 h^{-1} with reductive defluorination (8.71 µM F^- accumulation, accounting for 4.8% of the total F in the ~12 µM PFOA) with a pseudo-zero-order rate of 0.11 µM/h during the 77-hour test.

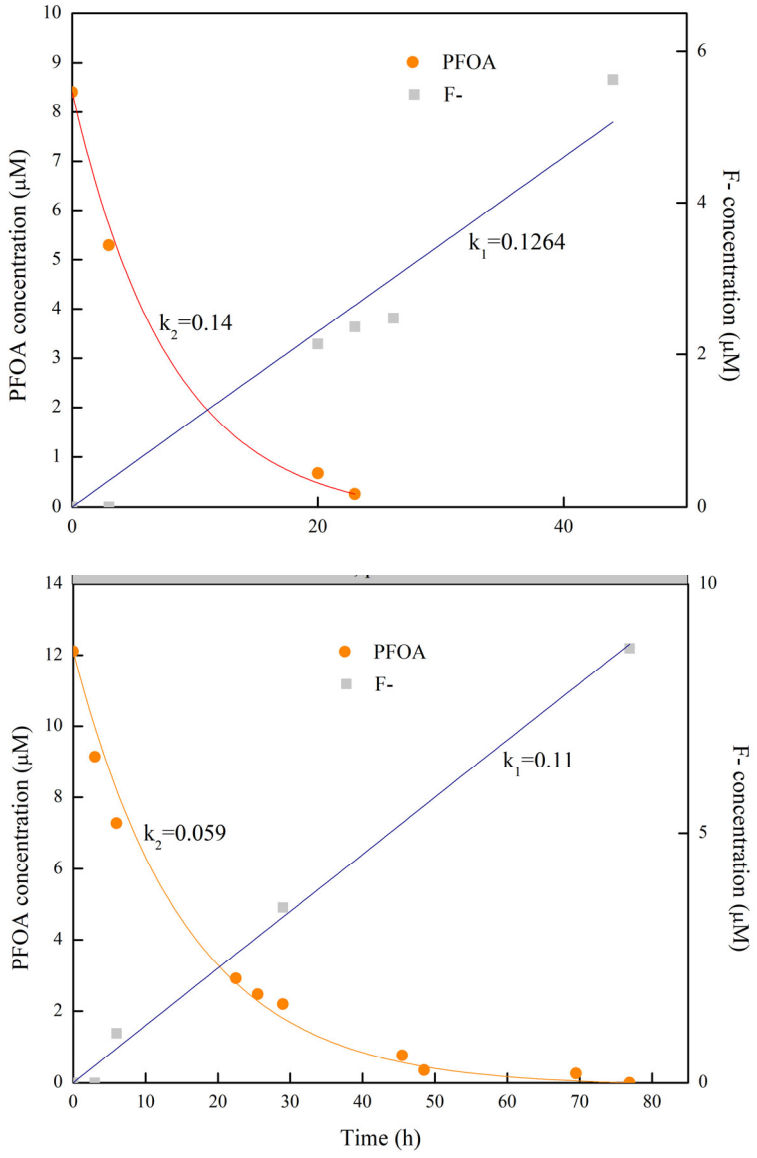

Figure 11. Concentrations of PFOA and F^- released in the batch test of catalytic reductive defluorination of ~10-µM PFOA in the MCfR with 11 mM/m^2 Pt^0 at pH 4 (top) and 7 (bottom) with H_2 supplied at 20 psig.

Ru: The results of PFOA and F^- concentrations for RuNPs are shown in Figure 12. At pH 4, over 99% PFOA was depleted at a pseudo-first-order rate of 0.1 h^{-1} along with slow reductive defluorination (6.3 µM F^-, accounting for 4.5% of the total F in the ~9 µM PFOA) with a pseudo-zero-order rate of 0.14 µM/h in the H_2-MCfR during the 44-hour test. At pH 7, we detected over 67% PFOA depletion with a pseudo-first-order rate of 0.016 h^{-1}, but with almost no reductive defluorination (0 µM F^- accumulation) in the H_2-MCfR during the 77-hour test.

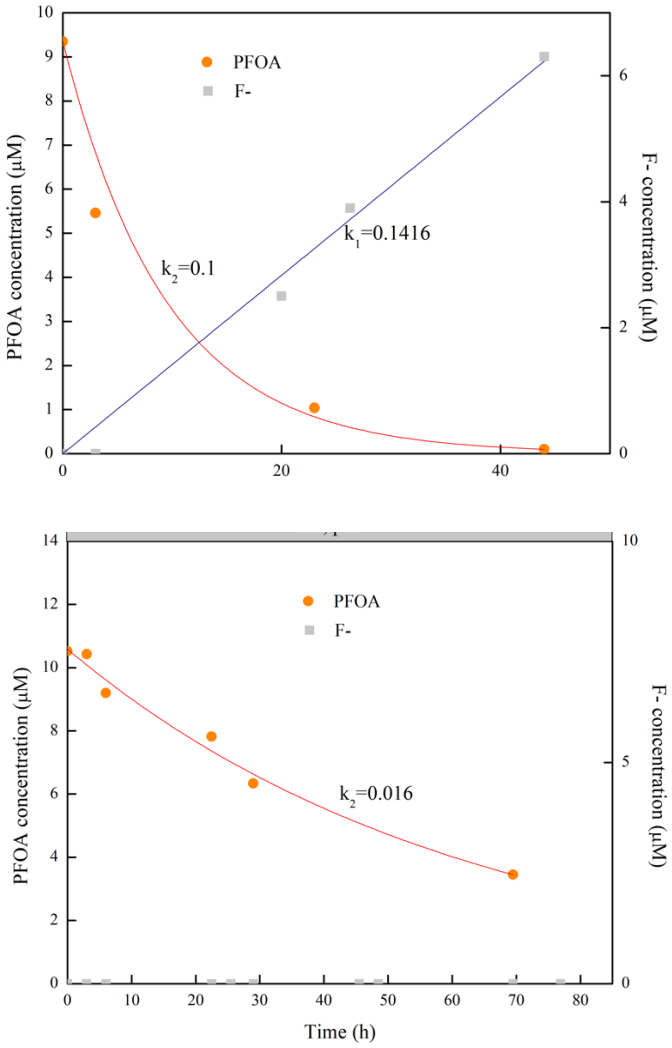

Figure 12. Concentrations of PFOA and F^- released in the batch test of catalytic reductive defluorination of ~10-µM PFOA in the MCfR with 11 mM/m^2 Ru^0 at pH 4 (top) and 7 (bottom) with H_2 supplied at 20 psig.

Rh: The results of PFOA and F^- concentrations for Rh are shown in Figure 13. At pH 4, over 99% of the 10 µM PFOA was depleted with a pseudo-first-order rate of 0.127 h^{-1}, along with accumulation of 8.8 µM F^- (accounting for 5.3% of the total F in the ~11 µM PFOA) at a pseudo-zero-order rate of 0.16 µM/h within 52 hours. At pH 7, we detected over 41% PFOA depletion with a pseudo-first-order rate of 0.008 h^{-1} with reductive defluorination (27.6 µM F^- accumulation, accounting for 22% of the total F in the ~9 µM PFOA) with a pseudo-zero-order rate of 0.36 µM/h during the 77-hour test.

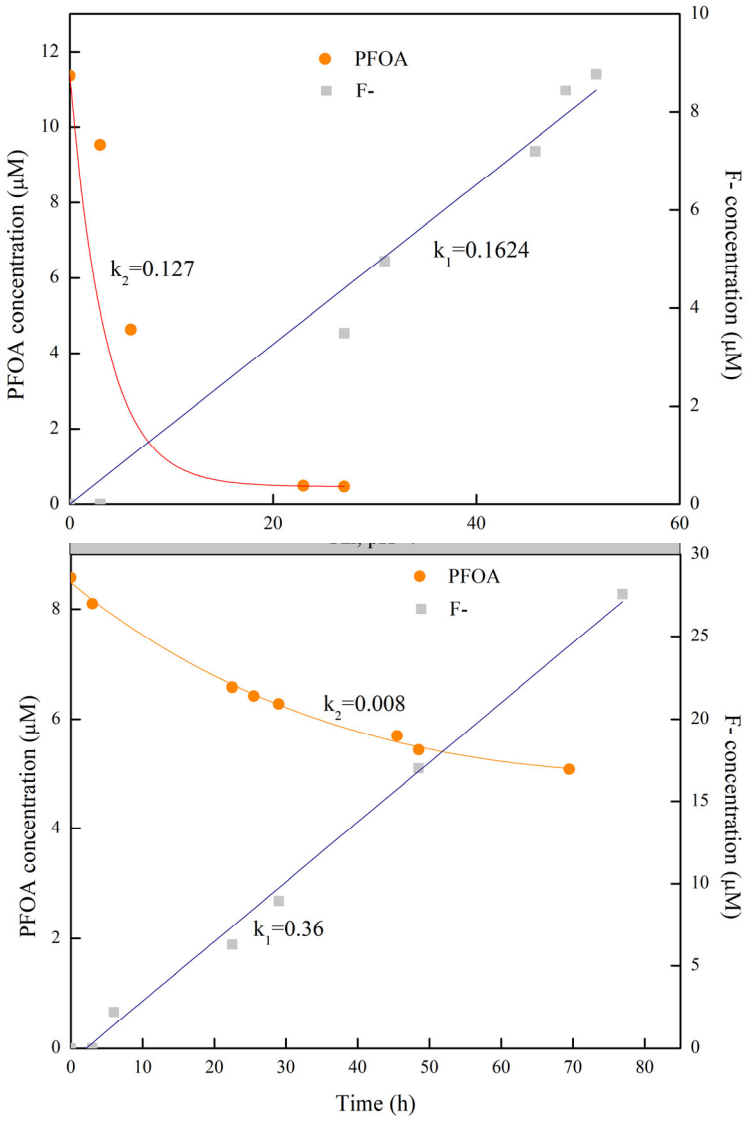

Figure 13. Concentrations of PFOA and F^- released in the batch test of catalytic reductive defluorination of ~10-µM PFOA in the MCfR with 11 mM/m^2 Rh^0 at pH 4 (top) and 7 (bottom) with H_2 supplied at 20 psig.

Figure 14 summarizes the rate constants for PFOA removal and defluorination catalyzed by the four types of precious metals at acidic and neutral pHs.[54,55] At acidic pH,

Pt^0, Ru^0, and Rh^0 exhibited moderately higher PFOA-removal rates than Pd^0, but Pd^0 had at least 15-fold higher defluorination kinetics (maximally 2.52 mM/hr) and capacity (77% within 50 hours) than the other three PGM catalysts. The advantage of Pd^0 probably was caused by its superior capacity for H_2 adsorption at acidic pH. At neutral pH, the trends were reversed. On the one hand, the PFOA-removal rate for Pd^0 (maximally 1.47 mM/hr) was fastest among the PGMs. On the other hand, Rh^0 yielded a slightly higher defluorination rate (maximally 0.36 mM/hr) and capacity (45% within 50 hours) than other PGMs, which indicates that Rh^0 might have higher catalytic activity at neutral pH. Pt^0 and Ru^0 displayed limited defluorination capability at both acidic and neutral pH, a finding similar to treating fluorinated pharmaceuticals.[58] Overall, Pd^0 was superior to the other PGMs in defluorinating PFOA at pH 4 and adsorbing PFOA at pH 7. In the following tests, we used Pd as the default catalyst.

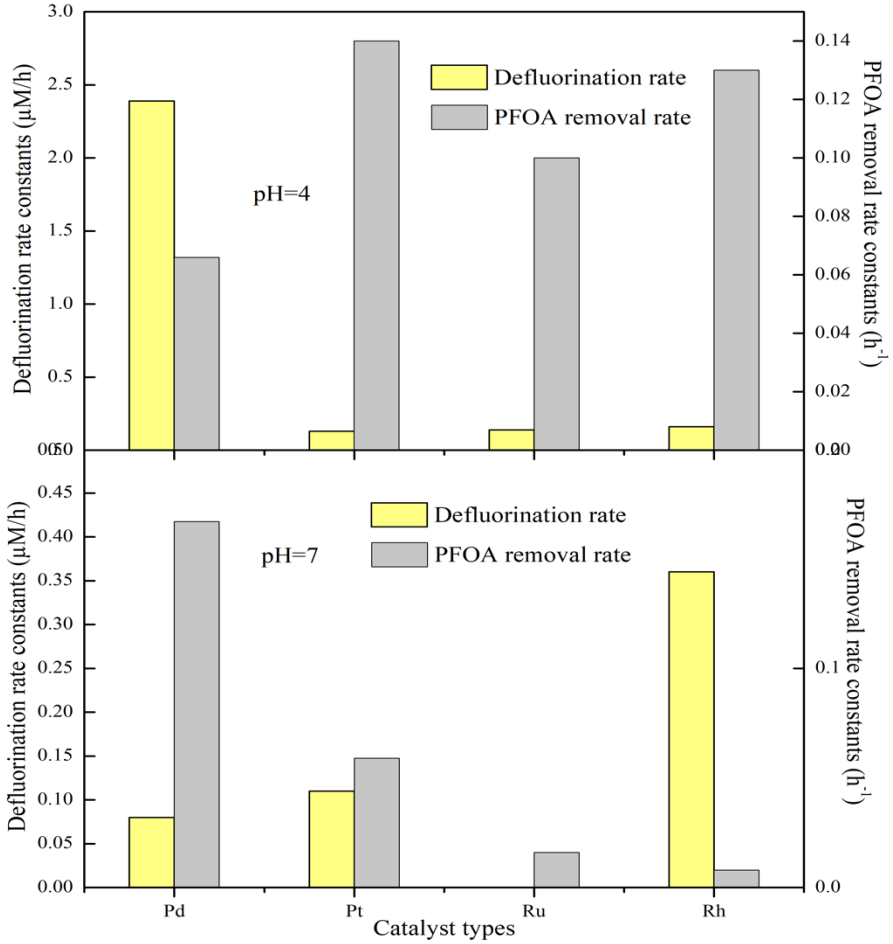

Figure 14. PFOA removal first-order rate constant and defluorination zero-order rate constant for the four precious-metal catalysts (Pd, Ru, Rh and Pt) in the batch tests of catalytic reductive defluorination of ~10-μM PFOA with 11 mM/m^2 catalyst at pH 4 and 7 with H_2 supplied at 20 psig.

4.1.2.3. Different catalyst loading

We investigated the defluorination of 10 µM PFOA at pH 4 catalyzed by *freshly synthesized* Pd^0NPs at different Pd^0 loadings (gPd^0/m^2) controlled by varying concentration of Pd precursors (as Na_2PdCl_4). We tested in parallel four different Pd precursor concentrations: 1, 3, 5, and 10 mM, which yielded 0.2, 0.7, 1.2, and 2.3 g-Pd^0/m^2 deposited on the membranes, respectively.

0.2 g/m² Pd^0: As shown in Figure 15, we detected over 99% depletion of 8 µM PFOA at a pseudo-first-order rate of 0.374 h^{-1} and 0.008 mM F^- accumulation (6% of the total F in in the initial PFOA) at a pseudo-zero-order rate of 0.0863 µM/h within 95 hours.

0.7 g/m² Pd^0: As shown in Figure 16, we detected over 99% depletion of 8 µM PFOA at a pseudo-first-order rate of 0.465 h^{-1} and 0.048 mM F^- accumulation (or 41% of the total F in the initial PFOA) at a pseudo-zero-order rate of 0.5 µM/h over 95 hours.

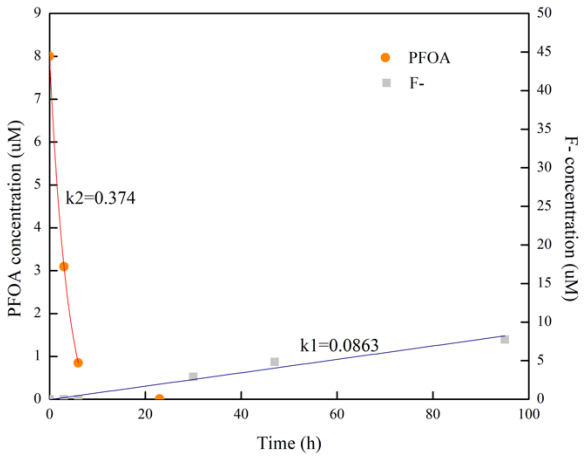

Figure 15. Concentrations of PFOA and F^- released in the batch test of catalytic reductive defluorination of ~10-µM PFOA in the MCfR with 0.2 g-Pd^0/m^2 at pH 4 with H_2 at 20 psig.

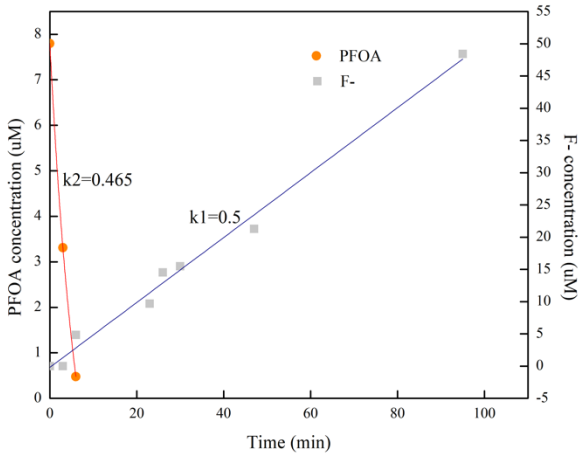

Figure 16. Concentrations of PFOA and F^- released in the batch test of catalytic reductive defluorination of ~10-µM PFOA in the MCfR with 0.7 g-Pd^0/m^2 at pH 4 with H_2 oat 20 psig.

1.2 g/m² Pd^0: As shown in Figure 17, we detected over 99% depletion of 10 µM PFOA at a pseudo-first-order rate of 0.066 h^{-1} and 118 µM F^- accumulation (77% of the total F in the initial PFOA) at a pseudo-zero-order rate of 2.4 µM/h within 95 hours.

2.3 g/m² Pd^0: As shown in Figure 18, we detected almost over 84% of the 11 µM PFOA depletion at a pseudo-first-order rate of 0.040 h^{-1} and 0.0025 mM F^- accumulation (or 1.5% of the total F in the initial PFOA) at a pseudo-zero-order rate of 0.063 µM/h over 47 hours.

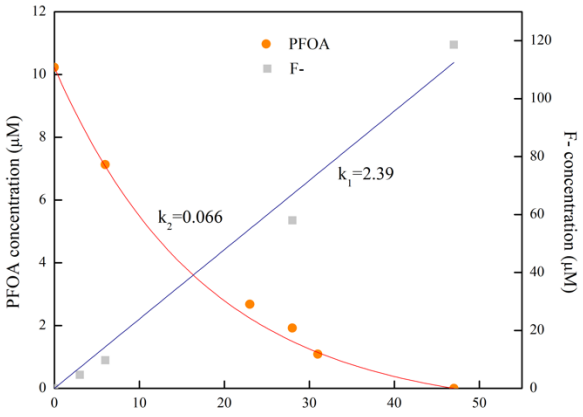

Figure 17. Concentration of PFOA and F^- released in the batch test of catalytic reductive defluorination of ~10-µM PFOA in the MCfR with 1.2 g-Pd^0/m^2 at pH 4 with H_2 supply at 20 psig.

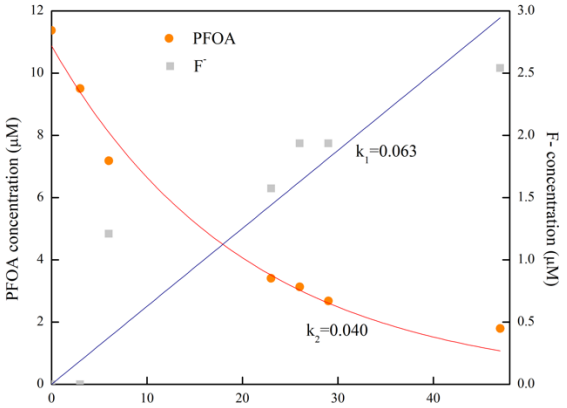

Figure 18. Concentration of PFOA and F^- released in the batch test of catalytic reductive defluorination of ~10-µM PFOA in the MCfR with 2.3 g-Pd^0/m^2 at pH 4 with H_2 supply at 20 psig.

Figure 19 summarizes the rate constants for PFOA removal and defluorination catalyzed by the four loadings of Pd^0 at pH 4. The PFOA-removal rate was greatest for 0.7 g Pd^0/m^2, but the defluorination rate was greatest for 1.2 g Pd^0/m^2. Both rates declined precipitously for 2.3 g Pd^0/m^2. The peaking of catalytic activity at 1.2 g Pd^0/m^2 probably occurred because the defluorination of PFOA with H_2 occurred mainly at the water-Pd^0 interface. Excessive Pd^0 coverage resulted in aggregation of Pd^0NPs, which decreased accessible specific surface area and led to lower catalytic activity.[27] In addition, a thick and agglomerated Pd-film may have hindered H_2 transfer to Pd^0 sites near the bulk liquid. This hypothesis is bolstered by the result for the catalyst-specific activity, which peaked at 1.2 g Pd^0/m^2. Because 1.2 g Pd^0/m^2 gave the best removal and defluorination performance, it was chosen as optimal for subsequent experiments in this study.

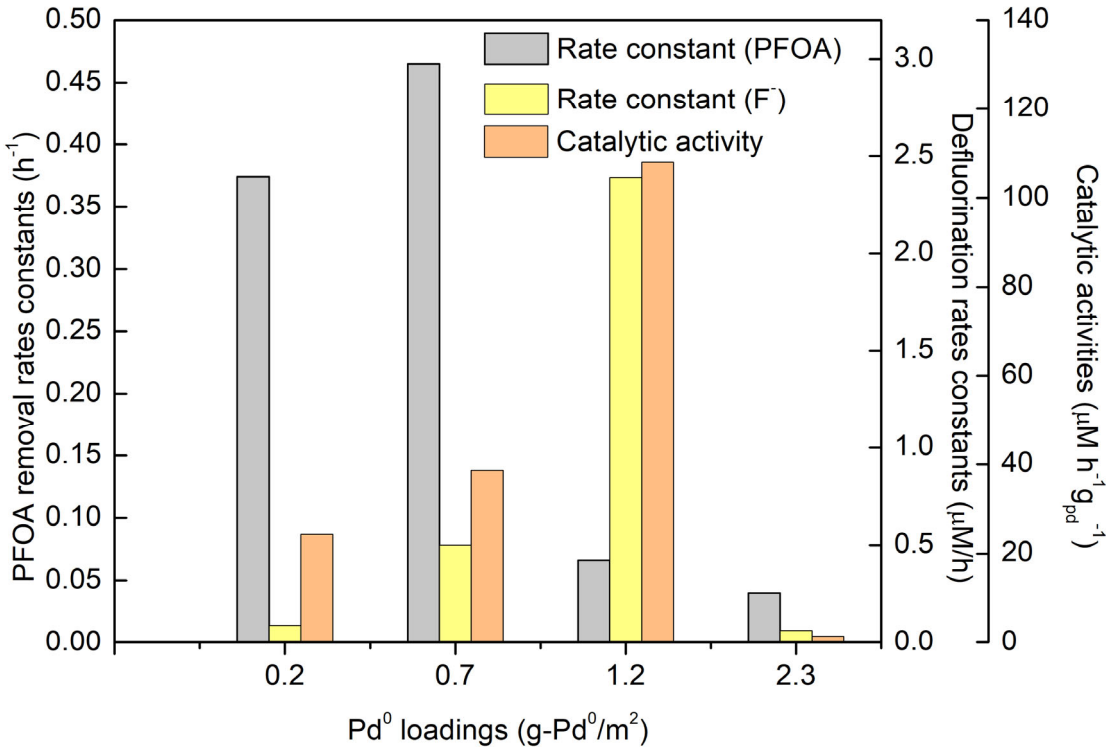

Figure 19. PFOA removal rate constant, defluorination rate constant, and catalytic activity of different Pd^0 loadings in the batch tests of catalytic reductive defluorination of ~10-μM PFOA at pH 4 and 20-psig H_2.

4.1.2.4. PFOS removal and defluorination catalyzed by Pd^0NPs

We investigated the defluorination of 10 μM perfluorooctanesulfonic acid (PFOS) at pH 7 catalyzed by *freshly synthesized* PdNPs with 1.2 g-Pd^0/m^2 deposited on the membranes. As shown in Figure 20, we detected over 97% depletion of 10 μM PFOS at a pseudo-first-order rate of 0.1 h^{-1} and 0.026 mM F^- accumulation (16% of the total F in the initial PFOA) at a pseudo-zero-order rate of 0.36 μM/h within 72 hours. The defluorination rate was significantly faster than for PFOA at pH 7, which supports that reductively defluorination with Pd^0NPs is a generalized mechanism for PFAS.

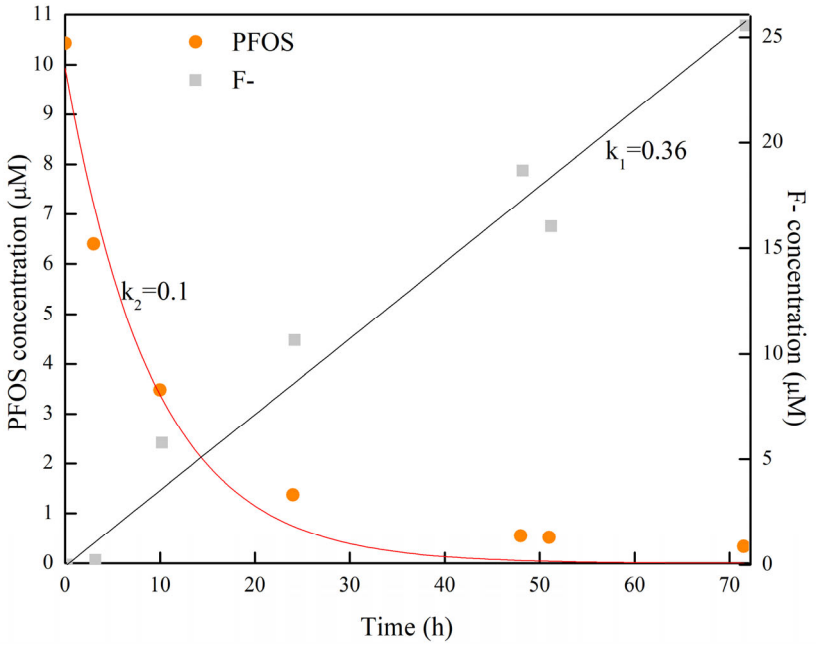

Figure 20. Concentrations of PFOA and F^- released in the batch test of catalytic reductive defluorination of ~10-μM PFOS in the MCfR with 1.2 g-Pd^0/m^2 at pH 7 and 20-psig H_2.

4.1.2.5. Mixed bimetallic catalysts on PFOA and PFOS removal and defluorination

To overcome the slow defluorination kinetics of Pd^0NPs at pH 7, we investigated of different mixed bimetallic catalysts in the defluorination of PFOA and PFOS at pH 7: Pd^0 prepared using the mixed format with Rh^0, Ru^0, Os^0, Pt, and Ir^0.

Pd/Rh: The results for PFOA and F^- concentrations for 2.5/2.5-mM Pd^0/Rh^0NPs are shown in Figure 21A. We detected over 60% PFOA depletion and reductive defluorination (43.8 μM F^- accumulation, accounting for 21.9% of the total F in the ~10 μM PFOA) with a pseudo-zero-order rate of 1.73 μM/h in the H_2-MCfR during the 29-hour test. The results of PFOS and F^- concentrations for 2.5/2.5-mM Pd/RhNPs are shown in Figure 21B. We detected over 75% PFOS depletion and reductive defluorination (35.1 μM F^- accumulation, accounting for 22.5% of the total F in the ~12 μM PFOA) with a pseudo-zero-order rate of 0.85 μM/h in the H_2-MCfR during the 41-hour test.

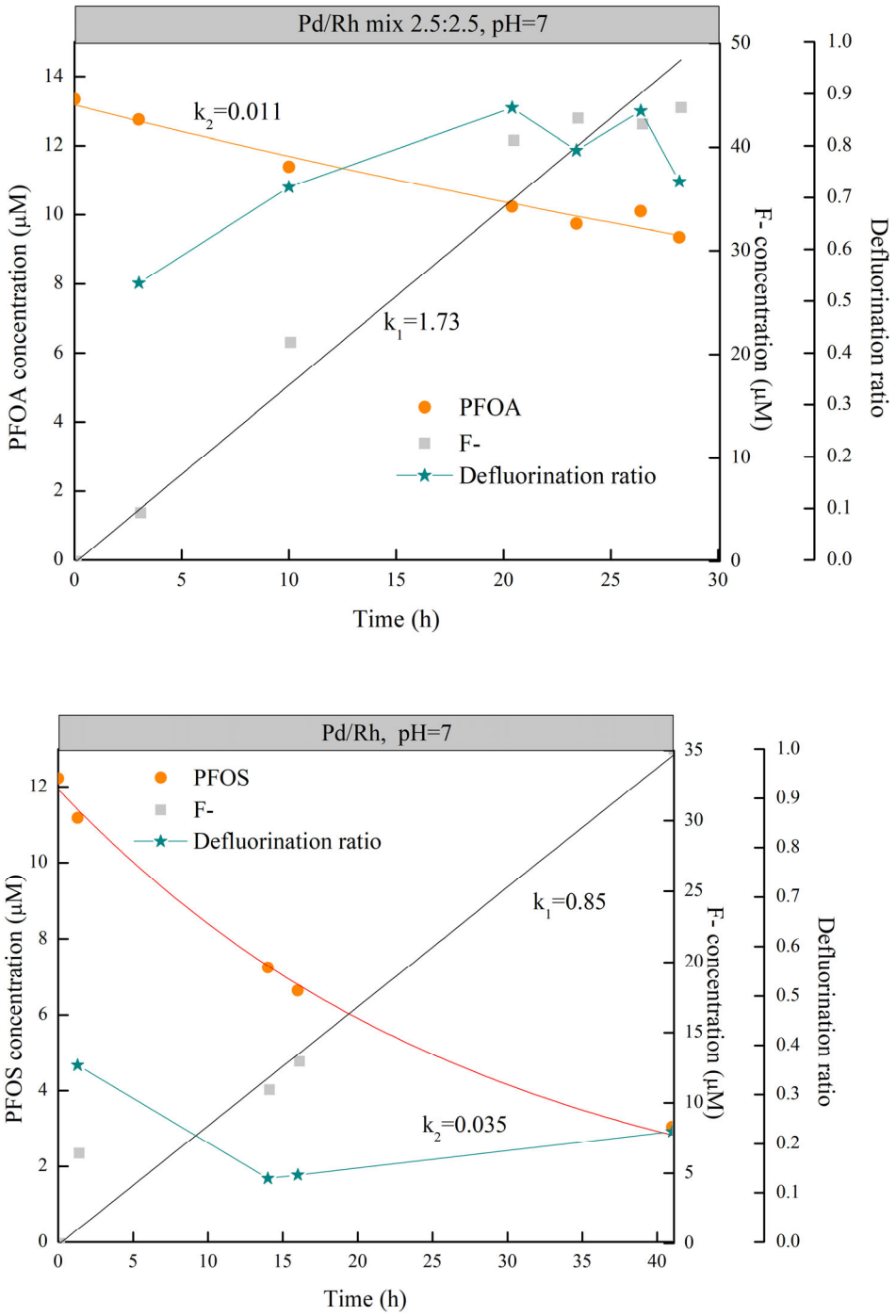

Figure 21. Concentrations of PFOA, PFOS, and F^- released and defluorination ratio in the batch test of catalytic reductive defluorination in the MCfRs with 2.5/2.5-mM Pd/RhNPs at pH ~ 7 with H_2 of 20 psig. (A) 10-μM PFOA (B) 10-μM PFOS.

Pd/Ru: The results of PFOA and F^- concentrations for 2.5/2.5-mM Pd^0/Ru^0NPs are shown in Figure 22A. We detected over 68% PFOA depletion with reductive defluorination (17.3 μM F^- accumulation, accounting for 8.1% of the total F in the ~14 μM PFOA) with a pseudo-zero-order rate of 0.21 μM/h in the H_2-MCfR during the 77-hour test. The results of PFOS and F^- concentrations for 2.5/2.5-mM Pd/RuNPs are shown in Figure 22B. We detected over 89.4% PFOS depletion with reductive defluorination (6.3 μM F^- accumulation, accounting for 3.6% of the total F in the ~11 μM PFOA) with a pseudo-zero-order rate of 0.06 μM/h in the H_2-MCfR during the 41-hour test.

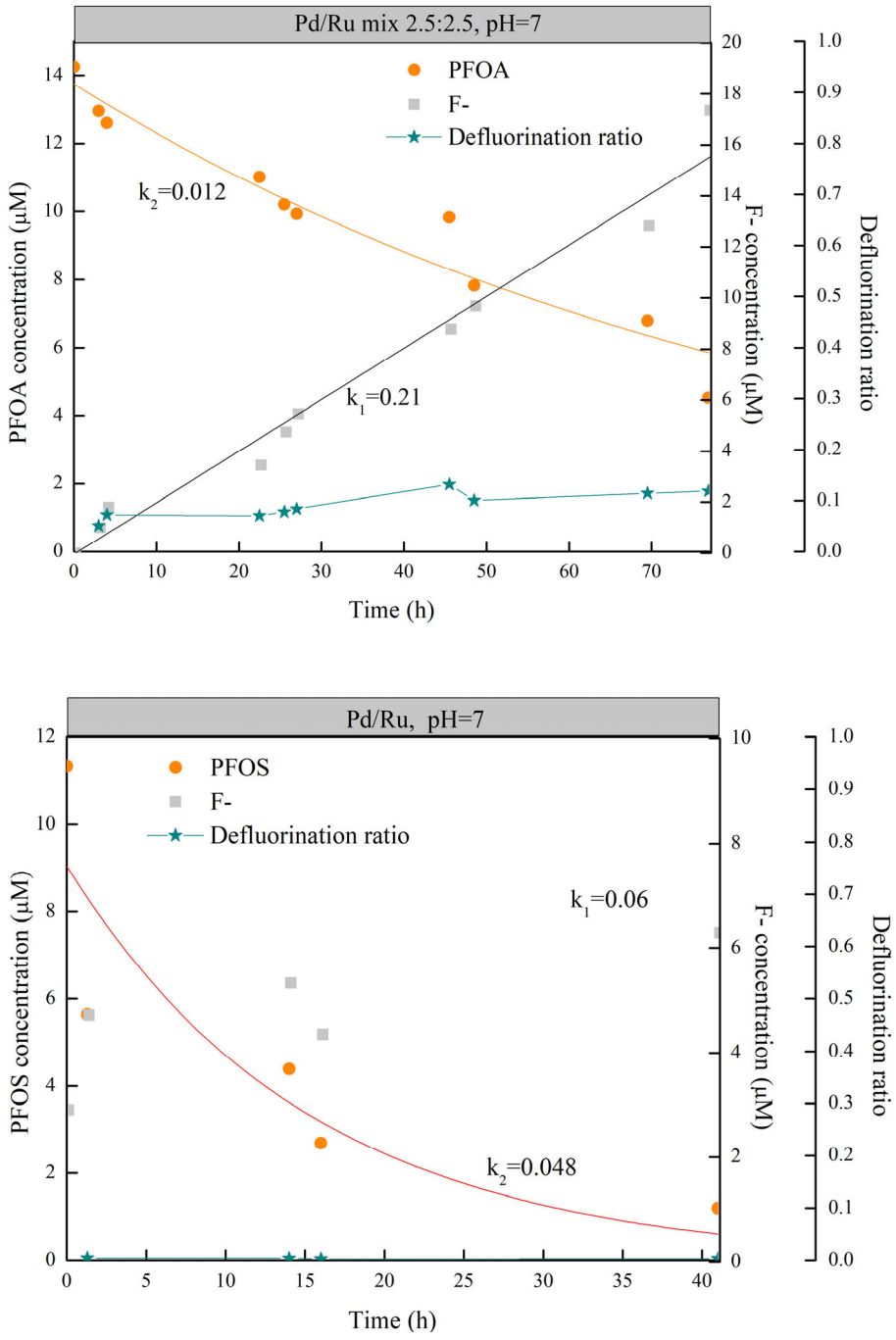

Figure 22. Concentrations of PFOA, PFOS, and F^- released and defluorination ratio in the batch test of catalytic reductive defluorination in the MCfRs with 2.5/2.5-mM Pd^0/Ru^0NPs at pH ~ 7 with H_2 of 20 psig. (A) 10-μM PFOA (B) 10-μM PFOS.

Pd/Os: The results of PFOA and F^- concentrations for 2.5/2.5-mM Pd^0/Os^0NPs are shown in Figure 23A. We detected over 33.4% PFOA depletion with a pseudo-first-order rate of 0.005 h^{-1} with reductive defluorination (7.9 μM F^- accumulation, accounting for 12.8% of the total F in the ~15 μM PFOA) with a pseudo-zero-order rate of 0.1 μM/h in the H_2-MCfR during the 72-hour test. The results of PFOS and F^- concentrations for 2.5/2.5-mM Pd/OsNPs are shown in Figure 23B. We detected over 36.2% PFOS depletion with a pseudo-first-order rate of 0.011 h^{-1} with reductive defluorination (~0 μM F^- accumulation, accounting for 0% of the total F in the ~11 μM PFOA) with a pseudo-zero-order rate of 0 μM/h in the H_2-MCfR during the 41-hour test.

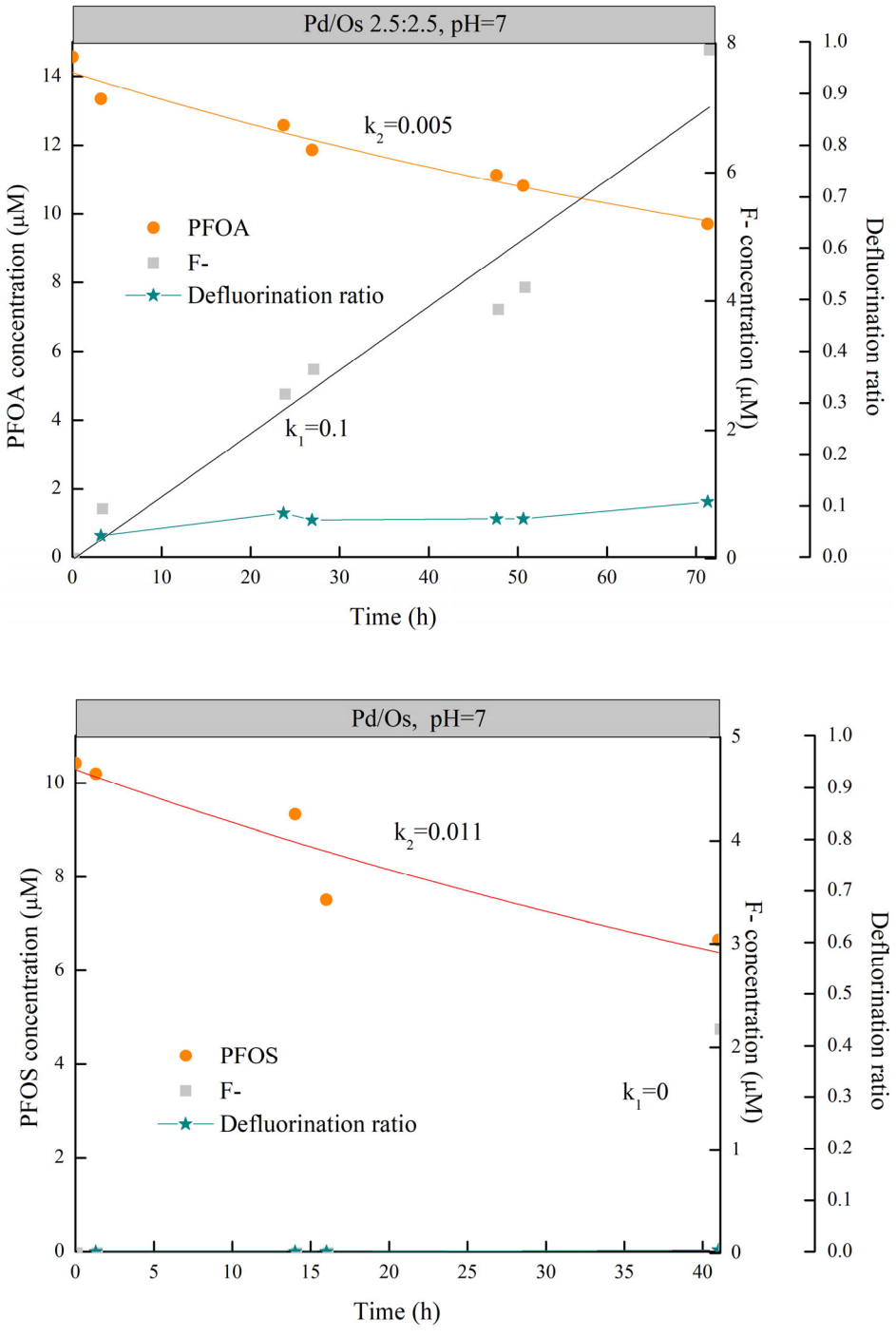

Figure 23. Concentrations of PFOA, PFOS and F^- released and defluorination ratio in the batch test of catalytic reductive defluorination in the MCfRs with 2.5/2.5-mM Pd^0/Os^0NPs at pH ~ 7 with H_2 of 20 psig. (A) 10-μM PFOA (B) 10-μM PFOS.

Pd/Ir: The results of PFOA and F^- concentrations for 2.5/2.5-mM Pd^0/Ir^0NPs are shown in Figure 24A. We detected 99% PFOA depletion with a pseudo-first-order rate of 0.215 h^{-1} with reductive defluorination (124.2 µM F^- accumulation, accounting for 65.2% of the total F in the ~7.6 µM PFOA) with a pseudo-zero-order rate of 1.12 µM/h in the H_2-MCfR during the 115-hour test. The results of PFOS and F^- concentrations for 2.5/2.5-mM Pd/IrNPs are shown in Figure 24B. We detected 87.8% PFOS depletion with a pseudo-first-order rate of 0.064 h^{-1} with reductive defluorination (29.6 µM F^- accumulation, accounting for 17.8% of the total F in the ~11 µM PFOA) with a pseudo-zero-order rate of 0.68 µM/h in the H_2-MCfR during the 41-hour test.

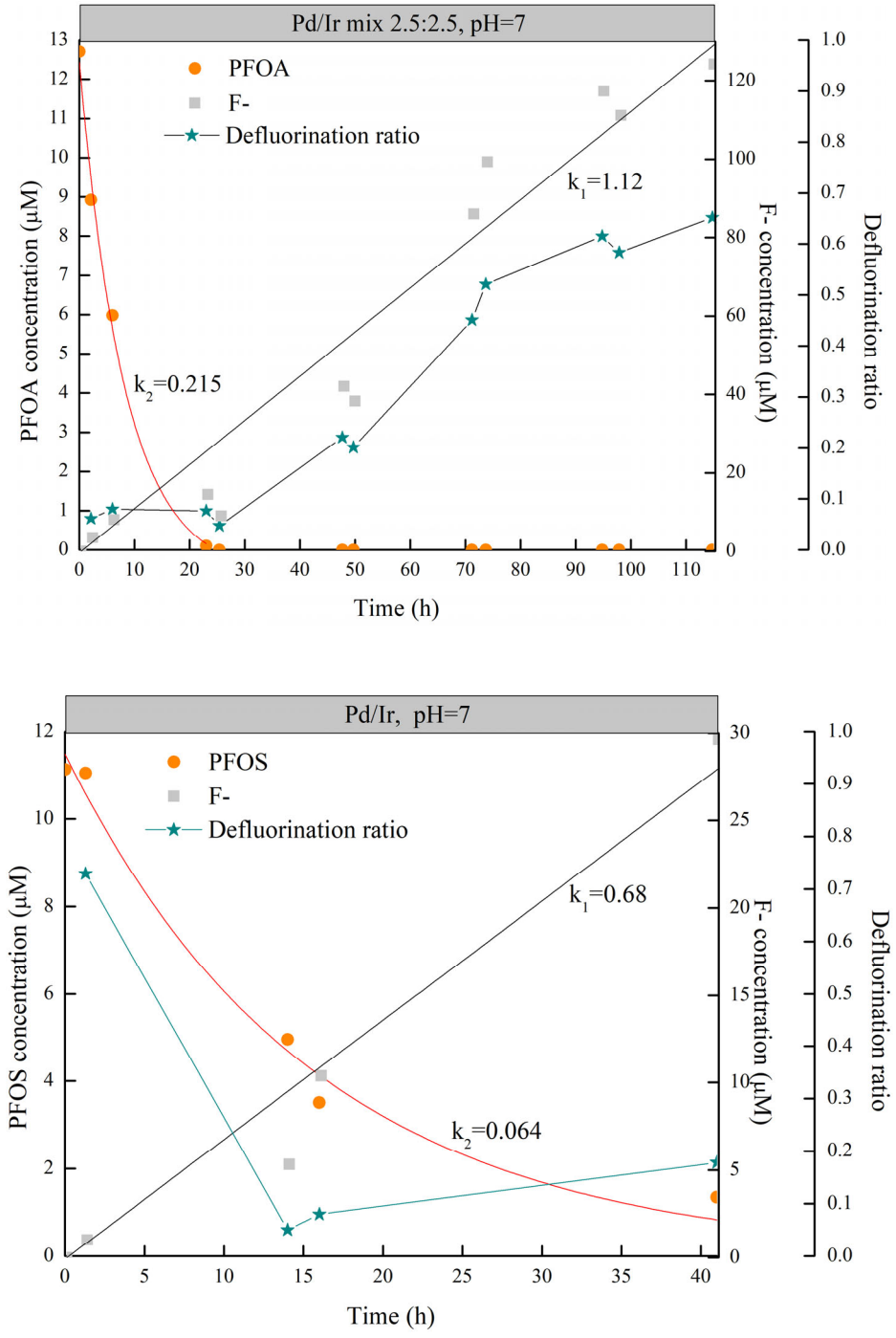

Figure 24. Concentrations of PFOA, PFOS and F^- released and defluorination ratio in the batch test of catalytic reductive defluorination in the MCfRs with 2.5/2.5-mM Pd^0/Ir^0NPs at pH ~ 7 with H_2 of 20 psig. (A) 10-μM PFOA (B) 10-μM PFOS.

Pd/Pt: The results of PFOA and F^- concentrations for 2.5/2.5-mM Pd^0/Pt^0NPs are shown in Figure 25A. We detected 94.6% PFOA depletion with a pseudo-first-order rate of 0.059 h^{-1} with reductive defluorination (39.1 μM F^- accumulation, accounting for 21.3% of the total F in the ~12.9 μM PFOA) with a pseudo-zero-order rate of 1.00 μM/h in the H_2-MCfR during the 46-hour test. The results of PFOS and F^- concentrations for 2.5/2.5-mM Pd/PtNPs are shown in Figure 25B. We detected 87.7% PFOS depletion with a pseudo-first-order rate of 0.035 h^{-1} with reductive defluorination (30.6 μM F^- accumulation, accounting for 17.9% of the total F in the ~11 μM PFOA) with a pseudo-zero-order rate of 0.80 μM/h in the H_2-MCfR during the 41-hour test.

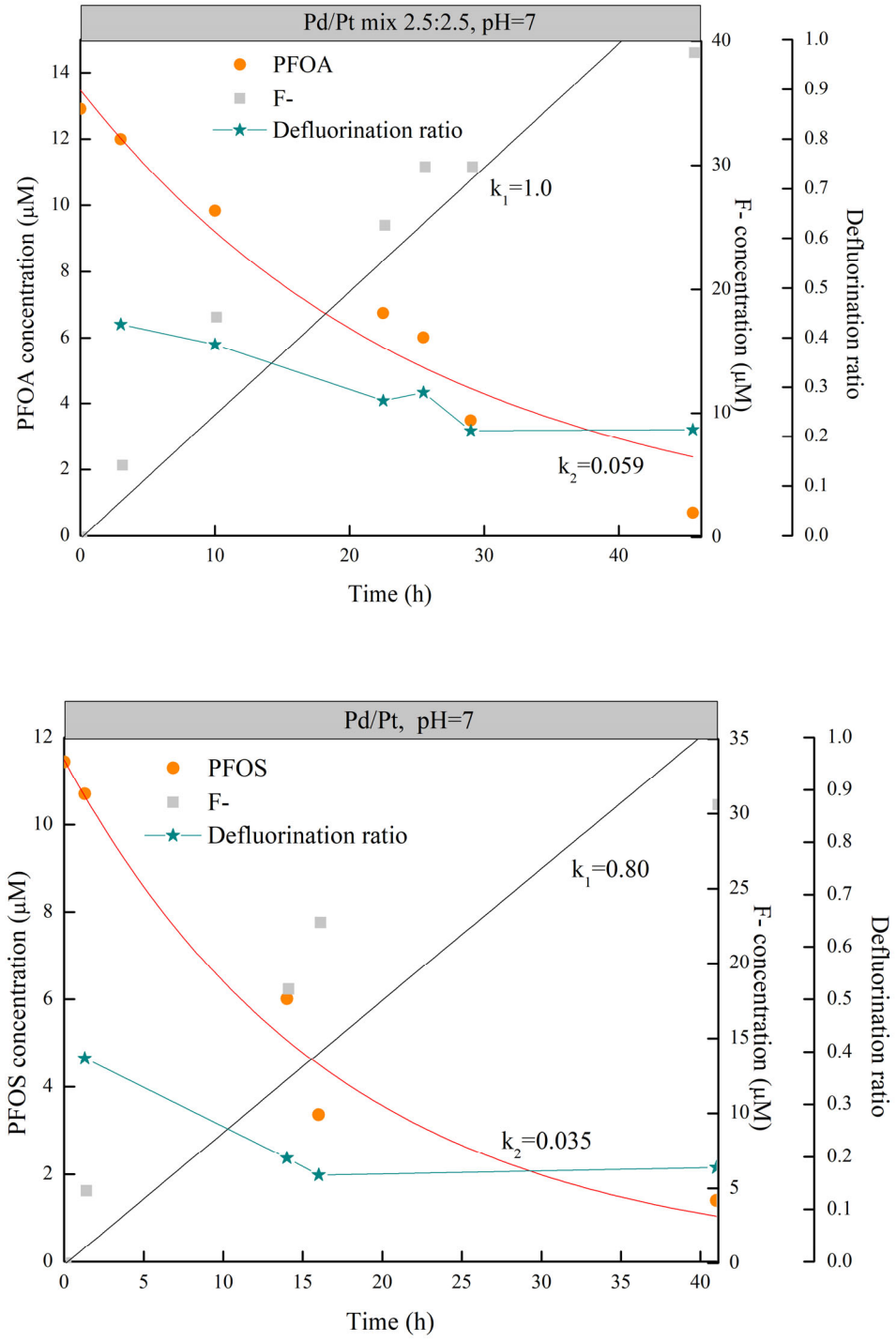

Figure 25. Concentrations of PFOA, PFOS and F^- released and defluorination ratio in the batch test of catalytic reductive defluorination in the MCfRs with 2.5/2.5-mM Pd^0/Ir^0NPs at pH ~ 7 with H_2 of 20 psig. (A) 10-μM PFOA (B) 10-μM PFOS.

Figure 26 summarizes the rate constants of PFOA removal, PFOS removal, and defluorination catalyzed by the five types of mixed bimetallic catalysts at neutral pH. Overall, bimetallic catalysts show higher defluorination ability in treating PFOA than that for PFOS. Of these bimetallic catalysts, Pd^0/Rh^0 catalyzed defluorination faster than the other four bimetallic catalysts at pH 7, but Pd^0/Pt^0 and Pd^0/Ir^0 were not far behind. Pd^0/Os^0 and Pd^0/Ru^0 showed limited ability to defluorinate PFOA and PFOS. Overall, Pd^0/Rh^0 and Pd^0/Ir^0 showed the highest capacity in removing PFOA and PFOS.

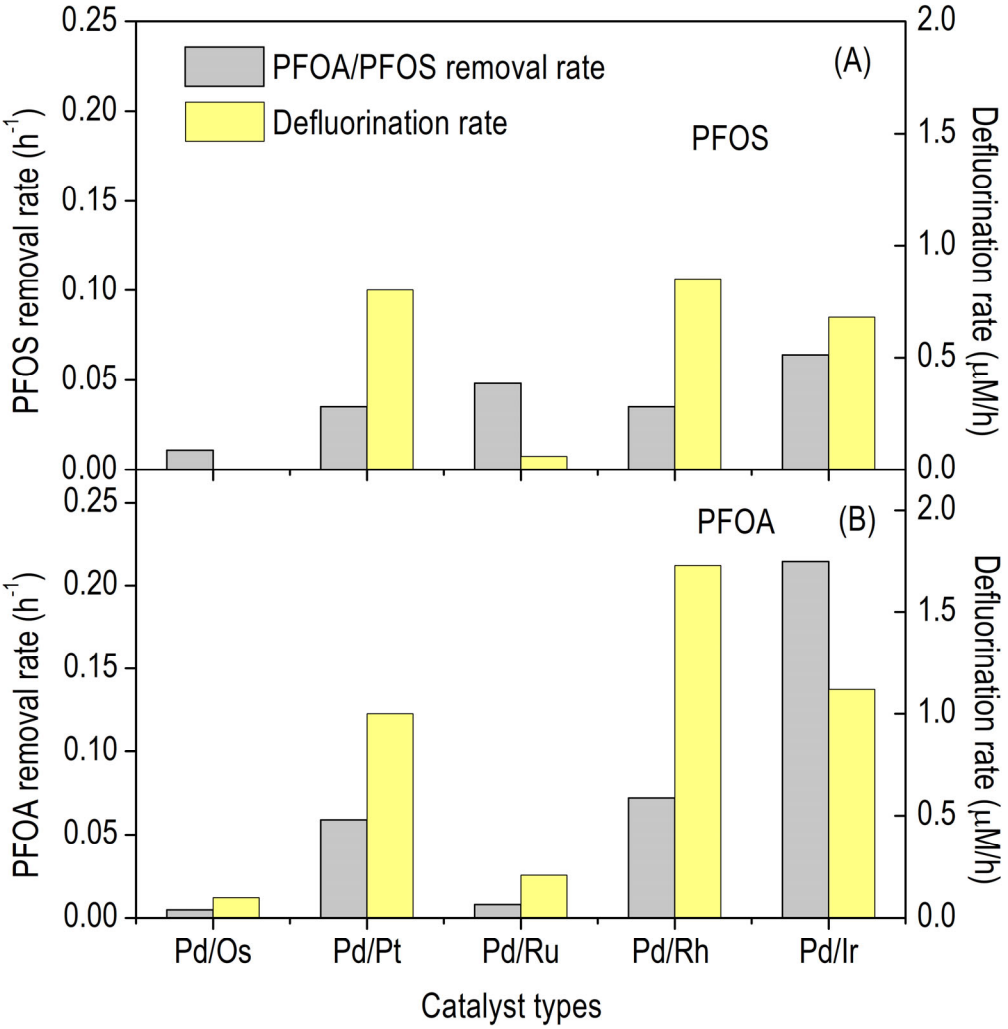

Figure 26. PFOA and PFOS removal first-order rate constant and defluorination zero-order rate constant for the five bimetallic catalysts in the batch tests of catalytic reductive defluorination of ~10-μM PFOA or PFOS with 11 mM/m^2 catalyst at 7 with H_2 supplied at 20 psig.

4.1.2.6 Decoration bimetallic catalysts for PFOA and PFOS removal and defluorination

We also tested different decoration bimetallic catalysts in the defluorination of PFOA and PFOS at pH 7: Pd^0/Rh^0, Pd^0/Ir^0, and Pd^0/In^0.

5:1 Pd/Rh (decor): The results of PFOA and F^- concentrations for 5/1-mM Pd^0/Rh^0NPs are shown in Figure 27A. We detected 28.2% PFOA depletion with a pseudo-first-order rate of 0.007 h^{-1} with reductive defluorination (19.6 µM F^- accumulation, accounting for 17.1% of the total F in the ~7.6 µM PFOA) with a pseudo-zero-order rate of 0.35 µM/h in the H_2-MCfR during the 48-hour test. The results of PFOS and F^- concentrations for 5/1-mM Pd^0/Rh^0NPs are shown in Figure 27B. We detected over 75% PFOS depletion and reductive defluorination (6 µM F^- accumulation, accounting for 4% of the total F in the ~12 µM PFOS) with a pseudo-zero-order rate of 0.14 µM/h in the H_2-MCfR during the 41-hour test.

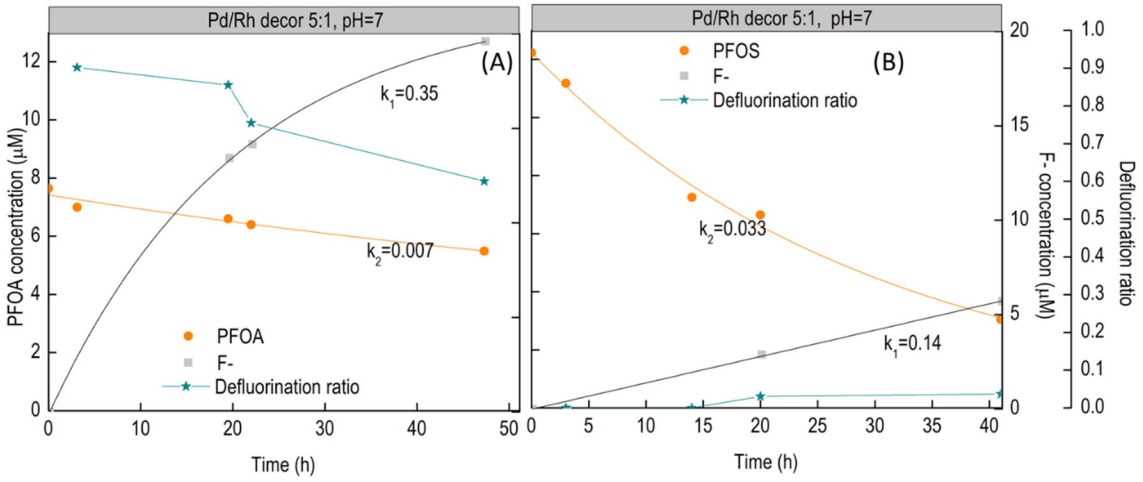

Figure 27. Batch tests of catalytic reductive defluorination of 10-µM PFOA (A) and 10-µM PFOS (B) in the MCfRs with 5/1-mM Pd^0/Rh^0 NPs, pH ~ 7, and 20 psig H_2 supply.

5:1 Pd/Ir (decor): The results of PFOA and F^- concentrations for 5/1-mM Pd^0/Ir^0NPs are shown in Figure 28A. We detected over 92.6% PFOA depletion with a pseudo-first-order rate of 0.054 h^{-1} with reductive defluorination (65.6 µM F^- accumulation, accounting for 36.8% of the total F in the ~12 µM PFOA) with a pseudo-zero-order rate of 1.30 µM/h in the H_2-MCfR during the 48-hour test. The results of PFOS and F^- concentrations for 5/1-mM Pd^0/Ir^0NPs are shown in Figure 28B. We detected 87.8% PFOS depletion with a pseudo-first-order rate of 0.057 h^{-1} with reductive defluorination (20 µM F^- accumulation,

accounting for 12% of the total F in the ~11 µM PFOS) with a pseudo-zero-order rate of 0.51 µM/h in the H_2-MCfR during the 41-hour test.

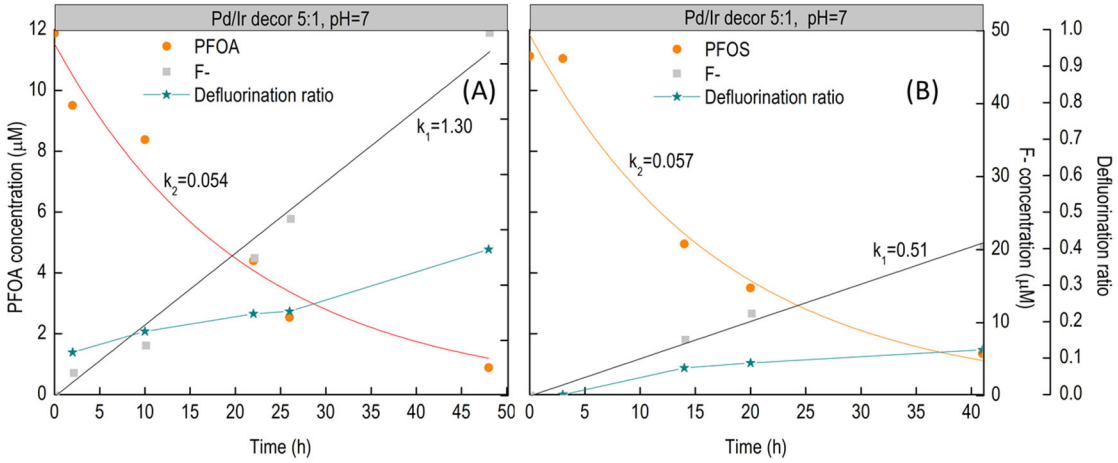

Figure 28. Batch tests of catalytic reductive defluorination of 10-µM PFOA (A) and 10-µM PFOS (B) in the MCfRs with 5/1-mM Pd/IrNPs, pH ~ 7, and 20 psig H_2 supply.

5:1 Pd/In (decor): The results of PFOA and F^- concentrations for 5/1-mM Pd^0/In^0NPs are shown in Figure 29A. We detected over 99% PFOA depletion with a pseudo-first-order rate of 0.143 h^{-1} with reductive defluorination (15 µM F^- accumulation, accounting for 12.7% of the total F in the ~8.0 µM PFOA) with a pseudo-zero-order rate of 0.35 µM/h in the H_2-MCfR during the 45-hour test. The results of PFOS and F^- concentrations for 5/1-mM Pd^0/In^0NPs are shown in Figure 29B. We detected 87.8% PFOS depletion with a pseudo-first-order rate of 0.054 h^{-1} with reductive defluorination (50 µM F^- accumulation, accounting for 29% of the total F in the ~11 µM PFOS) with a pseudo-zero-order rate of 1.15 µM/h in the H_2-MCfR during the 41-hour test.

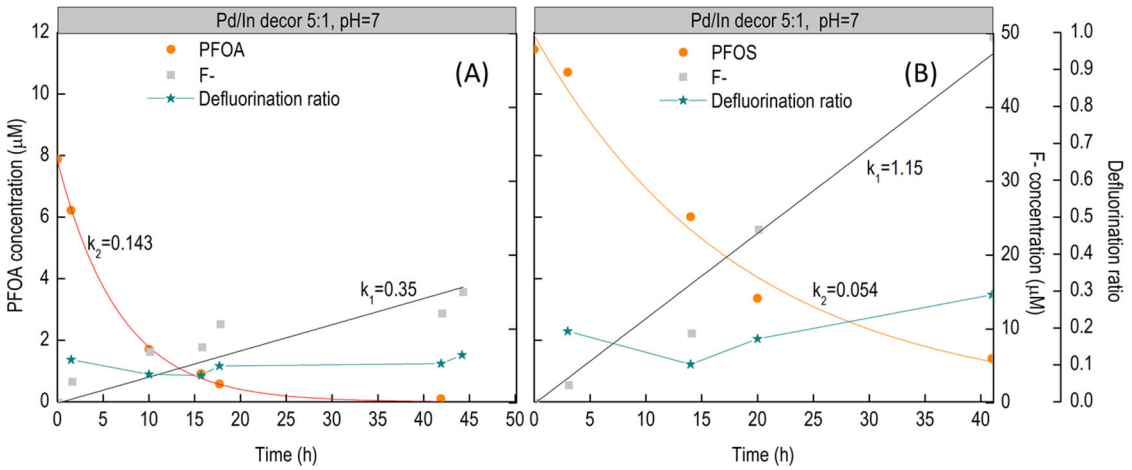

Figure 29. Batch tests of catalytic reductive defluorination of 10-μM PFOA (A) and 10-μM PFOS (B) in the MCfRs with 5/1-mM Pd^0/In^0NPs, pH ~ 7, and 20 psig H_2 supply.

4.1.2.7 Summary for Bimetallic Catalysts

Figure 30 summarizes the all the rate constants of PFOA and PFOS removal and defluorination catalyzed by different types of bimetallic catalysts and Pd alone at neutral pH. Overall, bimetallic catalysts had better defluorination ability for treating PFOA over PFOS, and they also had faster defluorination kinetics than Pd alone. Of these bimetallic catalysts, Pd^0/Rh^0 in the mixed method catalyzed defluorination faster than the other four bimetallic catalysts at pH 7. Pd^0/Ir^0 showed the highest capacity in removing PFOA and PFOS (similar to Pd alone), presumably due its greater adsorption capacity.

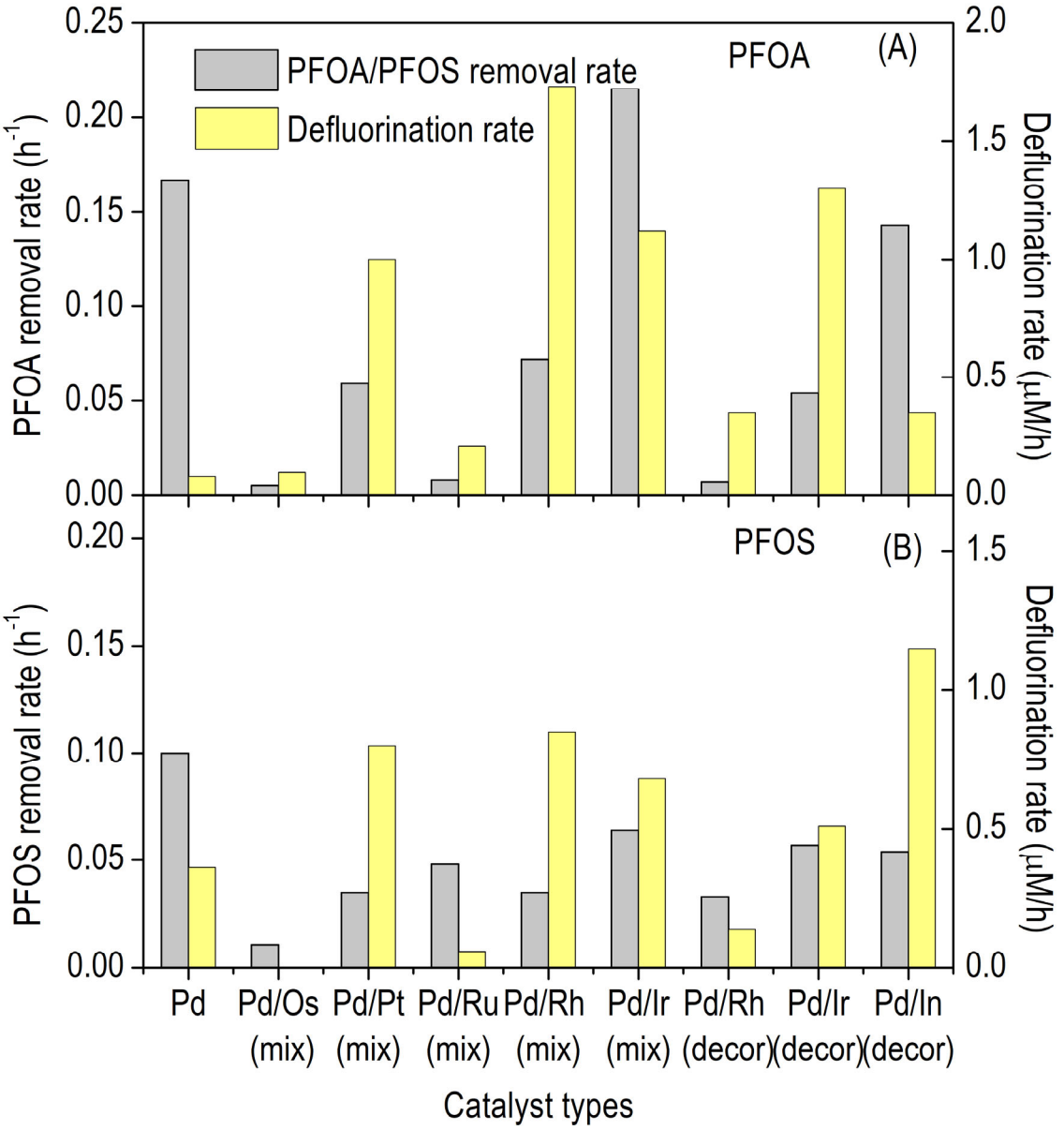

Figure 30. PFOA and PFOS removal first-order rate constant and defluorination zero-order rate constant for the bimetallic catalysts in the batch tests of catalytic reductive defluorination of ~10-μM PFOA or PFOS with 11 mM/m^2 catalyst at 7 with H_2 supplied at 20 psig.

4.1.2.8 Co-removal of PFOA and PFOS in bimetallic catalysts Pd/Rh

The results for co-removal of PFOA and PFOS and F^- concentrations for 2.5/2.5-mM Pd^0/Rh^0NPs are shown in Figure 31. We detected over 69% PFOA depletion, over 99% PFOS depletion and reductive defluorination (55 μM F^- accumulation, accounting for 39% of the total F

in the ~5 µM PFOA and PFOS) with a pseudo-zero-order rate of 1.07 µM/h in the H_2-MCfR during the 51-hour test. In comparison to PFOS, Pd has a better efficiency in defluorination and removal of PFOA. But, when PFOA and PFOS were removed together in the MCfR, the removal of PFOS improved, while the removal of PFOA deteriorated.

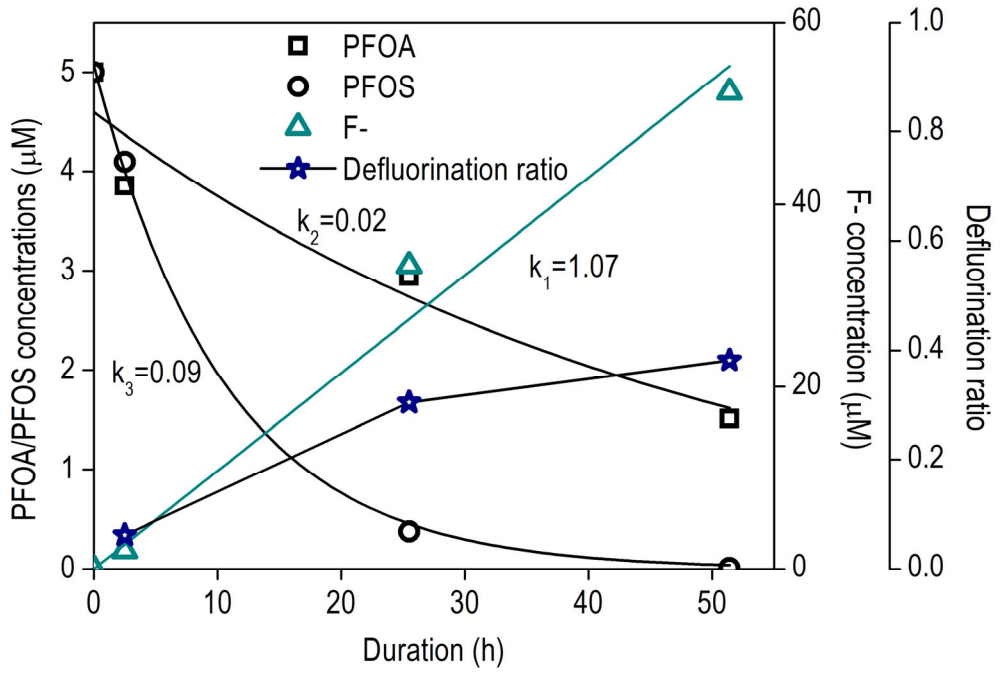

Figure 31. Concentrations of PFOA, PFOS, and F^- released and defluorination ratio in the batch test of catalytic reductive defluorination in the MCfRs with 2.5/2.5-mM Pd^0/Rh^0NPs at pH ~ 7 with H_2 of 20 psig.

4.1.3. Adsorption and Defluorination Mechanisms

Figure 32 shows the experimental results for the batch tests of PFOA depletion in the MCfRs. The default conditions included 0.9 g/m^2 Pd^0, 0.1 mM initial PFOA, pH 4, and constant 20 psig (2.36 atm absolute) gas pressure. In the absence of Pd^0 (i.e., bare membranes with H_2 supply; Figure 31A), the PFOA concentration did not change over 35 hours (Fig. 31A), indicating that PFOA did not react with the polypropylene membranes or other materials in the MCfR. With 0.9 g/m^2 Pd^0NPs loaded on the membrane surface and the same H_2 supply, 58% of the PFOA was depleted within 35 hours (Fig. 32B), along with gradual release of free fluoride ions (F^-) up to 0.49 mM (accounting for 55% of all F in the depleted PFOA).

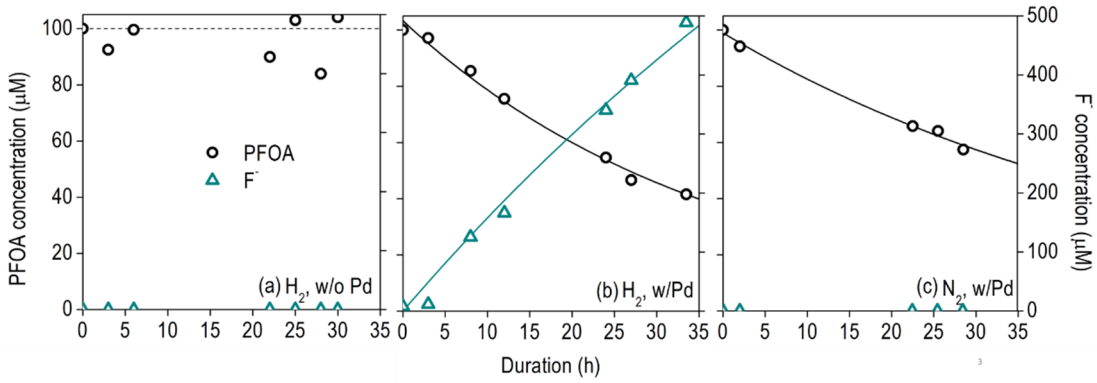

Figure 32. PFOA and F^- concentration changes over time of initial 0.1 mM PFOA and released F^- with H_2 delivery (a) without and (b) with the Pd^0 catalyst (0.9 g/m^2 areal loading), and (c) with N_2 delivery with the Pd^0 catalyst. Reaction conditions: pH 4 and MCfR operating with recirculating flow rate of 150 mL/min.

HPLC-QTOF-MS analyses in Figure 33 further reveal that, while PFOA ($C_8HO_2F_{15}$) was the only fluorinated carboxylic acid ($C_aH_bO_2F_d$) detected initially, at least four partially fluorinated octanoic acid (OA) species ($C_8H_2F_{14}O_2$, $C_8H_3F_{13}O_2$, $C_8H_7F_9O_2$, and $C_8H_8F_8O_2$) and non-fluorinated OA ($C_8H_{16}O_2$) were identified in the bulk liquid of the H_2-MCfR after 35 hours. These results verify our hypothesis and document for the first time that Pd^0 is capable of catalyzing reductive defluorination of PFOA into partial and non-fluorinated OAs. The HPLC-QTOF-MS results suggest the following reactions occurred:

$$C_8HF_{15}O_2 + 2H_{ads}^* \rightarrow C_8H_2F_{14}O_2 + F^- + H^+ \quad (2)$$
$$C_8HF_{15}O_2 + 4H_{ads}^* \rightarrow C_8H_3F_{13}O_2 + 2F^- + 2H^+ \quad (3)$$
$$C_8HF_{15}O_2 + 12H_{ads}^* \rightarrow C_8H_7F_9O_2 + 6F^- + 6H^+ \quad (4)$$
$$C_8HF_{15}O_2 + 14H_{ads}^* \rightarrow C_8H_8F_8O_2 + 7F^- + 7H^+ \quad (5)$$
$$C_8HF_{15}O_2 + 30H_{ads}^* \rightarrow C_8H_{16}O_2 + 15F^- + 15H^+ \quad (6)$$

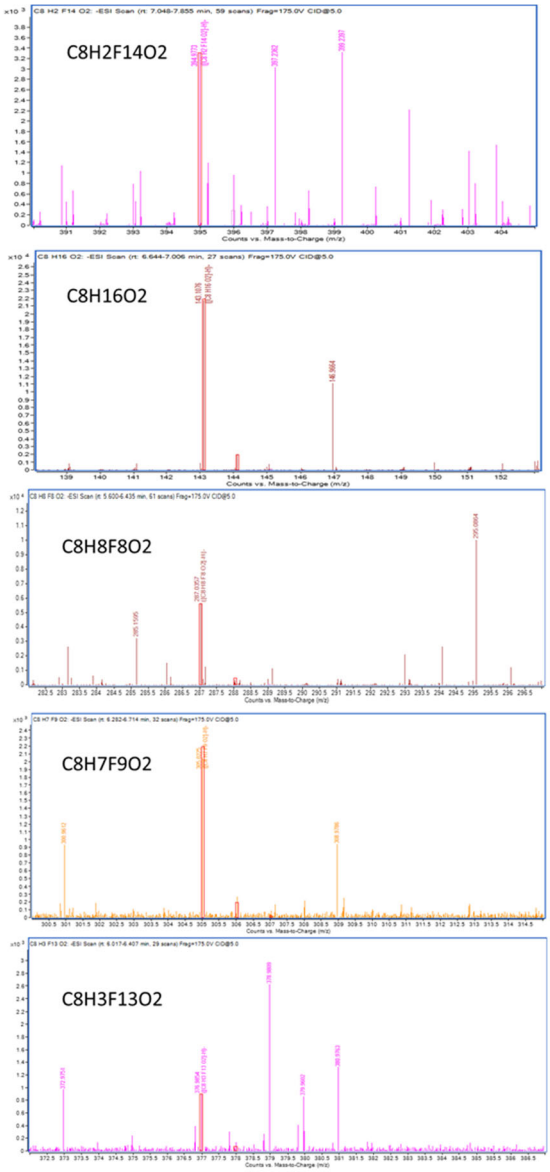

Figure 33. HPLC-QTOF-MS results for Pd^0-catalyzed reduction of PFOA.

When H_2 was replaced by N_2 at the same pressure of 20 psig, we detected 41% PFOA removal, but no F^- release within 30 hours (Figure 32C). No partially defluorinated carboxylic acids were detected by HPLC-QTOF-MS. These results reveal that, in the absence of H_2 as the electron donor, no defluorination or other chemical reactions occurred, but the H_{ads}*-free Pd^0 still was able to adsorb PFOA.

To explore further this observation of PFOA adsorption on H_{ads}*-free Pd, we carried out an extended two-week batch test; the results are in Figure 34. Over 99.9% of the initial 0.05 mM PFOA was adsorbed by the Pd^0 within 67 hours using N_2. After 6 days, we replaced N_2 with H_2, but did not observe F^- release for the following 6 days. This suggests that the adsorbed PFOA on the H_{ads}*-free Pd^0 surface was not able to be defluorinated in the presence of H_2. We then re-spiked 0.01 mM PFOA and observed >99% PFOA removal along with 46% defluorination within

50 hours. This implies that Pd^0 still had active sites available for H_{ads}*, and the H_{ads}* was able to defluorinate newly introduced PFOA from the bulk liquid, but not PFOA already adsorbed prior to the presence of H_{ads}*.

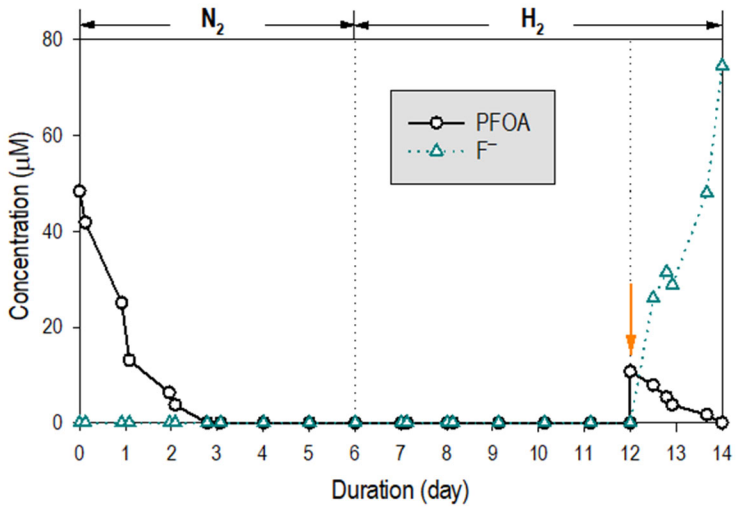

Figure 34. PFOA and F^- concentrations over time in the extended batch test for 0.9 g/m^2 Pd^0 at pH 4 in the MCfR supplied with 20 psig N_2 for 6 days followed by 20 psig H_2 for 8 days. The orange arrow refers to PFOA re-spiking into the liquid in the MCfR on day 12.

Overall, the batch results identify two distinct adsorption patterns involved in PFOA removal by Pd^0: H_{ads}*-independent non-reactive adsorption and H_{ads}*-dependent reactive (defluorinating) adsorption. We further propose that the two adsorption patterns are associated not only with H_{ads}*, but also with different adsorptive positions and orientations.

The hypothesis of different adsorption orientations is based on DFT modeling, whose results are summarized in Figure 35. Because reported pK_a values for PFOA are ≤ 2.8, PFOA predominantly exists in the deprotonated form as the $C_7F_{15}COO^-$ anion. DFT calculations reveal that, when H_2 is absent (Fig. 35A&C), $C_7F_{15}COO^-$ tends to bind to active Pd^0 sites in a perpendicular orientation, because of its more favorable adsorption energy ($\Delta E^{ads}_{Pd/PFOA}$= -1.28 eV) when a metal-oxygen bond can form compared to a parallel orientation ($\Delta E^{ads}_{Pd/PFOA}$= -0.79 eV), characteristic of physisorption. The non-reactive adsorption occurs through the carboxylate head group of PFOA binding via chemisorption by the formation of a Pd-O complex. The tail group is oriented off the surface, which keeps C-F bonds away from the Pd surface and thus minimizes chances of contact-based hydrodefluorination even when H_{ads}* is introduced.

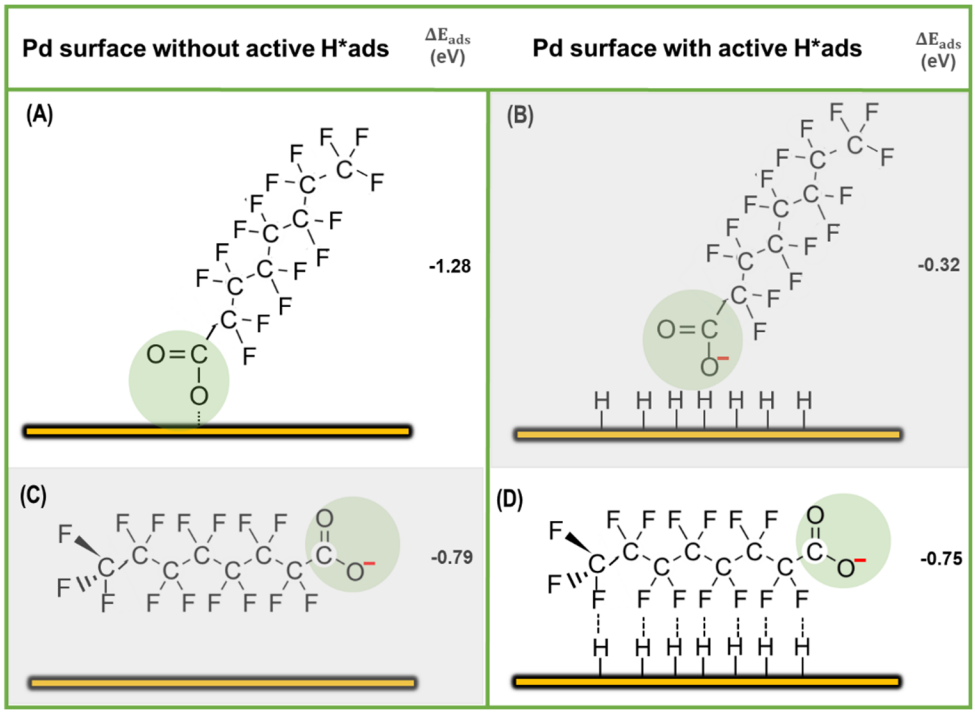

Figure 35. Two distinct adsorption mechanisms of PFOA. Perpendicular (non-defluorinative) and parallel (defluorinative) adsorption modes of PFOA to the Pd (111) surface at different conditions along with respective adsorption energies (in eV). Shaded adsorption modes represent the less favorable mode for each condition. The gold lines represent Pd0 surfaces. The H connected on the Pd^0 represents activated H*. The green circles identify PFOA's carboxyl heads.

In contrast, when H_2 is present (Fig. 35B&D), the high amounts of H_{ads}^* on the surface block Pd-O bond formation, which favors parallel binding orientation ($\Delta E_{Pd/PFOA}^{ads}$= -0.75 eV, compared to -0.32 eV for the perpendicular orientation) through van der Waals attraction. Parallel adsorption allows maximum contact of C-F bonds and H_{ads}* on Pd^0 surface, which promotes catalytic reduction of PFOA via surface H addition or F/H substitution. After the reaction, defluorinated products and fluoride desorb from Pd surface,[59,60] which frees Pd^0 active sites for continued defluorinative adsorption of PFOA. This DFT-based atomistic-scale insight into PFOA adsorption on the Pd^0 surface agrees with the adsorption trends observed experimentally.

4.1.4. Proposed Pathway of PFOA Hydrodefluorination

In the batch experiment with 1.2 g Pd^0/m^2 on the membrane fibers, presented in Figure 36A, over 99% of the initial 10 µM PFOA was depleted within 58 h, which was accompanied by steady F^- release up to 0.12 mM (77.3% of the F originally present on the depleted PFOA) at the end of the experiment. The HPLC-QTOF-MS results in Fig. 36B reveal the presence of six partially hydrodefluorinated fluorooctanoic acids (FOAs) -- $C_8H_2F_{14}O_2$, $C_8H_3F_{13}O_2$, $C_8H_5F_{11}O_2$, $C_8H_8F_8O_2$, $C_8H_{10}F_6O_2$, and $C_8H_{12}F_4O_2$ – along with completely hydrodefluorinated OA ($C_8H_{16}O_2$) in the bulk liquid during the batch experiment. These products again confirm that Pd^0-catalytic PFOA conversion was exclusively via reductive hydrodefluorination:

$$C_7F_{15}COOH + nH_2 \rightarrow C_7H_nF_{15-n}COOH + nH^+ + nF^- \ (1 \leq n \leq 15) \quad (7)$$

The defluorination ratio increased from 20% in the first 6 h to 77% at 58 h, which supports that PFOA was sequentially hydrodefluorinated after being removed from the water. Among the defluorination products, lightly defluorinated $C_8H_2F_{14}O_2$ and $C_8H_5F_{11}O_2$ accumulated during the first 6-23 hours, but then were depleted. More completely defluorinated products, such as $C_8H_{10}F_6O_2$ and $C_8H_{16}O_2$, appeared once $C_8H_2F_{14}O_2$ and $C_8H_5F_{11}O_2$ began to decline (Fig. 36B). These trends further support stepwise hydrodefluorination. Because the lightly defluorinated species appeared and then declined in solution, they desorbed and then resorbed onto the Pd^0NP surfaces for further defluorination:

$$C_7H_nF_{15-n}COOH + mH_2 \rightarrow C_7H_{n+m}F_{15-n-m}COOH + mH^+ + mF^- \ (1 \leq m \leq n) \quad (8)$$

This stepwise phenomenon is similar to Pd^0-catalyzed hydrodehalogenation of chlorophenol to phenol, followed by hydrogenation to cyclohexanone.[61]

Fig. 36C shows OA and three partially defluorinated OAs in the digested solution of the Pd-film after the 58-hour batch test. All four species also were found in the bulk liquid during the batch test (Fig. 36B). This indicates that defluorination products were retained on the Pd^0 surface, which infers that desorption was slower than defluorination. Slow desorption of the FOAs contrasts to Pd^0-catalyzed dehalogenation trichloroacetic acid, in which desorption was not a rate-limiting step.[53,62] This difference probably was caused by higher adsorption affinity of longer-chain fatty acids from PFOA.[63]

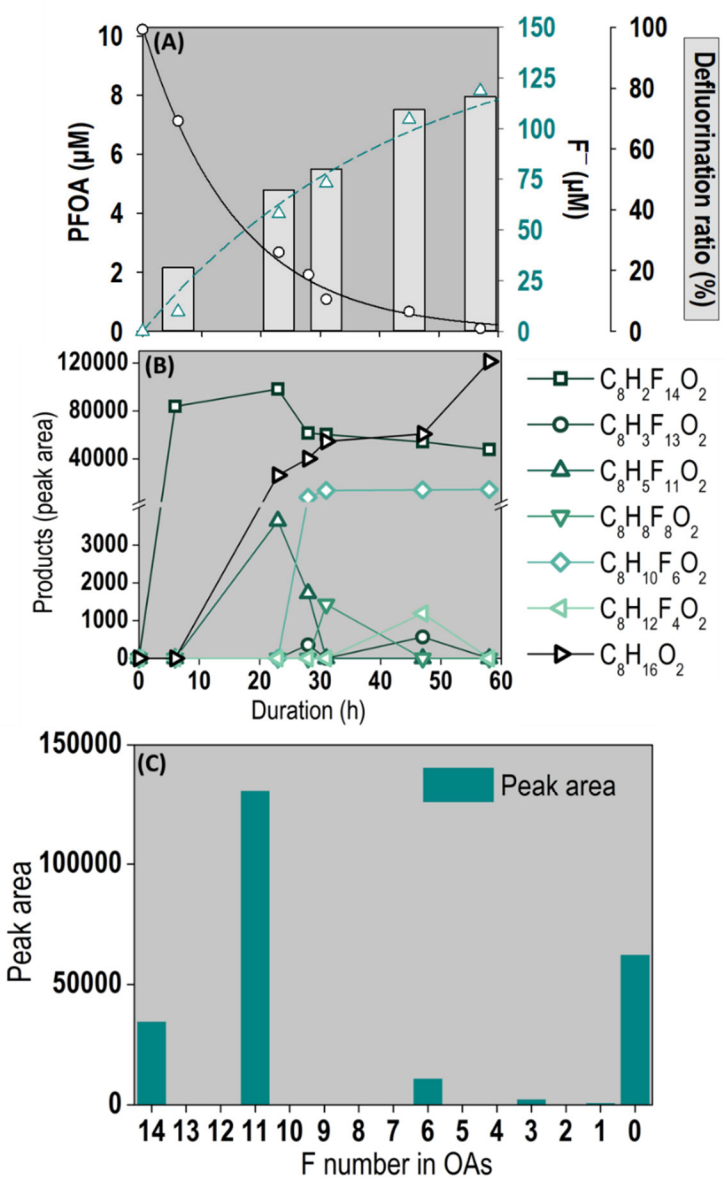

Figure 36. (A) Concentrations of PFOA and F^- released in the batch test of catalytic reductive defluorination of ~10-μM PFOA in the MCfR with 5-mM Pd^0NPs at pH ~ 4 with H_2 of 20 psig. (B) Products detected in the bulk liquid. (C) Compounds adsorbed on the Pd surface.

The persistence of surface-bound FOA complexes may affect the catalyst's activity. Figure 37 presents results from a set of batch experiments with higher initial concentrations of PFOA in different MCfRs. Initial first-order rates of PFOA removal and defluorination were considerably lower as the PFOA concentration increased from 10 to 1000 μM. In particular, PFOA removal halted after 40 h, and defluorination was minimal when the initial PFOA concentration was 1000 μM. FTIR spectra of the Pd-films in the three MCfRs at the end of the experiments reveal the symmetric (1450 cm^{-1}) and asymmetric (1650 cm^{-1}) stretching of the COO^- group for 100 μM

PFOA, and the signals were higher for 1000 μM PFOA.[64–66] This supports that retained Pd-FOA complexes retarded PFOA hydrodefluorination by blocking active sites on the Pd^0 surface.

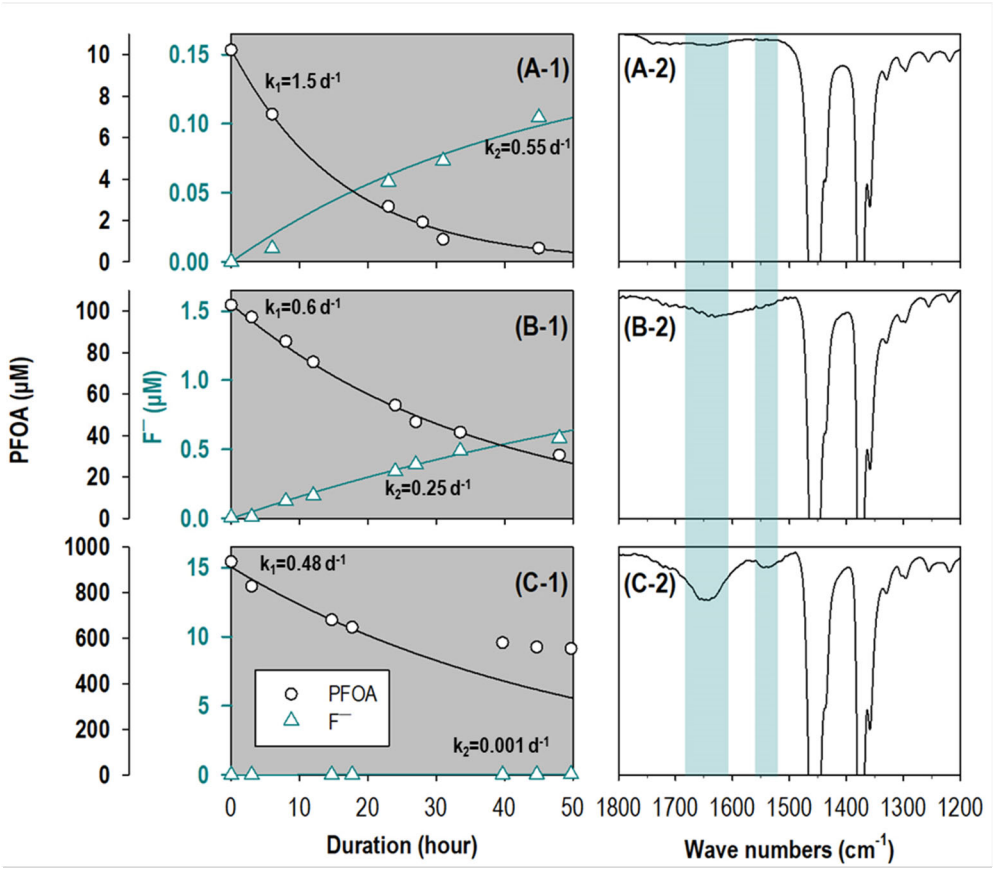

Figure 37. (Left panels) Concentrations of PFOA and F^- released in the batch test with influent concentration of 10, 100, or 1000 μM PFOA catalyzed by 1.2 g Pd^0/m^2 at pH 4 in the MCfR. (Right panels) Corresponding FTIR spectrum of the Pd surface after the reactions. First-order rate coefficients for PFOA loss (k_1) and F^- release (k_2) are in units of d^{-1}.

Based on the products detected from the liquid and the Pd^0 surface, we propose in Figure 38 a pathway of PFOA hydrodefluorination catalyzed by Pd^0NPs in the presence of H_2. After H_2 diffused through the nonporous membrane and reached the Pd^0 surface, it dissociated into the single activated H atoms adsorbed on the Pd^0 surfaces (i.e., H^*_{ads}) on the bulk-liquid side.[62] PFOA in the bulk liquid adsorbed on Pd^0 surfaces, forming Pd-PFOA complexes. Then, F was reductively substituted by H^*_{ads},[67] transforming $C_7F_{15}COOH^*$ (i.e., Pd-PFOA) to $C_7H_nF_{15-n}COOH^*$ (i.e., Pd-$C_7H_nF_{15-n}COOH$):

$$C_7F_{15}COOH^* + nH^*_{ads} \rightarrow C_7H_nF_{15-n}COOH^* + nF^- \ (1 \leq n \leq 15) \qquad (9)$$

Partially defluorinated complex could be further reduced, hydrodefluorinated and, desorbed into the bulk liquid as the free $C_7H_nF_{15-n}COOH$ form:

$$C_7H_nF_{15-n}COOH^* + nH^*_{ads} \rightarrow C_7H_nF_{15-n}COOH + nH^+ \ (1 \leq n \leq 15) \qquad (10)$$

We postulate that desorption became the rate-limiting step of the entire defluorination process, and it also led to the accumulation of partially defluorinated products on the Pd^0NP active sites.

Some of the released products were resorbed by Pd^0NP, formed $C_7H_nF_{15-n}COOH^*$, and were hydrodefluorinated into $C_7H_{n+m}F_{15-n-m}COOH^*$:

$$C_7H_nF_{15-n}COOH^* + mH^*_{ads} \rightarrow C_7H_{n+m}F_{15-n-m}COOH^* + mF^- \ (1 \leq m \leq n) \qquad (11)$$

Further reduction, hydrodefluorination and desorption steps were possible:

$$C_7H_{n+m}F_{15-n-m}COOH^* + mH^*_{ads} \rightarrow C_7H_{n+m}F_{15-n-m}COOH + mH^+ \ (1 \leq m \leq n) \qquad (12)$$

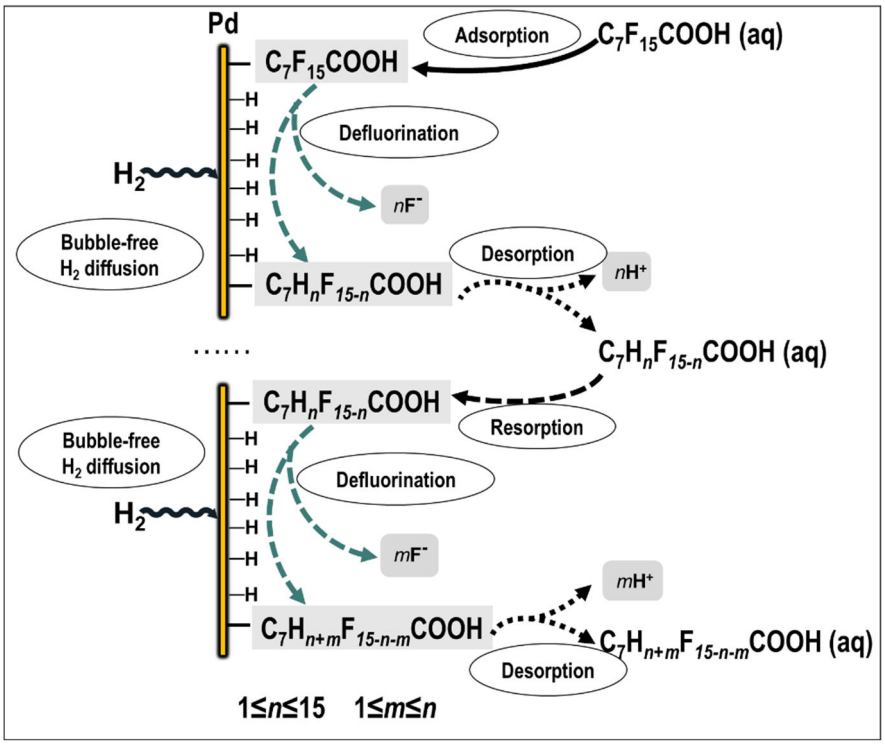

Figure 38. Proposed pathway of PFOA hydrodefluorination by Pd^0NPs in the MCfR.

4.1.5. Continuous tests of PFOA removal and defluorination in the H_2-MCfRs

4.1.5.1 Calculation of the H_2-supply capacity

The driving force behind gas transfer in an MCfR system is the concentration gradient across the membrane wall. The H_2 flux through an MCfR membrane can be described by:[68]

$$J_{H_2,max} = 0.8 D_m \frac{K_m}{Z_m} K_l P_0 \left(\frac{d_m - z_m}{d_m}\right) \quad (13)$$

where D_m is the H_2-diffusion coefficient in the membrane (1.4×10^{-7} m^2/d for polypropylene fibers), K_m is H_2 solubility coefficient in membrane (1.29 m^3 H_2 @ standard temperature and pressure/m^3 membrane bar), K_L is coefficient that converts H_2 from volume to mass (1 g/0.0112 m^3@ standard temperature and pressure), P_0 is H_2 pressure in the hollow-fiber lumen (bar), d_m is hollow-fiber outer diameter (200 μm for polypropylene fibers), and z_m is membrane thickness (55 μm for polypropylene fibers). $J_{H2,\,max}$ also equals the e^- eq flux, since each mmol of H_2 contains 2 e^- meq in 2 mg of H_2.

We also calculated the maximum electron fluxes towards PFOA by using Eq. (14).[67]

$$J_{pfoa,max} = 15 C_{PFOA}^{in} \frac{Q}{A} \quad (14)$$

where J is the flux of electron for reducing PFOA to OA (e^-meq/m^2/day); C is the concentration of influent PFOA (mM); Q is the flow rate (L/day); A is the total fiber surface area (18.48×10^{-3} m^2); and 15 is the electron equivalent (e^--eq/mole) for full PFOA reduction to OA.

Based on Eqs. (13) and (14), we calculated that the maximum H_2 flux was 230 e^- meq/m^2-day from the polypropylene fibers at 20 psig, and the surface loading of 0.01 mM PFOA (J_{max}) had a maximum electron-equivalent demand of 1.2 e^-meq/m^2/day. This confirms that the H_2 supply capacity we used was well in excess of the H_2 demand for full reductive defluorination of PFOA. This reinforces the possibility of increasing the Pd^0NP surface loading, since the H_2 supply is not limiting.

4.1.5.2 Continuous tests of PFOA removal and defluorination in the H_2-MCfRs

4.1.5.2.1 Continuous performance at HRT = 6 h

Figure 39a shows the PFOA and F^- concentrations in the influent and effluent of the MCfR at pH 4 during the initial 30 days. The concentration of effluent PFOA decreased sharply to 5.2 μM (or 57% removal) within 6 hours because of rapid adsorption, with the highest removal flux reaching 0.79 e^-meq/m^2/day. The PFOA concentration then increased gradually and even exceeded the influent concentration by 33.8%, probably due to desorption. F^- rose to 25 μM (14% of the total F in the influent PFOA, or 55% of the F in the depleted PFOA) within 50 hours, and it then decreased to 0 μM within 300 hours. The trends indicate that the Pd^0NPs were gradually deactivated after being exposed to PFOA or its defluorination products for the conditions of this

experiment, which featured a high PFOA concentration compared to what is found in most environmental samples.

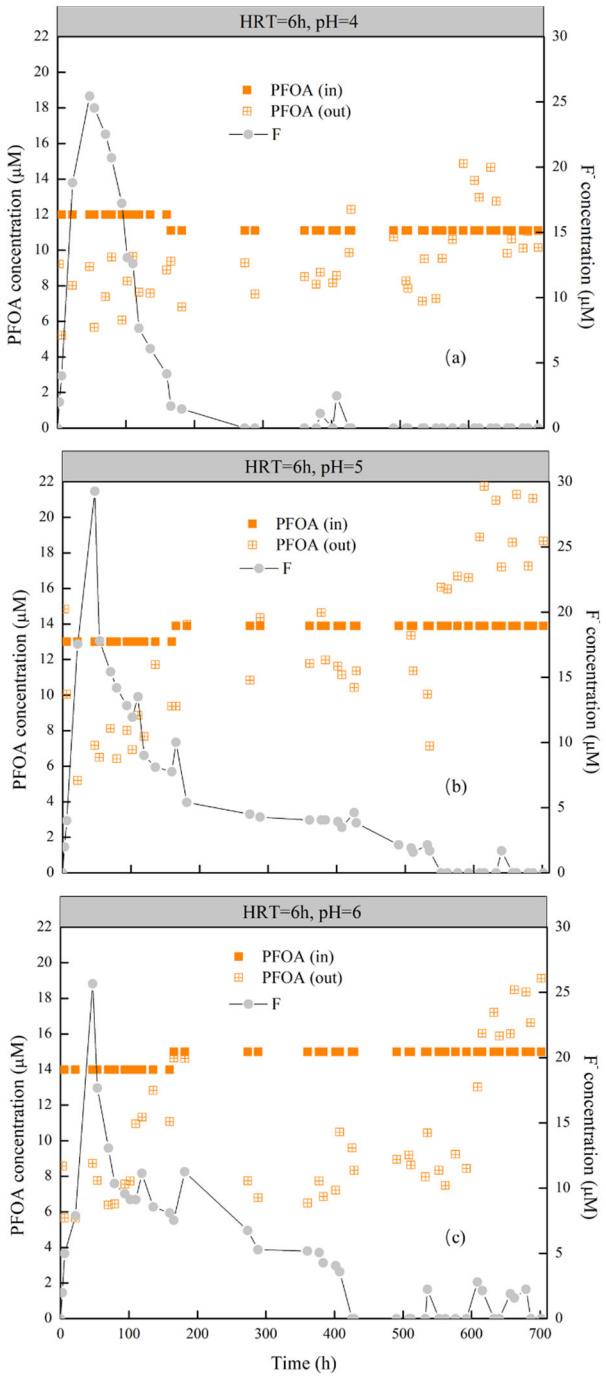

Figure 39. Concentrations of PFOA and F^- released in the continuous operation of catalytic reductive defluorination of ~10-μM PFOA in the MCfR with 5-mM Pd^0NPs at pH ~ 4 (a), pH ~ 5 (b), pH ~ 6 (c) with H_2 supplied at 20 psig.

As shown in Figure 39b for the MCfR with the pH adjusted to 5, the concentration of effluent PFOA decreased sharply from 13 μM to 2 μM (or 84.6% removal) within 6 h because of rapid adsorption, with the highest removal flux reaching 1.26 e^-meq/m^2/day, and then it increased gradually to higher levels, with the highest effluent concentration exceeding 56% of the influent PFOA concentration, probably due to desorption. Accordingly, the released F^- concentration rose to maximally 0.029 mM F^- accumulation at about 50 h, accounting for 15% of the total F in ~13 μM PFOA and 33% of the F in ~5.83 μM depleted PFOA. Then, F^- decreased gradually to 0 mM at 550 hours because of the deactivation of PdNPs caused by continuous exposure to PFOA or its products.

Figure 39c displays the PFOA and F^- concentrations in the influent and effluent of the MCfR at pH 6. Similar to the lower pH conditions, the concentration of effluent PFOA decreased sharply to 5.2 μM (or 59% removal) within 6 hours, with the highest removal flux reaching 0.97 e^-meq/m^2/day, and then the PFOA concentration increased gradually to exceed the influent PFOA concentration by 27%. F^- rose to 26 μM (12% of the total F in the influent PFOA, or 32% of the F in the depleted PFOA) within 50 hours, and then it decreased gradually and fluctuated between 0 mM and 0.002 mM F^- out to 700 h. The trends again indicate that the Pd^0NPs were gradually deactivated from being exposed to PFOA or its defluorination products for the experimental conditions.

After these three PdNPs had been deactivated, we used DI water to wash the three membranes for two days. We monitored the PFOA concentration in these days, as shown in Figure 40. The PdNPs at pH = 4 still retained all the adsorbed PFOA, while the PdNPs at pHs 5 and 6 released 15.5% and 0.6% of the adsorbed PFOA after 43 hours of being soaked in DI water. These phenomena are in accord with the results at the end of 700 h in each continuous-flow condition: that Pd^0NPs at pH = 5 and pH = 6 definitely desorbed PFOA, although the fractions were small.

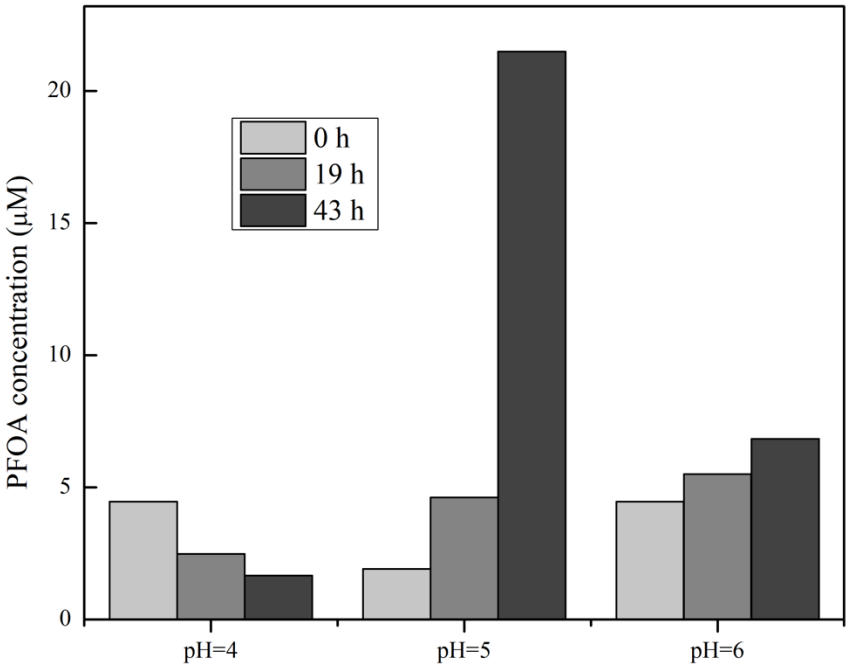

Figure 40. PFOA concentrations in the MCfR with DI water at different time points. (0 h represents that we drained all the liquid in the reactor and fed it with DI water, and some PFOAs were washed out immediately.)

We calculated the cumulative amount of removed PFOA and released F^- in each MCfR. During the 700-hours of operation, 17, 9, and 26% of the total ~22.6 mg of PFOA were removed (through adsorption and/or defluorination), and 2.5, 2.7, and 2.4% of the total 15.6-mg F^- were released through defluorination from the influent at pHs of 4, 5, and 6, respectively. This re-confirms that higher pH promoted the adsorption of PFOA.

Right after the DI-water wash, we conducted a batch test of catalytic reductive defluorination of ~10-μM PFOA on each membrane at each pH condition; the results are shown in Figure 41. After the desorption process, the Pd^0NPs at pH 5 and 6 recovered the ability to adsorb PFOA, with the PFOA concentration decreasing and fluctuating due to the adsorption and defluorination of PFOA by the PdNPs. We detected accumulation of 0.004 mM F^- (accounting for 2.7% of the total F in the ~10 μM PFOA) within 50 hours at pH 5 and accumulation of 0.009 mM F^- (accounting for 6.7% of the total F in the ~9 μM PFOA) at pH 6. In contrast, the Pd^0NPs at pH 4 did not show significant adsorption or any F^- release. In summary, washing the membrane with DI water partially reactivated the PdNPs for adsorption and defluorination for pH of 5 and 6, but not 4.

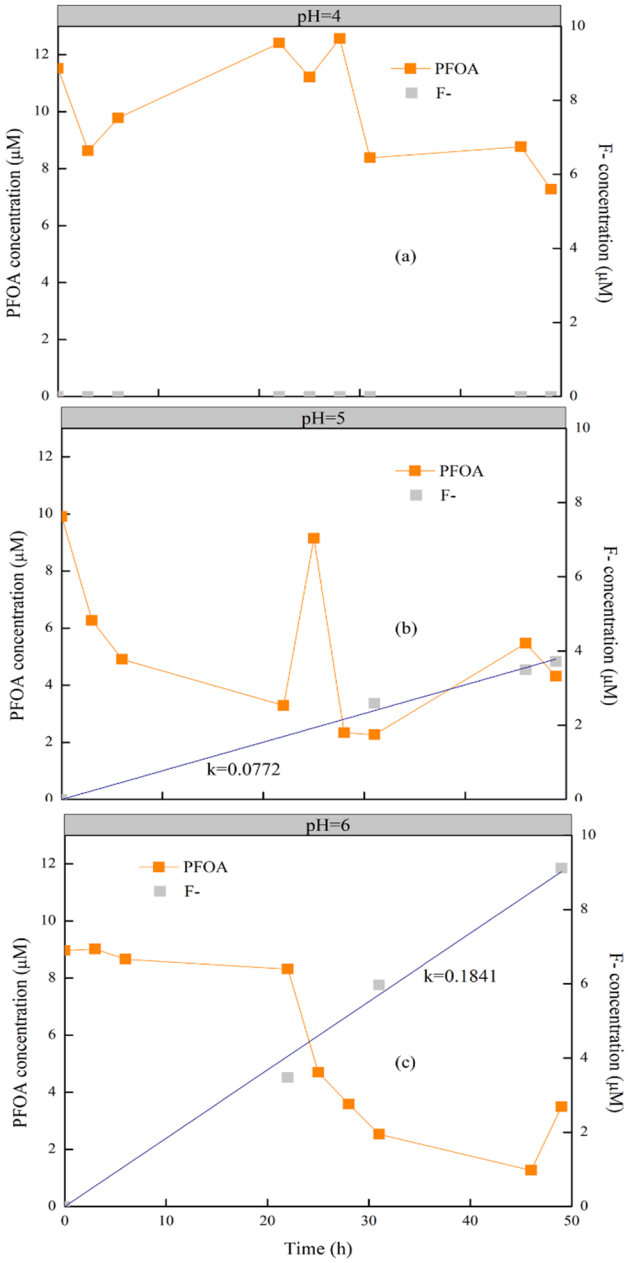

Figure 41. Concentrations of PFOA and F^- released in the batch test of catalytic reductive defluorination of ~10-μM PFOA in the MCfR with 5-mM Pd^0NPs at pHs 4 (a), 5 (b), and 6 (c) with H_2 supplied at 20 psig.

4.1.5.3. Continuous performance at HRT = 24 h

pH 6 gave the best balance of overall PFOA removal, resistance against adsorptive deactivation, and reactivation. Furthermore, pH 6 is closer to the optimal pH (~7) for the biofilm in the O_2-MBfR. Therefore, we set up one H_2-MCfR for continuous operation at pH = 6 and HRT = 24h.

Figure 42a shows the PFOA and F^- concentrations in the influent and effluent of the MCfR over 135 days. The effluent concentration of PFOA stabilized at 2.72±0.83 μM (or 67.9±11.2% removal and a 3.9±0.6 mg/m^2/day PFOA-removal flux), along with 8.5±2.2 μM of F^- release (6.9% and 10.5% of the total F in the influent PFOA and the depleted PFOA, respectively) for about 80 days. These trends support our hypothesis that the Pd^0NPs were deactivated to a low extent with the lower surface loading, compared with Figure 42b. However, PFOA removal started to deteriorate after Day 90, as reflected by a gradual increase of the effluent concentration up to 9.83 μM (over 100% of the influent) on Day 120. Correspondingly, the effluent F^- decreased gradually to 1.57 μM on the 106th day, which is only 1.1% of the total F in the influent PFOA or 2.9% of the F in the depleted PFOA. After the desorption of PFOA from days 118 to 125, the Pd^0NPs spontaneously reactivated to recover some of the ability to adsorb and defluorinate PFOA, with the highest fluoride release reaching 19.5 μM (13.9 % of the total F in the influent) on the 128th day. This partial reactivation may have been due to PFOA desorption, which made active sites available again on the surface of Pd^0NPs.

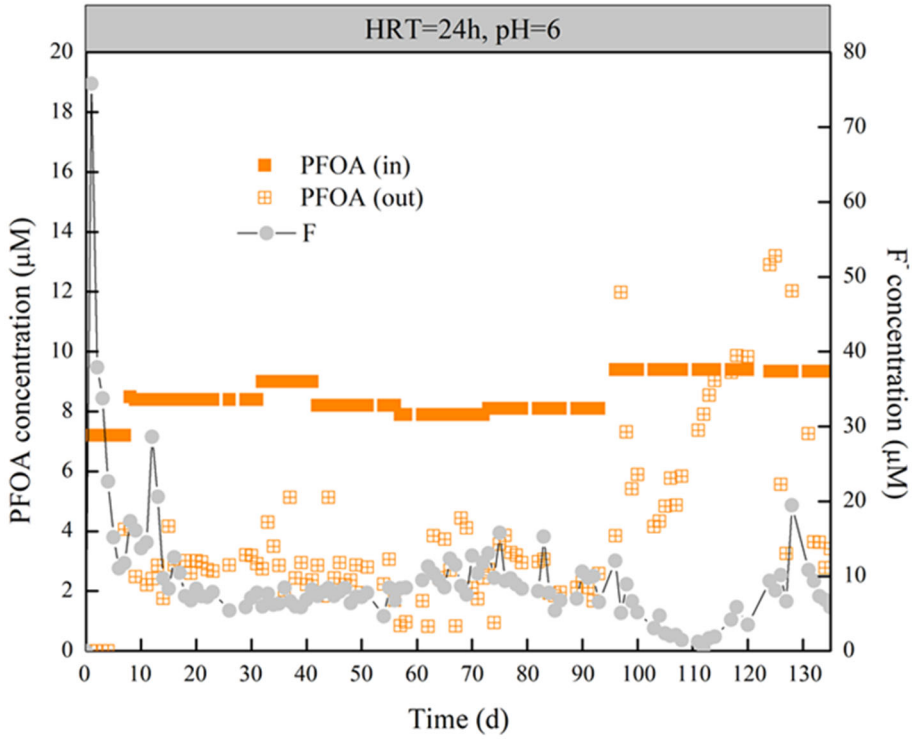

Figure 42. Concentrations of PFOA and F^- released in the continuous operation of catalytic reductive defluorination of PFOA in the MCfR with 5-mM Pd^0NPs at pH ~ 6 with H_2 of 20 psig. Orange solid squares: influent PFOA the H_2-MCfR; Orange open squares: effluent PFOA in the H_2-MCfR; Grey dots: F^- in the H_2-MCfR.

4.1.5.4. Continuous performance at environmental relevant concentrations of PFOA and PFOS.

We lowered the PFOA surface loading by making the PFOA influent concentrations much smaller; this ought to retard deactivation, which was accentuated in our tests with relatively high influent concentration of PFOA. We set up two separate MCfRs for testing the continuous removal of PFOA and PFOS at environment-relevant concentrations (0.5-1 ppb in the influent) at pH 6. We routinely monitored the substrates. We were not able to quantify F^- because its concentrations in the effluent are below the IC detection limit (0.5 μM), even if PFOA were 100% defluorinated.

Figure 43 shows the PFOA concentrations in the influent and effluent of the H_2-MCfR during the initial 213 days. Within 4 days, the effluent PFOA decreased gradually to < 100 ppt (or 87% removal). Then, the effluent concentrations of PFOA stabilized around the EPA health advisory level (70 ppt) with an average concentration of 66±29 ppt (or 87±5% removal) for the following 101 days.

Unfortunately, all liquid was accidentally drained out of the MCfR for one day due to the broken tubing held by the circulating pump, and the effluent of PFOA increased up to 287 ppt (or 54% removal). The performance fluctuated until day 139. From day 140 to day 213, the effluent

of PFOA decreased and eventually stabilized again at 72±32 ppt (or 88±5% removal). This shows the system can recover after a disturbance by external factors. In this case, the broken tubing and liquid draining out allowed the catalysts to be exposed to the air and affected catalyst activity. However, system recovery was not fast once the problem had been fixed.

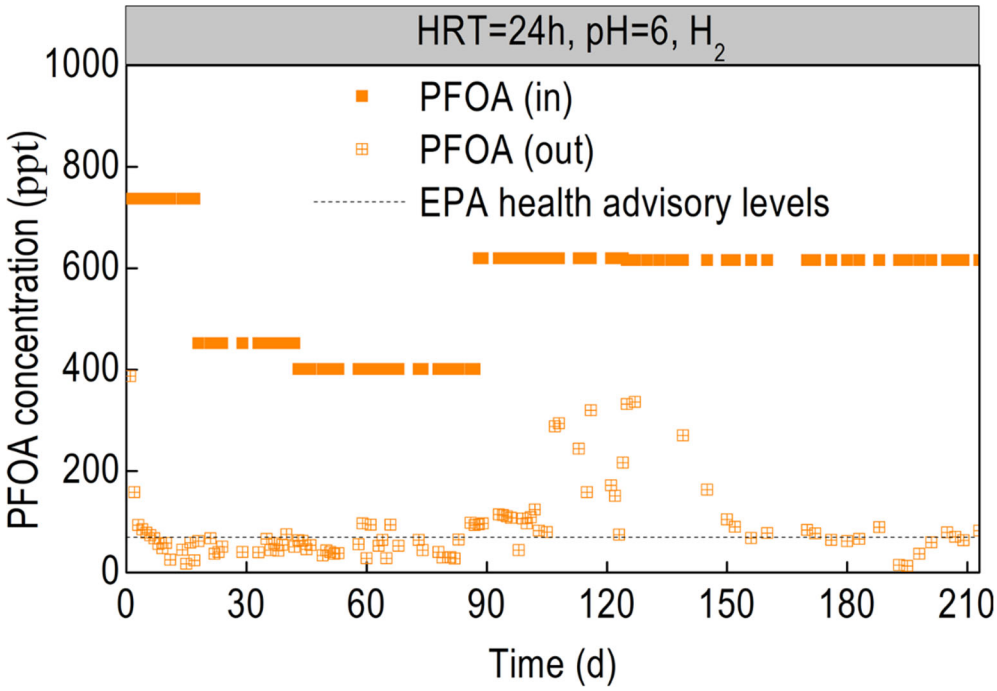

Figure 43. Concentrations of PFOA in the continuously operated MCfR with 5-mM Pd^0NPs and 20 psig H_2 supply. The blue arrow indicates the time when the tubing was accidentally broken.

Figure 44 shows the PFOS concentrations in the influent and effluent of the H_2-MCfR at pH 6 during the 105 days. After 1 day, the effluent concentrations of PFOS stabilized around the EPA health advisory level (70 ppt), and the average concentration was 26±14 ppt (or 95±2% removal) for the following 22 days. On day 23, we increased the influent PFOS concentration to ~900 ppt, and the effluent PFOA stayed below the EPA health advisory level (70 ppt), with an average concentration of 27±30 ppt (or 95±6% removal) for the following 46 days.

On day 70, we began to add ~900 ppt PFOA along with ~900 ppt PFOS into the influent. The effluent concentrations began to increase and fluctuate, with the average PFOA concentration at 261±106 ppt (or 70±12% removal) and average PFOS concentration at 160±92 ppt (or 84±9% removal) from day 70 to day 105. This result suggests a competitive effect for adsorption and defluorination between PFOA and PFOS when both are input at ~900 ppt.

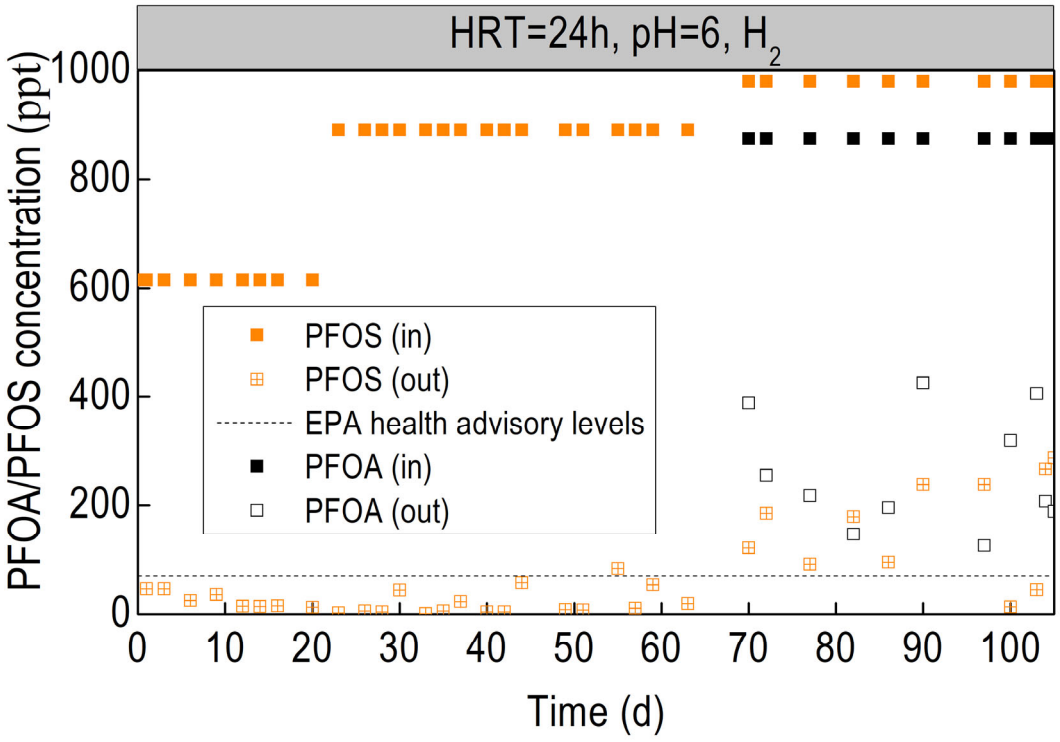

Figure 44. Concentrations of PFOA and PFOS in the continuous MCfR with 5-mM Pd^0NPs and 20 psig H_2 supply.

4.1.5.5. Continuous performance of PFOA, PFOS and co-removal of PFOA and PFOS

Figure 45A shows the PFOA and F^- concentrations in the influent and effluent of PFOA-only MCfR #10 during the first 90 days. The effluent concentrations of PFOA were constantly 1.53±1.72 ppb (96.7±4% removal) for 90 days, indicating that the PFOA adsorption sites had not been saturated. F^- release was initially stable at 1.66±0.12 µM (88.6±6.6% defluorination ratio) for the first 60 days, but then started to decrease gradually to 1.29 µM (72% defluorination ratio) on day 90, suggesting possible deactivation of the catalysts over time.

Figure 45B shows the PFOA, PFOS, and F^- concentrations in the influent and effluent of the PFOA+PFOS MCfR #11 during the first 90 days. The effluent concentration of PFOA were 0.10±0.20 ppb (99.5±0.9% removal) during the first 23 days, and then they moderately increased to 3.7±1.7 ppb (83.0±7.7% removal) during the following 67 days. Compared to PFOA, PFOS removal had a similar trend, but better performance: 0.35±0.34 ppb effluent concentration (98.8±1.2% removal) during the first 30 days and 1.2±0.5 ppb effluent concentration (95.9±1.9% removal) during the following 60 days. The effluent F^- was stably averaging 1.83±0.41 µM (89.5±13.8% defluorination ratio) except for a brief decrease to 1.06 µM (62.9% defluorination ratio) on day 31 for unknown reason.

Figure 45C shows the F^- concentrations in the influent and effluent of the PFOS-only MCfR #12 during the first 31 days. PFOS removal was stably at 88% during the 30 days. F^- release, however, decreased to only 0.21 μM (12% defluorination ratio) on day 31.

Pd showed high efficiency in defluorination and removal of PFOA when PFOA was the sole substrate. The defluorination performance of PFOS alone was considerably poorer than PFOA. When PFOA and PFOS were co-removed in MCfR #11, the removal of PFOS was negligibly affected, but the removal of PFOA was noticeably inhibited. The underlying mechanism needs further investigation.

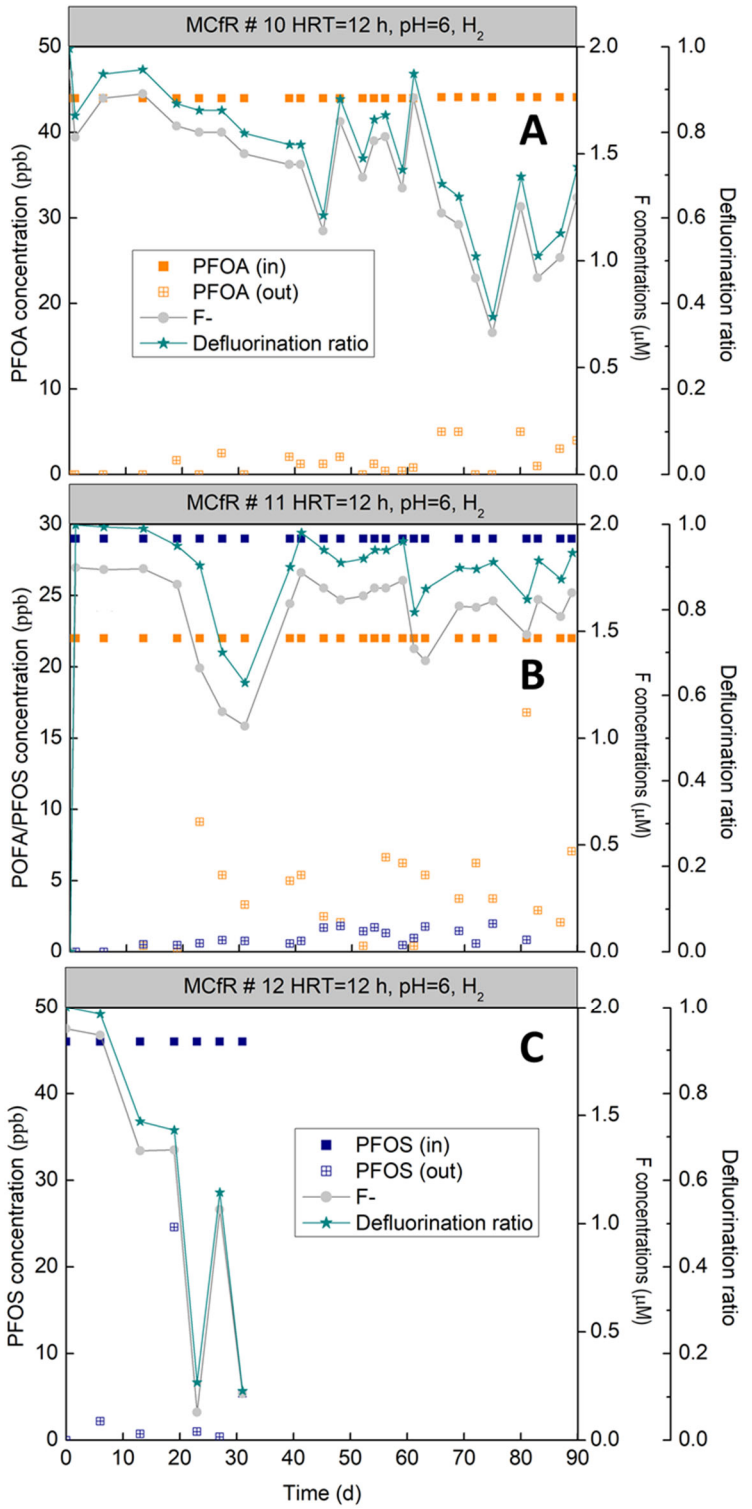

Figure 45. Concentrations of PFOA and F- in continuous operation of MCfRs #10, #11, and #12 in different conditions.

4.2. Task 2: Oxidative defluorination and mineralization of partially fluorinated OA/OS in the O_2-MBfR

4.2.1. Removal of partially fluorinated OA in the O_2-MBfR

We continuously operated an OA-consuming O_2-MBfR with a 12-hr HRT. Figure 46 shows the substrate concentrations in the influent and effluent over time. We measured the concentration of OA, 2-fluorooctanoic acid (2-FOA), and free F^- released in the effluent at the beginning of Stage 1-2, when we started to add 2-FOA. In stage 1-1, the O_2-MBfR achieved complete removal (> 99%) of 0.5 mM OA from the influent. In stages 1-2 and 1-3, it took about 2 months to have biofilm acclimate to 2-FOA biodegradation. The fluorine atom on 2-FOA was released to the bulk liquid as free F^- ion, and the concentration was well-matched to the removed 2-FOA. In stage 1-4, featuring 0.5 mM OA and 0.01 mM 2-FOA (mono-fluorinated OA) in the influent, the removal of 2-FOA was stable at about 99% for more than 10 days. The results reveal that bacteria were able to efficiently degrade partially fluorinated 2-FOA with OA as the primary substrate.

Next, we maintained continuous operation of the OA-consuming O_2-MBfR (still having a 12-hr HRT) in stage 2 by adding 2H,2H-perfluorooctanoic acid (2H-PFOA) into the influent. With 2H-PFOA at 10 μM in the influent in Stage 2-1 (Figure 46B) to test the effects of a more fluorinated OA on the biofilm. During this stage, OA removal remained >99%. The 2H-PFOA started to be removed, and the removal reached about 10% by 10 days. In the following 20 days, however, 2H-PFOA removal gradually decreased to 5%. F^- release always was less than 0.1 μM, which accounted for less than 10% of the total F in the removed 2H-PFOA. The slow rate of defluorination (perhaps even a zero rate) for 2H-PFOA supports that more-fluorinated OA is less biodegradable, a trend that we anticipated. The mismatch of F^- release to 2H-PFOA removal suggests that the removal of 2H-PFOA in the O_2-MBfR is not by defluorination, but perhaps by adsorption or biotransformation that does not involve F^- release. The low biodegradation rate of 2H-PFOA may be caused by the toxicity of highly fluorinated OA and the biofilm need time to adapt to new substrate. Therefore, we decreased influent concentration of 2H-PFOA concentration to 5 μM.

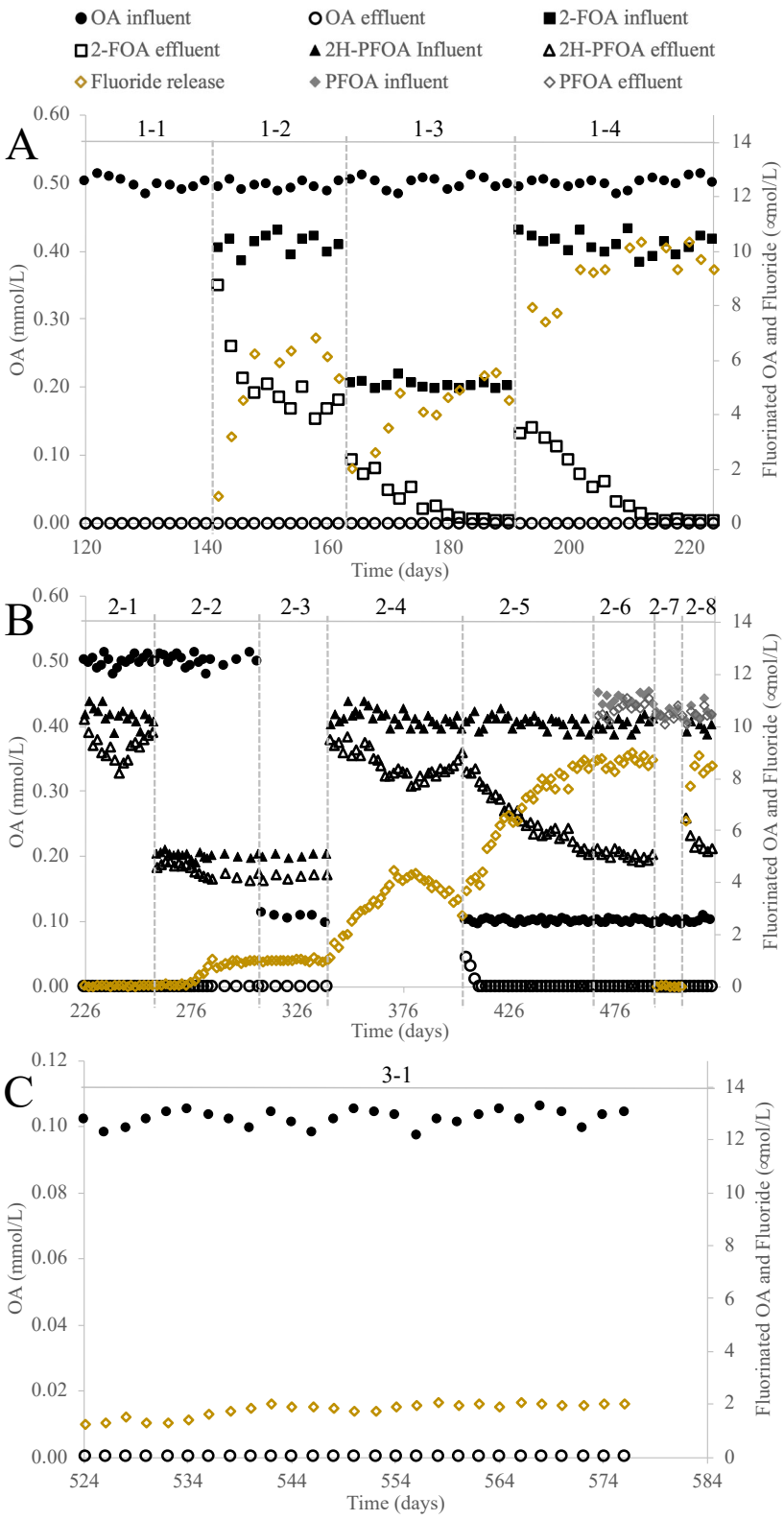

Figure 46. Continuous operation for fluorinated and non-fluorinated OA biodegradation in the O_2-MBfR.

During stage 2-2, OA removal remained >99%, while 2H-PFOA removal gradually increased to 15% at the end of the stage. F^- release also increased and reached a steady-state of 1.0 μM, which accounted for about 13% of the total F in the removed 2H-PFOA (based on 2H-PFOA data for the first 26 days of this stage). On the one hand, the relatively lower level of defluorination for 2H-PFOA (compared to 2-FOA) supports that a more-fluorinated OA is less biodegradable (as expected). On the other hand, the stable 2H-PFOA removal and F^- release indicates that the biofilm in the O_2-MBfR obtained 2H-PFOA removal and defluorination capabilities, probably through co-metabolic biodegradation.

In Stage 2-3, we decreased the influent concentration of OA to 0.1 mM, thereby increasing the 2H-PFOA/OA mole ratio to 1/20, which we expected to selectively enrich for 2H-PFOA-oxidizing bacteria. OA removal remained >99%, while 2H-PFOA removal gradually increased to 16% at the end of the stage. The concentration of released F^- ion was stable at about 1.1 μM, which accounts for about 11% of total fluorine of removed 2H-PFOA, and the mole ratio of released F^-per removed 2H-PFOA was about 1.4.

In Stage 2-4, we removed OA from the influent to selectively enrich the functional bacteria capable of degrading highly fluorinated OA without OA. In the last two weeks, we observed a ~24% slowdown of 2H-PFOA removal and F^- release, probably caused by biomass loss due to energy deficiency (90% less energy input without OA). The trend reinforces that a primary substrate (like OA) is crucial to support biofilm growth and the initial steps of reductive defluorination.

In stage 2-5, we added back 0.1 mM OA to the influent as the primary substrate to support the biofilm growth and 2H-PFOA biodegradation. In the first 6 days, the removal of OA increased from 55% to over 99%, which indicated that the biofilm still was capable of utilizing OA as carbon and energy source, but it needed to have new synthesis to regain its early performance for OA removal; this coincides with our explanation of the gradual loss of 2H-PFOA removal. With the increasing removal of OA, the 2H-PFOA biodegradation gradually increased from 1.0 μM to 4.8 μM (or flux from 3.8 to 18.3 $mg/m^2/d$). The released F^- concentration also increased from 1.8 to 8.6 μM, which accounts for about 14% of the total fluorine in the removed 2H-PFOA. The latest molar ratio of released F^- to removed 2H-PFOA was about 1.8. The removal of 2H-PFOA and fluoride release is at steady-state now, since the standard deviation is smaller than 3% of average in 12 days (6 data point). The promoting effects to 2H-PFOA removal efficiency from adding OA back into the influent further proves that extra carbon and energy source are required for 2H-PFOA biodegradation.

In Stage 2-6, we added 10 mM PFOA to the influent to investigate the potential for PFOA biodegradation and its inhibition effect on 2H-PFOA biodegradation. In the first month, the removal of OA did not change, staying over 99%. 2H-PFOA remained at steady-state removal of 48% (or a flux of 18.3 $mg/m^2/d$). The released F^- concentration was 8.6 μM, which accounts for about 14% of the total fluorine in the removed 2H-PFOA. The latest molar ratio of released F^- to removed 2H-PFOA was about 1.8. The effluent concentration of PFOA was decreased by < 8% of the influent during the initial 14 days, but it gradually increased back to 97% of the influent. This suggests initial adsorption followed by desorption of PFOA to the reactor material or the biofilm. Overall, the 28-day results of Stage 2-6 reveal that PFOA probably was not biodegraded

(as we expected), but its presence had no acute effect on biodegradation of partial- or non-fluorinated OA.

In new stage 2-7, we removed 2H-PFOA from the influent and left 10 μM PFOA and 100 μM OA as the substrates. In two weeks, the removal of OA did not change, staying over 99%. The effluent PFOA concentrations showed no PFOA removal through biodegradation in O_2-MBfR. The effluent concentration of F^- was constantly below 0.1 μM. In stage 2-8, we added back 10 μM 2H-PFOA to the influent and removed PFOA. In two weeks, the removal of OA did not change, staying over 99%. Within one day after 2H-PFOA re-introduction, the 2H-PFOA removal bounced back to 40%, and the system soon reached steady-state for 48% removal (or a flux of 18.3 $mg/m^2/d$). Accordingly, the released F^- concentration reached 8.6 μM, which accounts for about 14% of the total fluorine in the removed 2H-PFOA, or 1.8 of the molar ratio between released F^- to removed 2H-PFOA; these values are close to those in the previous 2H-PFOA stage (Stage 2-6) before the PFOA test. Overall, the 14-day results of Stage 2-8 reveal that the biofilm maintained its capability of 2H-PFOA biodegradation and was ready for PFOA reductive defluorination products biodegradation tests.

Stage 3-1 involved feeding the same O_2-MBfR with H_2-MCfR effluent that contained featuring 7 mM remaining PFOA, 2 mM F^-, and unidentified defluorinated products. 0.1 mM OA was added in the solution as the primary electron donor. The removal of OA did not change, staying over 99%; this confirms that the products from the H_2-MCfR had no observable inhibition on OA biodegradation (Figure 46C). The effluent F^- concentration decreased from 8.6 μM to 1.5 μM in the first week, indicating lower concentration of biodegradable compounds or less biodegradability (at least in terms of defluorination) of the partially defluorinated compounds from the collected effluent, compared to 10 μM 2H-PFOA, at least initially. After two months enrichment, the effluent F^- changes (difference between influent and effluent concentration) gradually increased from 1.5 μM to 2.0 μM and reached steady-state, indicating that the biofilm needed time to adapt to the new substrates (products of H_2-based defluorination). According to the HPLC-MS-MS results for the O_2-MBfR effluent from day 524 to 538 (first two weeks of stage 3-1), the dominant (relatively high peak area) shorter chain per-fluorinated carboxylic acid was perfluorohexanoic acid (C6), plus trace-level heptafluorobutyric acid (C4). These two biodegradation products indicate that the defluorinated products in the H_2-MCfR effluent could be 2H-PFOA and 6H-PFOA:

$$C_8HF_{15}O_2 + 2H_2 \rightarrow C_8H_3F_{13}O_2 + 2HF$$

$$C_8HF_{15}O_2 + 6H_2 \rightarrow C_8H_7F_9O_2 + 6HF$$

$$C_8H_3F_{13}O_2 + 2O_2 \rightarrow C_6HF_{11}O_2 + 2HF + 2CO_2$$

$$C_8H_7F_9O_2 + 5O_2 \rightarrow C_4HF_7O_2 + 2HF + 4CO_2 + 2H_2O$$

Other highly defluorinated products, like monofluorooctanoic acid and difluorooctanoic acid, could have been completely mineralized in the O_2-MBfR. The residual PFOA in the MBfR effluent was about 7 mM, which means that no significant PFOA removal occurred in the O_2-MBfR (as expected).

4.2.2. Removal of partially fluorinated OS in the O_2-MBfR

An O_2-based OS-consuming membrane biofilm reactor (O_2-MBfR-OS) was built and inoculated with sludge (Northeast Wastewater Reclamation Plant, Mesa, AZ) plus the OA enriched culture. The O_2-MBfR-OS was continuously fed with 1 mM OS at an HRT of 12 hours (Stage I). One month after inoculation, the removal of OS gradually increased to over 99% (results in Figure 47), along with the observable accumulation of biofilm. The biofilm samples were collected and stored in the -80ºC refrigerator for subsequent microbial community sequencing. After day 68, we started stage 2 by adding 0.1 mM 1H,1H,2H,2H-Perfluorooctanesulfonic acid (4H-PFOS) to the influent, along with 0.9 mM OS (Stage II). The concentration of released F^- gradually increased from 8 mM to 38 mM, which indicated a F^-/4H-PFOS mole ratio of 0.38. We expect more F^- being release during longer-term continuous operation.

In stage III, we added 0.1 mM PFOS into the influent, and the removal of OS and release of F^- did not change significantly. In stage IV, we used the PFOS hydrodefluorination products (from an MCfR) as the influent for O_2-MBfR, with 1 mM OS as the primary substrates. The released F^- concentration gradually increased to about 20 mM, which indicated the further biodegradation and defluorination of PFOS hydrodefluorinated products.

We conducted a batch test of 4H-PFOS biodegradation in the O_2-MBfR with new medium in which we used H_2CO_3/HCO_3^- as the pH buffer instead of phosphate. With the phosphate peaks removed, we were able to monitor the 4H-PFOS, 2H-PFOA, C6-PFA, and fluoride ion concentrations using IC. Figure 48 shows the results of a ten-day batch test, in which about 100 mM 4H-PFOS was removed with 100 mM C6-PFA produced as the major product. At the same time, about 200 mM F^- and 100 SO_4^{2-} were released during the biodegradation of 4H-PFOS. The mole ratio of F^- releasing to 4H-PFOS removal was about 2. The mass balances of carbon, sulfur, and fluorine are well established (<5% discrepancies) and support a β-oxidation pathway:

$$C_8H_5F_{13}SO_3 + 1.5O_2 \rightarrow C_8H_3F_{13}O_2 + H_2SO_4$$

$$C_8H_3F_{13}O_2 + 2O_2 \rightarrow C_6HF_{11}O_2 + 2HF + 2CO_2$$

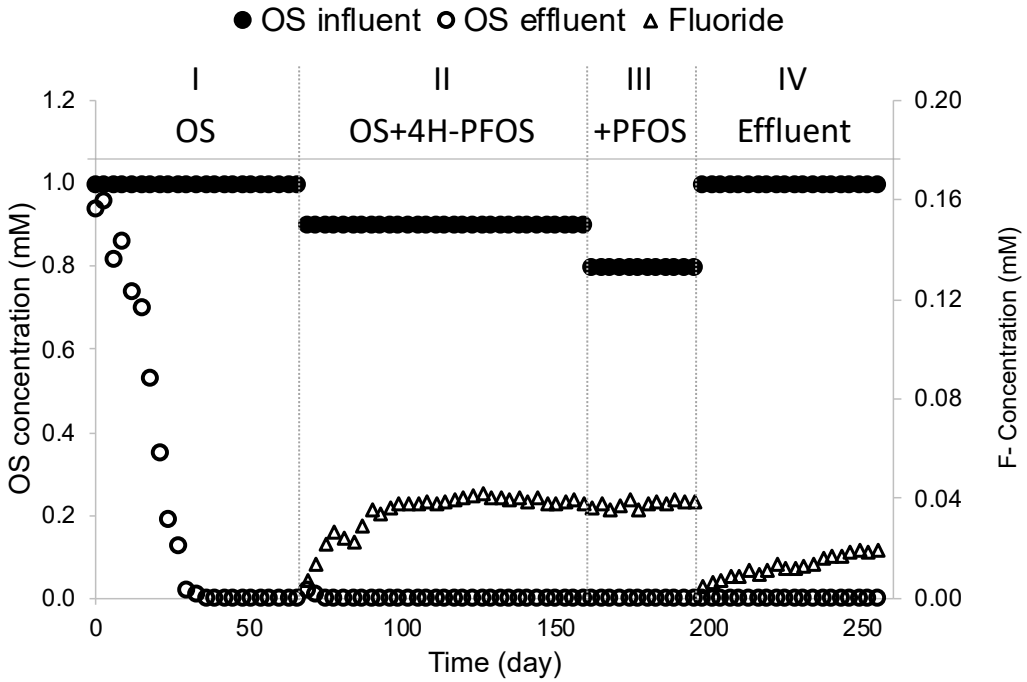

Figure 47. The influent (closed circles) and effluent (open circles) concentration of OS in the O_2-based MBfR.

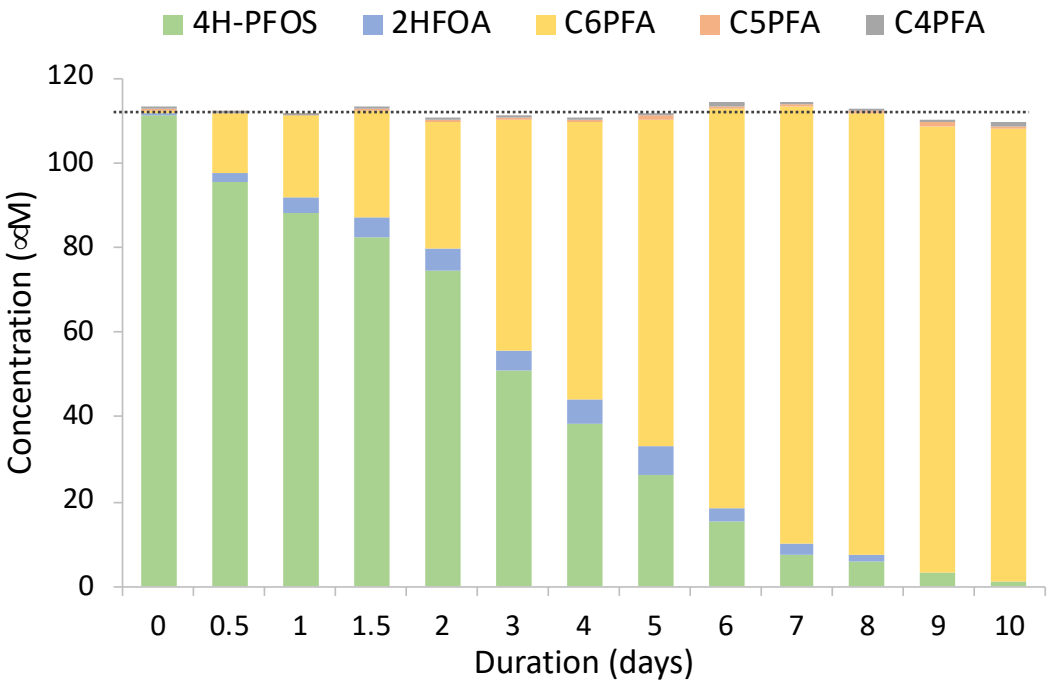

Figure 48. Batch tests of 4H-PFOS biodegradation in O_2-based MBfR.

4.2.3. Biofilm community with removal of partially fluorinated OA in the O_2-MBfR

We conducted shallow metagenomic sequencing DNA from the biofilm of the O_2-MBfR of removal OA and FOAs. Figure 49 shows that bacteria of genera *Cupriavidus* (7%~49%), *Mesorhizobium* (1%~9%), and *Dokdonella* (1%~8%) were dominant in the biofilm community. Some bacterial strains in the genus *Dokdonella* are known to biodegrade the 6:2 fluorotelomer alcohol (6:2 FTOH), which is a partially fluorinated 8C alcohol.[69,70] From stages II-2 to II-6, when the influent concentration of 2H-PFOA increasing in relation to O, the relative abundance of *Cupriavidus* gradually decreased, from 49% to 7%. The bacteria in the genus *Cupriavidus* may have been inhibited by the highly fluorinated octanoic acid. The genomic results point out that the substrate switch from less fluorinated octanoic acid (2-FOA) to highly fluorinated octanoic acid (2H-PFOA and PFOA) significantly shaped the community structure of the biofilm.

Table 2 shows the relative abundance of genes related to β-oxidation. Among the functional genes, *ACADM* (encoding acyl-CoA dehydrogenase), *fadE* (encoding acyl-CoA dehydrogenase), *paaF* (encoding enoyl-CoA hydratase), *fadN* (encoding 3-hydroxyacyl-CoA dehydrogenase), *fadJ* (encoding 3-hydroxyacyl-CoA dehydrogenase), and *fadA* (encoding acetyl-CoA acyltransferase) had relatively higher abundances (CPM > 100) than other genes. These results support that the biofilm communities were able to perform β-oxidation, the metabolic oxidation pathway for catabolism of fatty acids and that has been associated with the oxidation of partially fluorinated FOAs.[71] In general, little research has been published on the functional genes for OA/FOAs biodegradation. Our work is providing important new insights about OA/FOAs functional gene and the bacteria that harbor them.

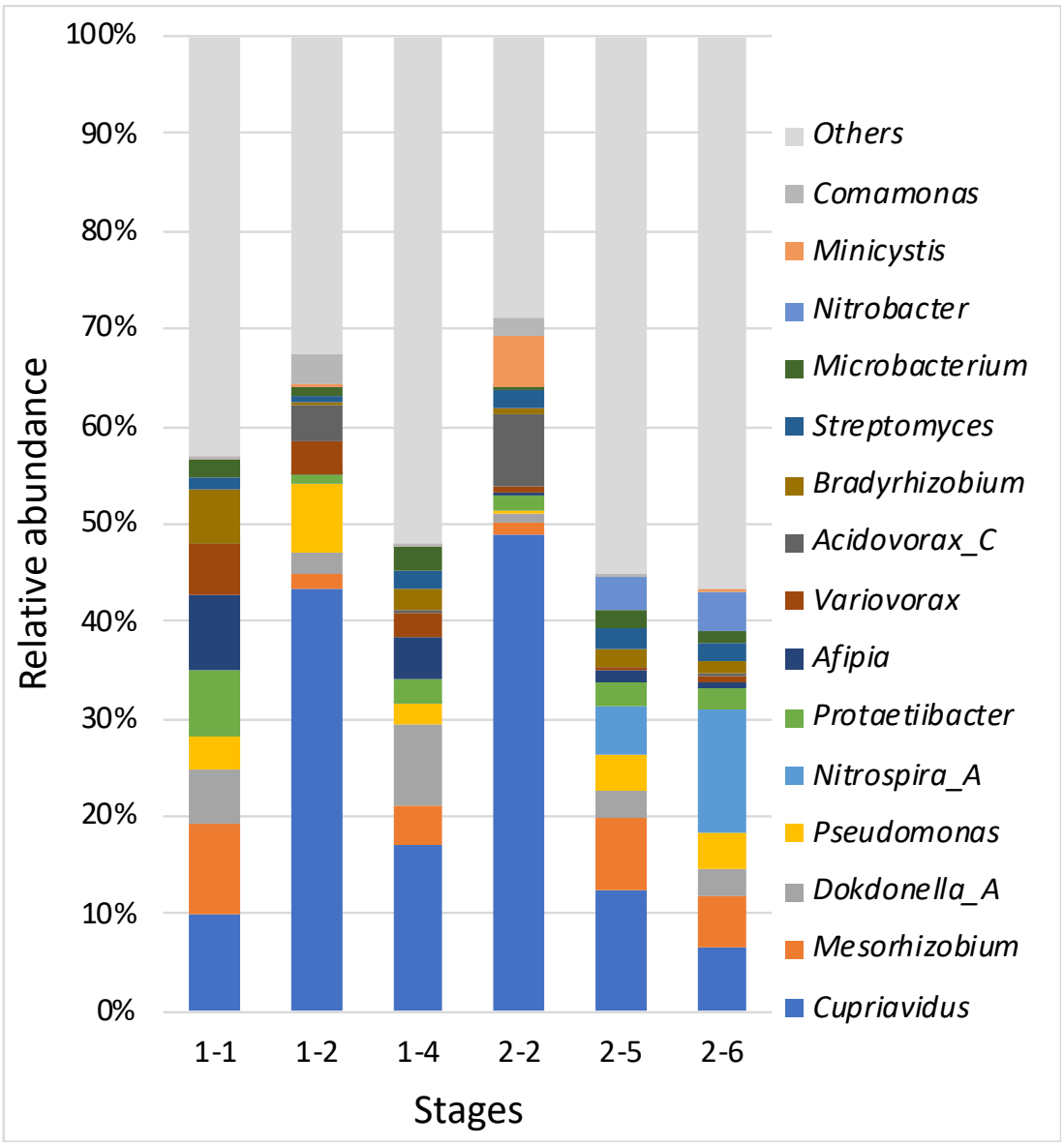

Figure 49. Community structure at the genus level of the O_2-MBfR biofilms able to oxidize partially fluorinated OAs.

Table 2. Relative abundances of functional genes related to β-oxidation

KO	Gene	Function	1-1	1-2	1-4	2-2	2-5	2-6
K00232	*ACOX1*	acyl-CoA oxidase	28.0	2.4	18.2	4.8	14.1	20.7
K00249	*ACADM*	acyl-CoA dehydrogenase	487.4	684.0	417.6	880.3	310.8	283.3
K00255	*ACADL*	ong-chain-acyl-CoA dehydrogenase	22.0	20.4	10.5	12.2	26.3	22.8
K06445	*fadE*	acyl-CoA dehydrogenase	97.9	98.4	115.2	95.7	90.9	133.2
K09479	*ACADVL*	very long chain acyl-CoA dehydrogenase	0.0	9.7	0.0	4.1	7.1	5.3
K01692	*paaF*	enoyl-CoA hydratase	311.9	419.9	249.4	575.3	175.8	169.7
K07511	*ECHS1*	enoyl-CoA hydratase	109.6	75.7	70.5	86.8	67.6	76.8
K13767	*fadB*	enoyl-CoA hydratase	0.0	0.0	0.0	0.0	4.6	0.0
K00022	*HADH*	3-hydroxyacyl-CoA dehydrogenase	3.1	0.0	10.4	0.0	0.0	0.0
K07516	*fadN*	3-hydroxyacyl-CoA dehydrogenase	155.2	254.4	194.9	275.9	129.7	167.3
K01825	*fadB*	3-hydroxyacyl-CoA dehydrogenase	11.2	9.9	9.6	13.2	7.5	6.5
K01782	*fadJ*	3-hydroxyacyl-CoA dehydrogenase	85.7	84.2	110.3	27.2	105.3	108.2
K07514	*EHHADH*	enoyl-CoA hydratase	8.2	0.0	0.0	0.0	5.1	5.7
K07515	*HADHA*	enoyl-CoA hydratase	0.0	0.0	3.2	0.0	0.0	0.0
K10527	*MFP2*	enoyl-CoA hydratase	0.0	0.0	0.0	0.0	3.7	0.0
K00632	*fadA*	acetyl-CoA acyltransferase	432.5	623.8	351.3	562.0	340.1	357.9
K07508	*ACAA2*	acetyl-CoA acyltransferase 2	1.4	0.0	0.0	9.1	3.6	0.0
K07509	*HADHB*	acetyl-CoA acyltransferase	11.1	0.0	5.6	5.7	7.2	3.6
K07513	*ACAA1*	acetyl-CoA acyltransferase 1	69.4	36.3	34.9	40.7	38.3	51.5
Unit: Counts per million (CPM); Color gradent:			0	50	100	200	400	900

4.2.4. Biofilm community in the O_2-MBfR removing partially fluorinated OS

Figure 50 shows that *Pseudomonas* (60%~70%), *Cupriavidus* (3%~10%), and *Dokdonella* (2%~8%) were the top three dominant genera in the biofilm community. The genus *Pseudomonas* is reported to oxidize alkane sulfonates.[72] The overall community structure did not show significant changes through the three stages, but they were greatly different compared to OA/FOAs biofilm community (Fig. 49). Thus, the primary substrate OS (versus OA) selectively shaped the community structure to *Pseudomonas* domination.

Table 3 shows the relative abundance of functional genes related to sulfonate and sulfate transformations in the biofilm community of the O_2-MBfR biodegrading OS/FOSs. From stage I to III, the overall trend of these functional genes was an increase through time. Since the OS/FOS molecules contain the sulfonic-acid functional group, the first step of OS/FOSs oxidative biodegradation likely is alkanesulfonate monooxygenation (catalyzed by *ssuD* encoded monooxygenase).[73] The increasing relative abundance of *ssuD* from 180 to 290 indicates that using OS as the primary substrate enhanced the biofilm's capacity for alkanesulfonate monooxygenation. During alkanesulfonate monooxygenation, the sulfite ion is released. In the O_2-MBfR, sulfite was further oxidized to sulfate, which was detected in the effluent, and the produced sulfate increased in parallel to the increase in sulfonate- and sulfate-related functional genes.

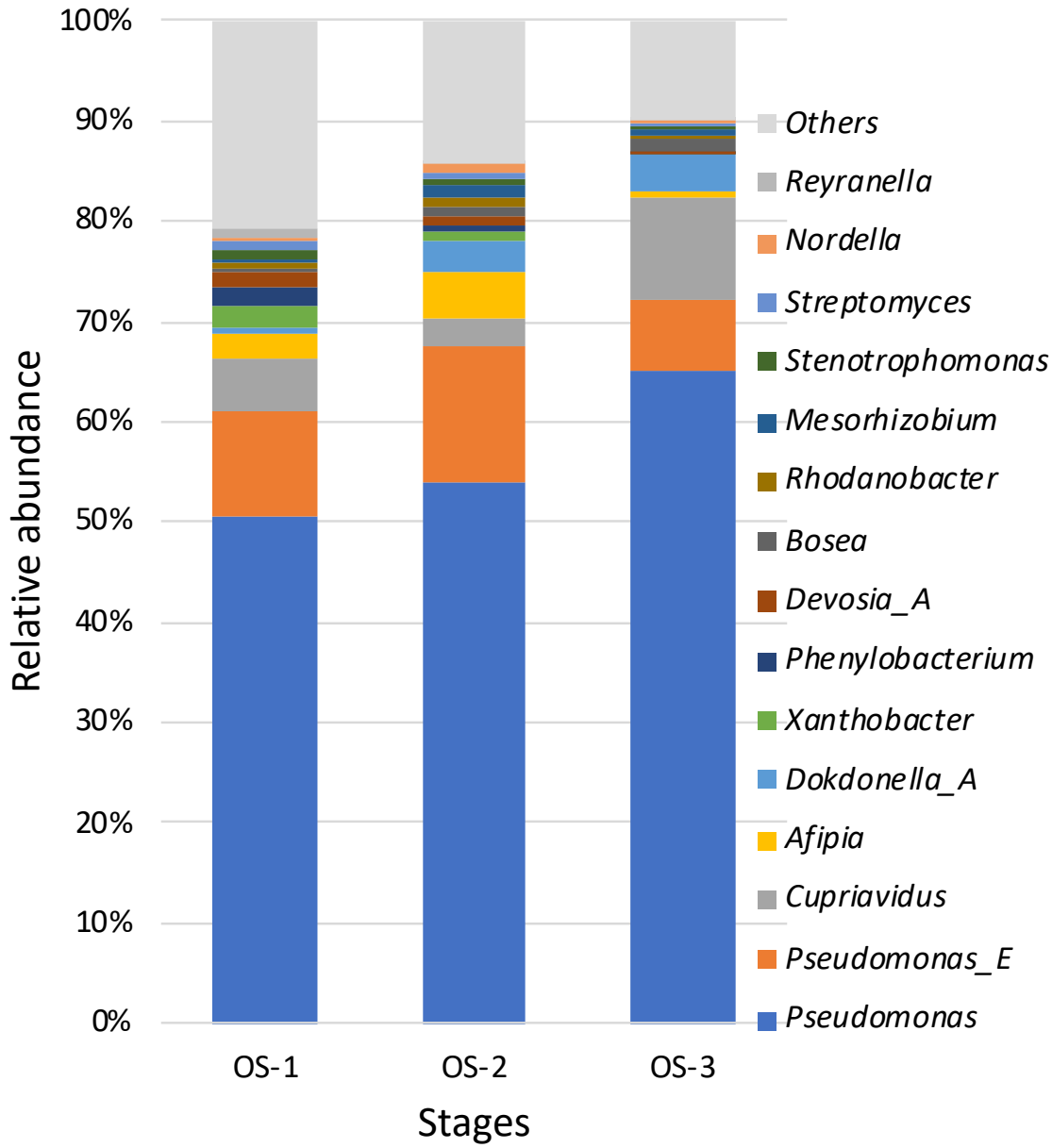

Figure 50. Community structure at the genus level of the biofilm in the O_2-MBfR biodegrading OS and partially fluorinated OSs.

Table 3. Relative abundances of functional genes related to transformations of sulfonate and sulfate

KO	Gene	Function	OS1	OS2	OS3
K15553	*ssuA*	sulfonate transport system substrate-binding protein	181.30	217.82	410.05
K15554	*ssuC*	sulfonate transport system permease protein	273.60	365.05	533.08
K15555	*ssuB*	sulfonate transport system ATP-binding protein	43.76	95.35	90.44
K04091	*ssuD*	alkanesulfonate monooxygenase	179.20	218.73	287.14
K03321	*TC.SULP*	sulfate permease	226.13	207.74	378.93
K01011	*sseA*	thiosulfate/3-mercaptopyruvate sulfurtransferase	111.19	168.74	189.34
K00957	*cysD*	sulfate adenylyltransferase subunit 2	108.63	121.01	154.46
K02046	*cysU*	sulfate/thiosulfate transport system permease protein	119.01	115.40	125.87
K02047	*cysW*	sulfate/thiosulfate transport system permease protein	95.42	102.27	157.83
K23163	*sbp*	sulfate/thiosulfate transport system substrate-binding protein	120.46	90.92	102.73
K00860	*cysC*	adenylylsulfate kinase	101.10	72.67	92.19
K22303	*atsK*	alpha-ketoglutarate-dependent sulfate ester dioxygenase	36.08	129.83	63.18
K02045	*cysA*	sulfate/thiosulfate transport system ATP-binding protein	73.78	60.81	86.63
K02439	*glpE*	thiosulfate sulfurtransferase	56.07	77.86	72.47
K00956	*cysN*	sulfate adenylyltransferase subunit 1	41.89	66.18	27.19
K05907	*APR*	adenylyl-sulfate reductase (glutathione)	27.05	37.39	54.15
K02048	*cysP*	sulfate/thiosulfate transport system substrate-binding protein	23.42	29.99	41.97
K19713	*tsdA*	thiosulfate dehydrogenase	27.57	26.43	32.86
K00390	*cysH*	phosphoadenosine phosphosulfate reductase	31.65	32.59	20.24
Unit: Counts per million (CPM); Color gradent:			0	250	500

4.3. Task 3: Synergistic defluorination of PFOA/PFOS

4.3.1. Synergistic defluorination of PFOA

We connected the effluent of an H_2-MCfR loaded with 0.84/0.36 g/m^2 Pd^0/Rh^0 to the influent of and O_2-MBfR and started continuous operation of this synergetic system. In the first stage, we added 10 μM PFOA to the influent medium, and the flow rate was 70 mL/day (HRT~24 hours). The PFOA surface loading in the H_2-MCfR was 9.1 mg/m^2-day (or 0.022 mmole/m^2-day). Figure 51 shows the concentrations of PFOA (left panel) and F^- (right panel) in the influent and MCfR/MBfR effluents.

Within the Pd^0-Rh^0NPs H_2-MCfR, over 90% of the influent PFOA was removed during the first 5 days of continuous operation, and the removal gradually decreased to 85% on day 8. The released-F^- concentrations in H_2-MCfR were around 5.3 μM (defluorination ratio 40%) at the beginning, and gradually decreased to 4.7 μM (defluorination ratio 35%). The deactivation of Pd^0-Rh^0NPs accelerated after two weeks' continuous operation, and the removal decreased to 33% on day 22. The released-F^- concentrations in H_2-MCfR also decreased to 2.1 μM (defluorination ratio 33%). The gradual deactivation may be caused by the accumulation of intermediate with incomplete defluorination, which was accentuated by the combination of moderately high PFOA loading and extended duration of the experiment.

In the subsequent O_2-MBfR, the effluent PFOA concentrations were similar to the effluent of H_2-MCfR (as expected). The released F^- through 10 days of continuous operation was around 5.8 μM (defluorination ratio 42%). Before day 8, the overall PFOA removal of the synergistic platform was about 89%, and the defluorination ratio was about 80% of removed PFOA. In the following two weeks, the overall PFOA removal decreased to 33% and the defluorination ratio was 75% of the removed PFOA.

To regenerate the deactivated Pd^0-Rh^0NPs, we continuously fed a 0.1%-HCl water solution to the H_2-MCfR for 3 days (HRT of 24 hours). In the first four days after regeneration, the overall removal of PFOA recovered to over 80%, and the defluorination ratio was about 85%. The results indicated that acid treatment can regenerate the activities of Pd^0-Rh^0NPs for PFOA removal and defluorination. The acid treatment may accelerate defluorination and desorption of adsorbed PFOA and intermediate, eventually achieves regeneration of active sites on the nano-particles surface.

After two weeks of continuous operation, the Pd^0-Rh^0NPs became deactivated again, with PFOA removal decreasing to 26% and F^- releasing decreasing to 2.2 μM (or 26% of the total organic F^- in removed PFOA). We regenerated the Pd^0-Rh^0NPs again to optimize the regeneration condition by lessening the HCl concentration (1 mM). After 1-week regeneration, we kept monitoring the PFOA and F^- concentrations in regenerated H_2-MCfR. The PFOA removal recovered to 90%, and F^- release increased to 5.4 μM and 6.1 μM in H_2-MCfR and O_2-MBfR, respectively. The released F^- were 36% and 39% of the total organic F^- in removed PFOA for reductive defluorination and biodegradation, respectively. The good recovery of PFOA reductive defluorination in H_2-MCfR indicates that the deactivation of Pd^0-Rh^0NPs is reversible. Low-concentration (1 mM) HCl seemed to accelerate the compete removal of the adsorbed PFOA and intermediates on the catalysts.

After another three weeks of continuous operation, the PFOA removal decreased to 32%, with F^- release decreasing to 1.1 μM (or 14% of the total organic F^- in removed PFOA). We did a third regeneration of Pd-Rh H_2-MCfR using 1 mM HCl with continuous feeding for 24 hours. After regeneration, the PFOA removal recovered to 92%, and F^- release increased to 5.5 μM and 6.0 μM in H_2-MCfR and O_2-MBfR, respectively. The released F^- were 39% and 40% of the total organic F^- in removed PFOA for reductive defluorination and biodegradation, respectively. The good recovery of PFOA defluorination indicated that 1 mM HCl continuous feeding is a good method for regeneration. However, after three regenerations, the time duration with >80% PFOA removal decreased from 11 days at the beginning to 5 days after for the third regeneration. This result suggests that some irreversible deactivation may happen through continuous operation and regeneration when the PFOA loading is high. The deactivation may have been caused by physical catalysts loss during regeneration (empty, refill, and washing the reactor). The fast deactivation of catalysts was accentuated by the high surface loading of PFOA.

We recoated the H_2-MCfR with 2.5 mM + 2.5 mM mixed Pd and Rh ion solution after the fourth continuous operation stage. In the new round of continuous operation, we decreased the influent PFOA concentration from 1 μM to 0.2 μM (or 414 ppb to 83 ppb). In the first two weeks, the effluent PFOA concentration was below IC detection limit (0.05 μM). The released F^- concentrations in MCfR and MBfR were 1.0 μM and 0.7 μM (or 40% and 30% of the total F on removed PFOA), respectively. The lower influent concentration enabled longer time (16 days) of good PFOA removal (>75%, or PFOA effluent below IC detection limit). And, the deactivation of Pd-Rh catalyst was slower, down from 20 days for >50 % removal to 30 days for >50% removal. The results also indicate that higher influent PFOA concentration (also PFOA surface loading) accelerated the deactivation of the catalyst. In practical use of the MCfR with typically low concentrations, the regeneration of catalysts could have a long repetition period, say over 3 months.

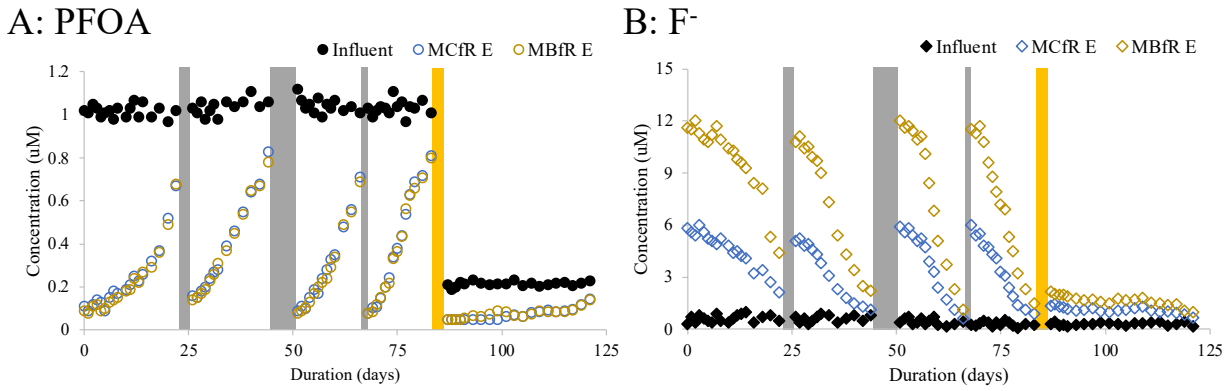

Figure 51. The PFOA (A) and F^- (B) concentrations of influent and MCfR/MBfR effluents for PFOA removal. Gray columns and yellow columns indicate the period of regeneration and recoating, respectively.

4.3.2. Synergistic defluorination of PFOS

In the synergistic platform for PFOS removal, the influent PFOS concentration was 10 μM, and the HRT was 24 hours. In the first day, the released F^- concentration in H_2-MCfR was 30 μM (or 20% of the total F^- in PFOS). Figure 52 shows that, during continuous operation, the effluent PFOS concentration in H_2-MCfR and O_2-MBfR gradually increased from 1.6 μM to 7 μM in 4 days (over all removal of PFOS from 84% to 27%). The released F^- concentration gradually decreased to about 5 μM (or 3% of the total organic F^- in PFOS). In the subsequent O_2-MBfR, the released F^- concentration through biodegradation decreased from 22 μM to 5 μM (or 15% to 3% of the total organic F^- in PFOS). The sulfate SO_4^{2-} concentrations did not change between the influent and two reactors' effluents (<1 μM difference). The results confirm that PFOS (like PFOA) can be removed by the synergistic platform. The decreasing concentration of released F^- indicated relatively rapid deactivation of Pd^0-Rh^0NPs with the high PFOS influent concentration. The negligible SO_4^{2-} concentration changes indicate that further biodegradation of defluorinated PFOS may not happen at the S side of PFOS. These results differ from what we saw with 4H-PFOS biodegradation, in which SO_4^{2-} was released during the reaction.

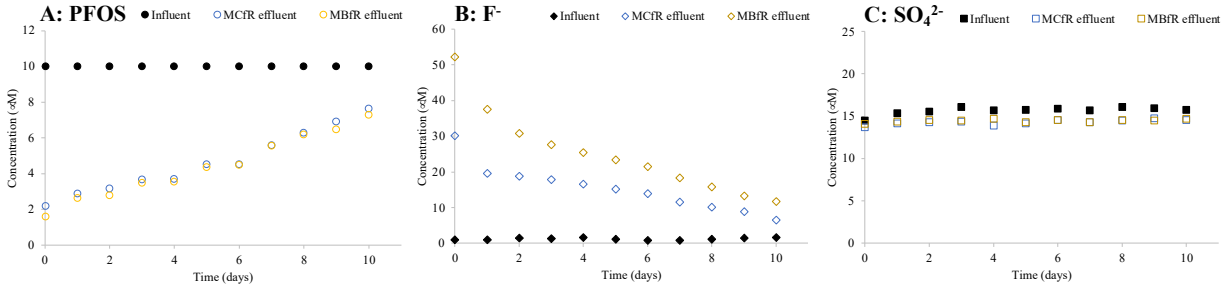

Figure 52. The F^- (A) and SO_4^{2-} (B) concentrations of influent and MCfR/MBfR effluents for PFOS removal.

We measured the PFOS and intermediates concentrations by HPLC-TOF. Figure 53A shows the relative abundances (based on the peak areas) of partially defluorinated PFOS, from 1H to 13H replacing F atoms in the PFOS molecule, for day 1 of the continuous PFOS removal in the synergistic platform. The less defluorinated PFOS (1H to 4H) were relatively more abundant than the highly defluorinated PFOS. Most of the partially defluorinated PFOS were not detected in the influent, although 1H to 4H and 7H were detected, probably due to contamination of the PFOS source. All the partially defluorinated PFOS had much higher concentrations in H_2-MCfR effluent than the O_2-MBfR effluent, which confirmed that partially defluorinated PFOSs produced in the H_2-MCfR were further removed and defluorinated in the subsequent O_2-MBfR.

Figure 53B shows the relative abundance of shorter chain perfluoro-carboxylic acids. PFOA was not detected in the synergistic platform. All the shorter chain perfluoro-carboxylic acids had higher relative abundance in the effluent of O_2-MBfR than the effluent of the H_2-MCfR or the influent. Trifluoroacetic acid (C2) had the higher abundance in O_2-MBfR, which indicates that it was the dominant biodegradation product. These results confirm that the partially defluorinated PFOSs produced in the H_2-MCfR were further oxidized to perfluoro-carboxylic acids in the subsequent O_2-MBfR.

Based on the HPLC-TOF results, we propose the three pathways shown in Fig. 53C for PFOS removal in the synergistic platform. In the H_2-MCfR, the reductive defluorination of PFOS replaced the F atoms near the S end/ C end or even the middle of carbon chain. Three different kinds of reductive defluorination products could lead to different biodegradation products. The S-end defluorination could enhance the removal of SO_3H group of PFOS and produce shorter chain perfluoro-carboxylic acids. The C-end defluorination could enhance carbon-side monooxygenation and produce the compounds with SO_3^- and COOH groups. The middle defluorination may lead to breaking the carbon chain in the middle. To prove the importance of the proposed pathways, we need to investigate for the presence of potential intermediates using HPLC-TOF; this would be a long-term effort.

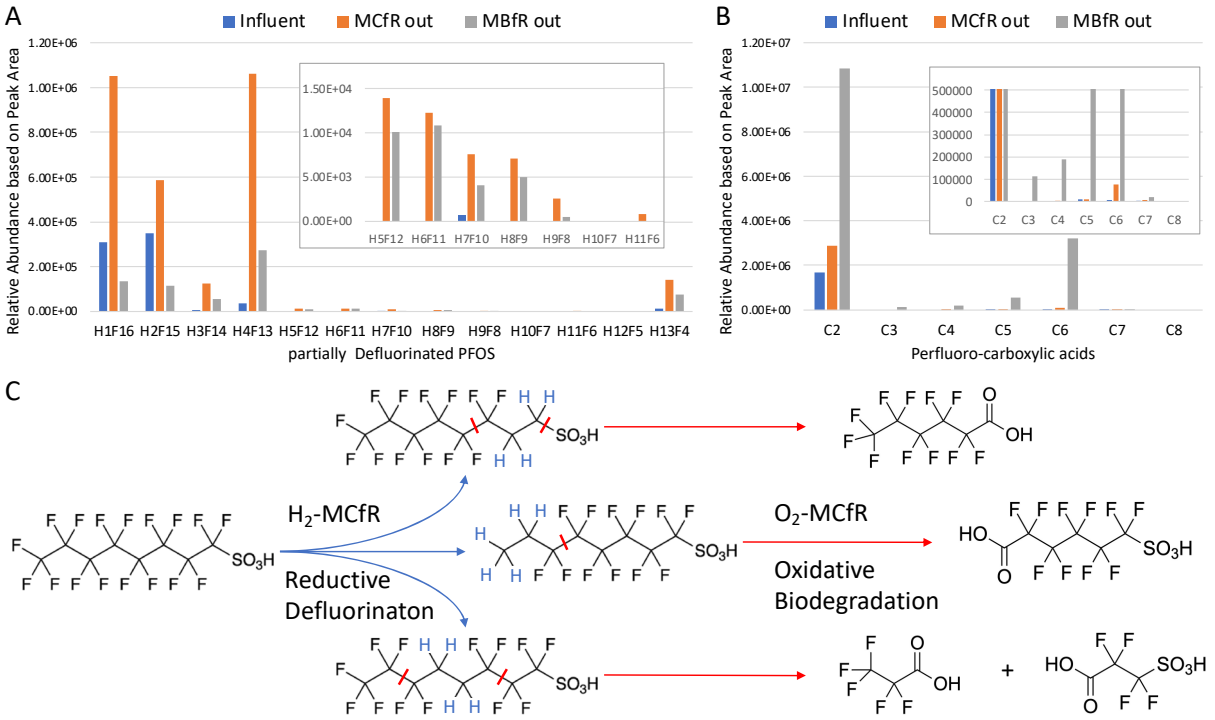

Figure 53. HPLC-TOF results for synergistic removal of PFOS on day 1. Measured concentrations of partially defluorinated PFOS (A) and shorter-chain perfluoro-carboxylic acids (B) in influent and in the effluents of the MCfR and MBfR. (C) A proposed PFOS-removal pathway in the synergistic platform.

4.4. Task 4: Cost analysis

Our goals for the cost analysis were to establish order-of-magnitude values for capital and operating costs and to identify the major factors contributing to costs. To do this, APTwater modified its design models to do a cost estimation for a H_2-MCfR along with an O_2-MBfR. Several different cost estimates were performed using results obtained directly from experimentation, along with what is believed to be achievable improvements for an ultimately optimized system. Each analysis assumed a typical flow rate of 100 gallons per minute. Additional common assumptions for each cost scenario may be found in Table 4. Each category of capital costs includes closely related component, as detailed in Table 5.

Table 4. Assumptions for a 100-gpm system

Assumption	Value	Unit
Influent flow rate	100	gpm
Surface area per module	143	m^2
Palladium unit cost	65	$/gram
Module replacement frequency	7	years

Table 5. Capital cost categories and component

Category	Component Details
Equipment	Auxiliary equipment for the modules, including tanks, pumps, piping, and instrumentation
ARoNite modules	The reactors themselves. Each are 6 feet in length, 1 foot in diameter, and contain 143 m^2 of available surface area.
Catalyst cost	Bulk cost for the catalyst required. No application cost included
System fabrication	The labor cost associated with building the system
Site improvement and design	The cost for permits, civil engineering, and design development of the system
Startup costs	The estimated cost for on-site support to start up the system
Contingency	20% of the total capital cost

For annual operating costs, $1/7^{th}$ the total cost for modules was included for module replacement each year. Each scenario assumed 100% destruction of PFOA and PFOS. Since H_2 demands were very small, H_2 generation was accomplished via on-demand electrolysis. O_2 for the MBfR was supplied by bulk liquid-O_2 cylinders. None of these costs included any mark up or separate costs for Pd deposition application.

The first cost-estimate scenario directly used the experimental results for a low influent concentration (500 ng/L for PFOA and 615 ng/L for PFOS). In this scenario, an O_2-MBfR was not utilized, because an H_2-MCfR alone should provide satisfactory removal of PFOA or PFOS. Table 6 contains the design basis for this "experimental" scenario. The Pd surface loading coating in this scenario was 1.2 mg/m^2, based directly on our previous SERDP project on MCfR with successful TCA/TCE dechlorination. Using these inputs, Table 7 shows the cost estimation for a 100-gpm system. The capital cost per gram of PFOA/PFOS removed was analyzed per year over a 10-year period. No discounted cash flow or inflation was accounted for in this number.

Table 6. Operational conditions and steady-state performances of an H_2-MCfR for environmental relevant (low) concentrations of PFOA and PFOS

Reactors		Operation Conditions	Parameters			
			Value 1	Unit 1	Value 2	Unit 2
MCfR1 PFOA	Operational conditions	Flow rate	1.67	mL/h	40	mL/day
		PFOA influent	500	ng/L	1.21	nmole/L
		PFOA loading	1099	ng/m^2-day	2.65	nmole/m^2-day
	Steady-state results	PFOA flux	956	ng/m^2-day	2.31	nmole/m^2-day
		PFOA removal	>87	%	>87	%
		PFOA effluent	<66	ng/L	<0.159	nmole/L
MCfR2 PFOS	Operational conditions	Flow rate	1.67	mL/h	40	mL/day
		PFOS influent	615	ng/L	1.23	nmole/L
		PFOS loading	1351	ng/m^2-day	2.7	nmole/m^2-day
	Steady-state results	PFOS flux	1321	ng/m^2-day	2.64	nmole/m^2-day
		PFOS removal	>97.8	%	>97.8	%
		PFOS effluent	<13	ng/L	<0.026	nmole/L

Using these inputs, Table 7 shows the cost estimation for a 100-gpm system. The capital cost per gram of PFOA/PFOS removed was analyzed per year over a 10-year period. No discounted cash flow or inflation was accounted for in this number.

Table 7. Budgetary capital and annual operating costs of a 100-gpm system (MCfR) for low PFOA and PFOS concentrations.

Budgetary Capital costs		
	Equipment (no modules) a	$6,306,683
	Aronite modules	$5,370,825
	Module Quantity	3769
	Catalyst cost	$42,039
	System fabrication	$695,000
	Site improvement and design	$1,225,000
	Startup costs	$52,800
	Contingency	$2,738,469
	Total installed cost	$16,430,817
	Installed cost per g of PFOA and PFOS over 10 year period	**$7,400**
Annual Operating Cost		
	Labor	$20,000
	Consumables	$0
	Parts and maintenance	$164,308
	Module Replacement	$773,266
	Power	$672,000
	Total annual costs	$1,629,575
	Total operating cost per g of PFOA and PFOS	**$7,300**

The next cost analysis, Scenario 2, used the same influent concentrations as Scenario 1, but assumed a 10-fold greater flux for PFOA and PFOS, since the influent concentration are orders of magnitude smaller than we used in the bench scale tests described in section 4.1.4.2. New fluxes were 9,560 ng/m^2-d for PFOA and 13,510 ng/m^2-d for PFOS. A Pd coating of 1.2 mg-Pd/m^2 again was used in this estimate. As with scenario 1, no MBfR was used in the cost analysis. Table 8 shows these cost estimate results. The increases in fluxes led to roughly 8-fold declines in per-g costs.

Table 8. Budgetary capital and annual operating costs of a 100-gpm system (MCfR) for 10 times higher PFOA and PFOS concentrations

Budgetary Capital costs (combined for PFOA and PFOS, no O_2 MBfR)		
	Equipment (no modules)	$863,000
	Aronite modules	$531,525
	Module Quantity	373
	Catalyst cost	$4,160
	System fabrication	$95,000
	Site improvement and design	$293,000
	Startup costs	$52,800
	Contingency	$367,897
	Total installed cost	$2,207,383
	Installed cost per g of PFOA and PFOS over 10 year period	**$990**
Annual Operating Cost (combined for PFOA and PFOS, no O_2 MBfR)		
	Labor	$20,000
	Consumables	$0
	Parts and maintenance	$22,074
	Module Replacement	$76,526
	Power	$69,600
	Total annual costs	$188,200
	Total operating cost per g of PFOA and PFOS	**$850**

We found comparable cost estimates in a CH2M-Hill report made for NAVFAC in 2020.[22] The report included a cost analysis using different technologies to treat a drinking-water well for PFOS located near the Oceana Naval Air Station in Virginia Beach, Virginia: GAC, ion exchange, and reverse osmosis were analyzed. No direct mention of the contamination load of PFOS or PFOA were mentioned, but it was noted that the level was above the USEPA Lifetime Health Advisory level of 70 ng/L. The assumption is the influent concentration was the same as in Table 5. The top of Table 9 shows highlights of the costs for ion exchange replacement and disposal for a treated flow of only 0.16 gpm, and the bottom of Table 9 extrapolates the costs to 100 gpm. Ion exchange was the least-cost option in the CH2M-Hill report. The 100-gpm costs in Table 9 are far higher than in Table 8 for the H_2-MCfR. For removing the same 615 ng/L PFOS at the same flow rate of 100 GPM, the capital cost of the ion exchange was $29 million. over one order of magnitude higher than the MCfR. The operating cost was $0.6 million, over three times thaty of the MCfR. Furthermore, all the processes tested in the CH2M-Hill project are non-destructive. This means that PFAS was transferred and concentrated from contaminated water, but not converted to less- or non-toxic compounds. Downstream treatment of the disposed materials containing concentrated PFAS is required and even more costly and energy-consuming. Overall, cost estimation and comparison confirm that destructive removal of PFAS using MCfR could be more efficient and economical than non-destructive approaches like GAC, ion exchange, and reversed osmosis.

Table 9. Summary of costs from the CH2M-Hill report made for NAVFAC.

Background NAS Oceana report		
influent	1115	ng/L PFOS and PFOA
Flow rate	7000	gal/month
resin cost	350	$/ft^3
resin amount	3	ft^3
exchange frequency	1	every two years
Exchange cost	525	$/yr
Capital Cost	47,810	$
Disposal costs		
$200 per disposal event		
$175 for profiling		
$49/ft^3 of material disposed		
Disposal cost	448.5	$/yr
Cost conversion for 100-gpm system		
Capital Cost	29,000,000	$
Exchange cost	324,000	$/yr
Disposal cost	277,000	$/yr

The next two cost scenarios use high influent concentrations of PFOS and PFOA (0.4 mg/L for PFOA and 0.5 mg/L for PFOS). The influent concentration s and fluxes are found in Tables 10 and 11; they are based directly on experimental results. Due to the high influent concentration, the two-stage synergistic platform is required. For the same reason, a greater Pd surface loading was used for the MCfR modules: 0.84 g-Pd/m^2.

Table 10. Operational conditions and steady-state performances for PFOA removal in the synergistic platform

Reactors			Parameters			
			Value 1	Unit 1	Value 2	Unit 2
MCfR	Operational conditions	Flow rate	1.5	mL/h	36	mL/day
		PFOA influent	0.4	mg/L	1	μmole/L
		PFOA loading	0.8	mg/m^2-day	2.0	μmole/m^2-day
	Steady-state results	PFOA flux	0.72	mg/m^2-day	1.79	μmole/m^2-day
		De-F flux	0.18	mg/m^2-day	9.49	μmole/m^2-day
		PFOA removal	90.5	%	-	-
		De-F rate	36.7	%	-	-
		PFOA effluent	0.04	mg/L	0.1	μmole/L
MBfR	Operational conditions	Flow rate	1.5	mL/h	36	mL/day
		PFOA influent	0.04	mg/L	0.1	μmole/L
		PFOA loading	0.08	mg/m^2-day	0.2	μmole/m^2-day
	Steady-state results	PFOA flux	0.072	mg/m^2-day	0.18	μmole/m^2-day
		De-F flux	0.16	mg/m^2-day	8.4	μmole/m^2-day
		PFOA removal	91.0	%	-	-
		De-F rate	69.2	%	-	-
		PFOA effluent	0.036	mg/L	0.09	μmole/L

Table 11. Operational conditions and steady-state performances for PFOS removal in the synergistic platform

Reactors			Parameters			
			Value 1	Unit 1	Value 2	Unit 2
MCfR	Operational conditions	Flow rate	1.5	mL/h	36	mL/day
		PFOS influent	0.5	mg/L	1	μmole/L
		PFOS loading	1.0	mg/m^2-day	2.0	μmole/m^2-day
	Steady-state results	PFOS flux	0.9	mg/m^2-day	1.79	μmole/m^2-day
		De-F flux	0.10	mg/m^2-day	5.37	μmole/m^2-day
		PFOS removal	90	%	-	-
		De-F rate	20.8	%	-	-
		PFOS effluent	0.05	mg/L	0.1	μmole/L
MBfR	Operational conditions	Flow rate	1.5	mL/h	36	mL/day
		PFOS influent	0.1	mg/L	0.1	μmole/L
		PFOS loading	0.10	mg/m^2-day	0.18	μmole/m^2-day
	Steady-state results	PFOS flux	0.05	mg/m^2-day	0.09	μmole/m^2-day
		De-F flux	0.07	mg/m^2-day	3.94	μmole/m^2-day
		PFOS removal	95	%	-	-
		De-F rate	36.0	%	-	-
		PFOS effluent	0.025	mg/L	0.05	μmole/L

Tables 12 and 13 summarize the costs for the high-concentration scenarios. Table 12 uses the experimentally established fluxes. Since the experimental results were of a proof-of-concept nature, not in any way optimized, realistic enhancements are to increase the fluxes of PFOA and PFOS to 10 mg/m^2-d, while lowering the Pd surface loading to 8.4 mg Pd/m^2, which was used successfully for continuous removal of TCE and TCA for over 90 days. Table 13, which summarizes the costs for this enhanced design of the synergistic platform, shows that it may be possible to treat PFOA or PFOS at unit costs around $1 per g installed capital cost (over 10 years) and $1/g operating costs using the synergistic platform.

Table 12. Budgetary capital and annual operating costs of a 100-gpm system (synergistic platform) for high PFOA and PFOS concentrations

Budgetary Capital costs (combined MCfR and MBfR)		
	Equipment (no modules)	$20,463,310
	Aronite modules	$18,176,425
	Module Quantity	12,743
	Catalyst Cost	$23,431,208
	System fabrication	$2,265,000
	Site improvement and design	$3,337,000
	Startup costs	$105,600
	Contingency	$13,555,709
	Total installed cost	$81,334,251
	Installed cost per g of PFOA and PFOS over 10-year period	**$45**
Annual Operating Cost (Combined MCfR and MBfR)		
	Labor	$30,000
	Consumables	$2,000
	Parts and maintenance	$813,343
	Module Replacement	$5,943,948
	Power	$2,267,000
	Total annual costs	$9,056,290
	Total operating cost per g of PFOA and PFOS	**$50**

Table 13. Budgetary capital and annual operating costs of a 100-gpm system (synergistic platform) for high PFOA and PFOS concentrations and lower Pd surface loading

Budgetary Capital costs (combined MCfR and MBfR)		
	Equipment (no modules)	$841,400
	Aronite modules	$374,850
	Module Quantity	263
	Catalyst Cost	$18,895
	System fabrication	$115,000
	Site improvement and design	$292,421
	Startup costs	$105,600
	Contigency	$349,633
	Total installed cost	$2,097,799
	Installed cost per g of PFOA and PFOS over 10-year period	**$1.2**
Annual Operating Cost (Combined MCfR and MBfR)		
	Labor	$36,667
	Consumables	$2,000
	Parts and maintenance	$20,978
	Module Replacement	$56,249
	Power	$54,200
	Total annual costs	$170,094
	Total operating cost per g of PFOA and PFOS	**$0.95**

4.5. Analytical Verification

PFOA and PFOS were coexisting compounds in verification samples. Samples 1-3 were the low-concentration influent, influent, and effluent of PFOA/PFOS, respectively. Table 14 compares the results from the Vista certified laboratory and the BSCEB (ASU) laboratory for the same samples. All measured values of samples 1-3 of the same order of magnitude, with differences from 9% to 38%. Both sets of data followed the same trend: effluent PFOA/PFOS concentration was about one order of magnitude lower for PFOA and at least three orders of magnitude lower for FFOS. Variations between the two laboratories can be best explained by the need for dilution and extraction steps.

Table 14. The PFOA and PFOS results obtained from the DoD certified lab (Vista, CA) compared to the BSCEB results

Sample #	ppt (ng/L)	Vista-PFOA	BSCEB-PFOA	Variation (%)-PFOA
1	Influent (low conc)	$7.6x10^3$	$5.5x10^3$	27
2	Influent	$1.3x10^7$	$1.2x10^7$	9.1
3	Effluent	$1.4x10^6$	$1.2x10^6$	18
#	ppt (ng/L)	Vista-PFOS	BSCEB-PFOS	Variation (%)-PFOS
1	Influent (low conc)	$1.7x10^4$	$1.03x10^4$	38
2	Influent	$1.1x10^7$	$1.3x10^7$	-18
3	Effluent	ND	$1.4x10^4$	NA

ND: not detectable with a detection limit of $1.2x10^4$ ng/L PFOS; NA: not available; Dilution factors were applied at 3X, 20X, and 10X for samples 1 to 3, respectively, for compound analysis at the Vista Laboratory; the same dilution factor was applied to sample 2, but not for samples 1 and 3 in the BSCEB laboratory.

4.6. Project Publications

1. Zhou, C., Y. Luo, C. Zheng, M. Long, X. Long, Y. Bi, X. Zheng, D. Zhou, and B. E. Rittmann 2021. H_2-Based Membrane Catalyst-Film Reactor (H2-MCfR) Loaded with Palladium for Removing Oxidized Contaminants in Water. *Environ. Sci. Technol*, 55(10), 7082-7093.

2. Long, M., Donoso, J., Bhati, M., Elias, W.C., Heck, K.N., Luo, Y.H., Lai, Y.S., Gu, H., Senftle, T.P., Zhou, C., Wong, M.S. and Rittmann, B.E., 2021. Adsorption and Reductive Defluorination of Perfluorooctanoic Acid over Palladium Nanoparticles. *Environmental Science & Technology*, 55(21), pp.14836-14843.

3. Long, M., Elias, W.C., Heck, K.N., Luo, Y.H., Lai, Y.S., Jin, Y., Gu, H., Donoso, J., Senftle, T.P., Zhou, C., Wong, M.S. and Rittmann, B.E., 2021. Hydrodefluorination of Perfluorooctanoic Acid in the H_2-Based Membrane Catalyst-Film Reactor with Platinum Group Metal Nanoparticles: Pathways and Optimal Conditions. *Environmental science & technology*, 55(24), pp. 16699-16707.

4. Long, M.; Elias, W. C.; Heck, K. N.; Senftle, T. P.; Luo, Y.-H.; Lai, Y. S.; Donoso, J.; Zhou, C.; Wong M. S.; Rittmann, B. E, 2022. Bimetallic Pd-Rh Nanoparticles Promoted H_2-Induced Catalytic Defluorination of PFOA at Neutral pH. (In preparation)

5. Luo, Y.H., Long, M., Lai, Y.S., Zhou, C. and Rittmann, B.E., 2022. Biodegradation of Fluorooctanoic Acid in the O_2-Based Membrane Bio-Film Reactor. (In preparation).

6. Luo, Y.H., Long, M., Lai, Y.S., Zhou, C. and Rittmann, B.E., 2022. Compete Mineralization of PFOA/PFOS by Reductive Defluorination Followed by Biodegradation in a Synergistic Platform. (In preparation).

5. Implications for Future Research and Benefits

5.1. Catalytic reductive defluorination

This study is the first report of Pd^0-based catalyzed defluorination of perfluorinated compounds. Fast adsorption of PFOA and PFOS and the release of F^- and partially and fully defluorinated compounds verified that the H_2-MCfR catalytically removed and destroyed PFAS. Defluorination preceded by PFOA adsorption in a parallel orientation enabled a fast reaction between F substituents on PFOA/S and activated H on the Pd^0 surface. The addition of a promoter metal enabled Pd-based bimetallic catalysts to defluorinate PFOA and PFOS at neutral pH. Operating under continuous flow, the MCfR was capable of sustained removal of PFOA at environmentally relevant concentrations, averaging 97% removal, to well below 70 ng/L, for more than two months.

The success is based on the efficient H_2 delivery to the nanoparticle catalysts in the MCfR. In the conventional heterogeneous catalysis, Pd^0 is supported on solid carriers, but H_2 is delivered from the headspace or by sparging. In that setting, non-reactive adsorption of PFOA/S occurs quickly due to slow H_2 mass transfer from the liquid phase to the catalyst surface; this leads to slow defluorination kinetics and accentuated deactivation. leading to no defluorination. In contrast, the nonporous membrane in the MCfR circumvents mass-transfer limitation delivering bubble-free H_2 directly to the Pd^0 film. Consequently, H* can be amply available at the Pd^0 surface of Pd^0, which blocks vertical non-defluorinative adsorption and promotes defluorination via parallel adsorption.

Hydrodefluorination at the MCfR's Pd^0 surface ought to be widely applicable for PFAS. Our results documented hydrodefluorination of PFOA, PFOS, and their partially defluorinated intermediates. This supports the generality of PFAS hydrodefluorination in the MCfR.

5.2. Biodegradation

The continuous oxidative biomineralization of partially defluorinated PFOA/S in the O_2-MBfR proved the capability of MBfR biofilms for further biodegradation and mineralization of PFOA/S-hydrodefluorination products from the H_2-MCfR. Metagenomic sequencing revealed dominant bacteria in the OA and OS biodegradation biofilm communities, and they contained the key functional genes for biotransformation of PFOA/S products. For example, the PFOA-biofilms had many genes for β-oxidation: e.g., β-oxidation of 2H-PFOA released two F^- and shortened the molecular from 8C to 6C. Likewise, the PFAS biofilms had monooxygenases able to release a sulfate from the 4H-PFOS molecule and produce 2H-PFOA. The results document the potential of the O_2-MBfR to biodegrade partially defluorinated PFOA/S.

5.3. Synergistic platform

Combining catalytic reductive defluorination and oxidative biodegradation creates the synergistic platform. Continuous experiments with the synergistic platform proved that the H_2-MCfR and O_2-MBfR worked as expected when linked together in the synergistic platform: partially defluorinated products from the MCfR were further defluorinated in the MBfR. The

defluorinated ratio in H_2-MCfR affected the biodegradation in O_2-MBfR, with more hydrodefluorination in thr MCfR allowing more oxidative biodefluorination in the MBfR. Compete mineralization of PFOA/S should be achieved when proper distribution of defluorination between the MCfR and MBfR is well-established by future research.

5.4. Cost analysis

Overall system cost depends strongly on the PFOA/S flux and the surface loading of catalyst required in the MCfR. The required flux is especially important, because it controls the number of modules, along with support equipment, including pumps, tanks, pipelines, and operating expenses that include maintenance and power. If PFOA/S flux and catalyst loading can be reduced through future research and development, capital and operating costs could become far less than for competing technologies.

5.5. Summary of future research needs

Low-concentration PFAS with the MCfR only. In most of the contaminated groundwaters and surface waters, PFAS concentrations less than 1 ppb. The MCfR has shown stable performance for removing environmental-relevant concentration of PFOA to below EPA health advisory level (70 ppt) for at least 3 months. Given that partially fluorinated hydrocarbons have not been regulated and the total concentrations of these products from the MCfR was minimal, we propose to focus on the H_2-MCfR for low-level contaminated water (e.g., < 100 ppb).

PFAS compounds other than PFOA/PFOS. The shorter chain PFAS (C2-C7) are found in contaminated soils and water, ranging from 0-2.5 ppb in groundwater and reaching up to 373,000 μg/kg in AFFF-contaminated sites.[74,75] An essential next step involves solidifying understanding of the hydrodefluorination capability and its underlying mechanisms by analyzing shorter-chain per-fluorinated carboxylic acids (PFCAs, C2 – C7). We hypothesize that longer chain PFAS will be more easily adsorbed by catalyst`s due to the higher adsorption affinity of longer-chain fatty acids; they also will be more readily defluorinated due to their lower carbon-fluoride dissociation energy. However, the shorter-chain (C2 – C7) PFCAs will products from the O_2-MBfR and must be evaluated.

Understanding the impact of chain length will require research that integrates experiments using catalysts *in situ* deposited on gas-transfer membranes; mechanistic modeling of the parallel adsorption, defluorination, and desorption reactions occurring at the NP surfaces; and DFT evaluation of PFASs competing adsorption modes and hydrogenation mechanisms. Special focus needs to be placed on the shorter-chain (C2 – C4) PFCAs, because they will not have PFOA's strong surface-adsorptive behavior. The C2-C4 PFCAs and their partially or fully hydrodefluorinated counterparts are water soluble, allowing for much easier product identification (fewer isomers), concentration quantification, and mass balance verification. Furthermore, the shorter-chain PFCAs are pollutants of emerging concern, e.g., at sites contaminated with AFFF formulations, and are even more difficult to remove from water than PFOA and other longer-chain PFAS using conventional approaches.[76–78]

High concentration with the synergistic platform with recycling. In some important situations, high concentrations of PFAS are present. For example, wastewater generated from the photolithographic process in a semiconductor industry was reported to have PFOS and PFOA in the concentration of 1,650-3,000 mg/L and 1,000 mg/L, respectively. The levels of PFOS and PFOA in surface water near industrial zone vary in range of 0.1 – 5,700 ng/L and 0.7 – 19,200 ng/L, and higher concentrations (up to several mg L^{-1} for PFOS and PFOA) have been measured in groundwater collected from military bases where aqueous film-forming foams (AFFF) are used for fire-training activities. The synergistic platform is most appropriate for these high-concentration situations. Reductive defluorination in H_2-MCfR yields partially fluorinated compounds (e.g., $C_8H_xF_{16-x}O_2$ and $C_8H_xF_{18-x}O_3S$), their subsequent biodegradation in O_2-MBfR eventually produces perfluorinated shorter-chain carboxylic or sulfonic acids (C<7). These perfluorinated acids, similarly to their longer-chain counterparts like PFOA and PFOS, probably cannot be further biodegraded in the MBfR, but can be reductively defluorinated in the MCfR. Thus, we propose recycling the O_2-MBfR effluent to the H_2-MCfR, as illustrated in Figure 54. Recycling should enable the shorter chain perfluorinated acids be reductively defluorinated in the H_2-MCfR, along with the original substrates (PFOA and PFOS). Several passes through the two-stage system should allow for complete defluorination and mineralization.

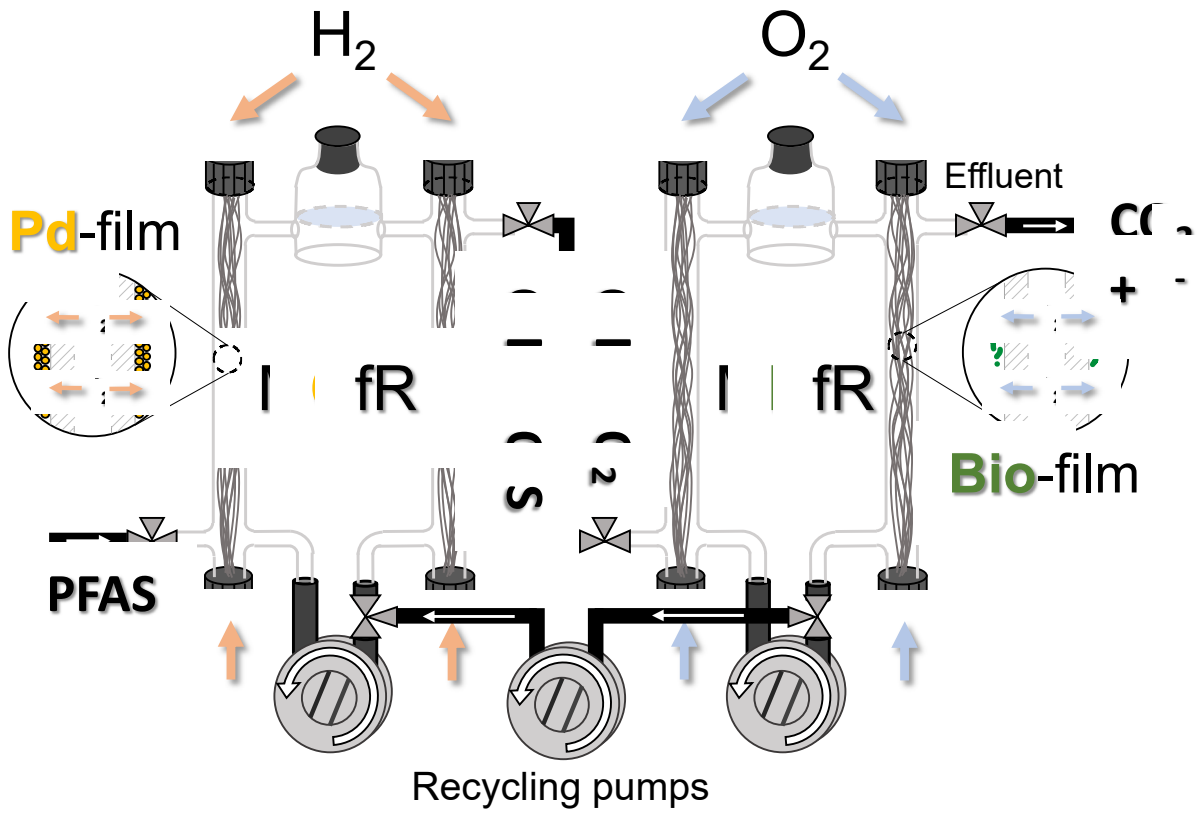

Figure 54. Schematic of the synergistic platform with recycling from the MBfR back to the MCfR.

Treatment of PFAS in real wastewater/groundwater. The presence of anions (e,g., sulfur components)[79,80] in real wastewater and groundwater could deactivate catalyst performance. In addition, real PFAS-contaminated waters contain many PFAS compounds, which may create competitive inhibition.[81–83]

Deactivation/poisoning could be associated with anions bonding with the Pd-NMP surface. The H_2-MCfR operated at lower pH (i.e., pH 4) has shown better defluorination performance than with higher pHs. The pH affects anion speciation and tendency to adsorb on the Pd surface. It would be valuable to understand how pH affects anion adsorption and potential deactivation.

Competition will be affected by differences of electronic and adsorptive affinities among the short and long alkyl chains of PFAS. On one hand, the presence of mother compounds, e.g., PFOA or PFOS, might inhibit their daughter products' further defluorination, or vice versa. On the other hand, our results already demonstrated competition between PFOA and PFOS. The active surface area of Pd^0 is finite, and strong surface adsorption by one compound could inhibit adsorption and the defluorination of others. Since adsorption competition among PFAS is far from understood, systematic evaluation of adsorption kinetics and thermodynamics will have large marginal benefits towards minimizing negative impacts of competition in actual PFAS-contaminated waters.

5.6. Future research priorities

Task 1 (first year of two years): Fundamental research on the MCfR

1) PFAS other than PFOA and PFOS (PFCAs)

Since our previous studies showed that Rhodium (Rh) was superior as the promoting metal, the team will continue evaluating Pd/Rh, along with mono-Pd. While a practical sub-goal is to obtain the smallest amount of the second metal that acts as an effective promoter, the mechanistic goal is to generate results that test our hypotheses about the interactions of adsorption and reductive defluorination on the NP surface. The team will begin by conducting a series of mechanism-oriented batch kinetics tests that systematically vary catalyst loading, H_2-supply pressure, and the PFCA. While the team will test the PFCA range of C2 – C7, it will focus on C2 – C4 in order to maximize our ability to gain mechanistic insight. The team also will operate in the continuous-flow mode to understand long-term performance for PFCAs co-removal and possible impacts of catalyst fouling or loss. To quantify removal and defluorination kinetics, the team will assay the influent and effluent for all possible (non)fluorinated carboxyl acid species using the high-performance liquid chromatography–quadrupole-time of flight mass spectrometry (HPLC-QTOF-MS) and F^- ions using ion-exchange chromatography (IC). The team also is able to extract PFCAs from the NPs at the end of an experiment, and this will allow the team to provide information on the reaction mechanisms. The team also will advance and apply DFT computation to understand the interactions between the PCFAs and the mono- and bi-metallic surfaces. This will include DFT evaluation of the competing PFCA-adsorption modes and their relative binding strengths, as well as evaluation of barriers for candidate hydrogenation mechanisms to identify the most favorable reaction path on surfaces with varying composition.

2) Impact of sulfur anions

Among the oxygenic chemicals present in the aqueous environment, sulfate is one of the important elements to study, because it is commonly present in contaminated waters and can be reduced to sulfite and sulfide, which are known catalyst poisons.[84] In addition, the functional group for PFOS is sulfonic acid, which can be released and then reduced to sulfide in the via H_2-MCfR. Therefore, it will be important to understand the impact of sulfur on catalytic performance. We will evaluate defluorination efficiency for ~5 ppm PFOA and PFOS in the presence of up to 120 mg/L input sulfate (0, 5, 10, 40, 80, and 120 mg/L). we will assay for sulfite and sulfide, as well as defluorination efficiency. If we see evidence of sulfur-related deactivation, we will evaluate sulfur speciation the catalysts' surface, i.e., direct inhibition by sulfate or a reduced sulfur compound.

Task 2 (first year): MCfR-MBfR synergy with recycling

Reductive defluorination in H_2-MCfR yields various partially fluorinated compounds (e.g., $C_8H_xF_{16-x}O_2$ and $C_8H_xF_{18-x}O_3S$), and their subsequent biodegradation in O_2-MBfR eventually produces perfluorinated shorter-chain carboxylic or sulfonic acids ($C \leq 7$). These perfluorinated acids, similarly to their longer-chain counterparts like PFOA and PFOS, cannot be further

biodegraded in the MBfR, but should be reductively defluorinated in the MCfR. Thus, we propose to evaluate a strategy featuring recycling of the O_2-MBfR effluent to the H_2-MCfR (Figure 54). To test this hypothesis, we will recycle the H_2-MBfR effluent with a peristaltic pump and monitor the products in effluents. By monitoring the products composition in H_2-MCfR and O_2-MBfR, we can test our hypothesis that biodegradation-produced per-fluorinated shorter-chain PFCAs can be further reduced through hydrodefluorination, ultimately leading to full mineralization in the MBfR. We will vary the recycling flow rate (e.g., ranging from 0.5 to 5 times of influent flow rate), evaluate the impact of recycling on the biofilm communities, and evaluate effects of recycled compounds (e.g., O_2 and bacteria secretions) on the H_2-MCfR.

Task 3 (in the second year of two years): Setup and test a small pilot-scale MCfR for low-concentration PFAS removal

2.1 Catalyst synthesis and deposition in mini modules (3-4 months)

APTwater can supply "mini modules" that have the same configuration as the full-scale ARoNite modules, but have about 8% of the surface area and 18% of the volume. They are ideal for small-scale pilot testing. The first step is to evaluate our ability to carry out nanocatalyst *in situ* synthesis and deposition. The *in situ* method has been simple and reliable with our bench-scale MCfRs, but the mini-modules are larger and have much higher membrane density. Therefore, we will need to develop a reliable *in situ* method for the mini-modules.

2.2 PFAS testing using synthetic water (3-4 months)

We will first obtain real water samples from some contaminated sites and conduct comprehensive analysis of the key components, including PFAS types and concentrations, pH, alkalinity, salinity, total organic carbon (TOC), and other possible co-contaminants (i.e., nitrate and sulfate). We will then synthesize in the lab a feeding medium mimicking the basic composition of the real water, except for some potentially inhibitory factors to be figured out in Task 1 (e.g., sulfur species). We will feed the synergistic MCfR-MBfR with the basic medium first.

2.3 PFAS testing using real contaminated water (3-4 months)

In this sub-task, we will feed the real water obtained in 2.1 and feed it directly to the MCfR-MBfR system (from 2.2) and test PFAS removal. Long-term performance of continuous removal of PFAS from real contaminated water will be documented and will support the feasibility of on-site implementation of larger-scale MCfR-MBfR systems in a follow up ESTCP study

2.4 Prepare a plan for a field pilot (2 months)

Assuming that the results in 2.1 – 2.3 are promising, we will prepare a plan for an ESTCP-supported pilot study in the field. We will engage industry partners for the field pilot.

Literature Cited

(1) Wang, Z.; Dewitt, J. C.; Higgins, C. P.; Cousins, I. T. A Never-Ending Story of Per- and Polyfluoroalkyl Substances (PFASs)? *Environ. Sci. Technol.* **2017**, *51* (5), 2508–2518. https://doi.org/10.1021/acs.est.6b04806.

(2) Moody, C. A.; Field, J. A. Perfluorinated Surfactants and the Environmental Implications of Their Use in Fire-Fighting Foams. *Environ. Sci. Technol.* **2000**, *34* (18), 3864–3870.

(3) Zareitalabad, P.; Siemens, J.; Hamer, M.; Amelung, W. Perfluorooctanoic Acid (PFOA) and Perfluorooctanesulfonic Acid (PFOS) in Surface Waters, Sediments, Soils and Wastewater–A Review on Concentrations and Distribution Coefficients. *Chemosphere* **2013**, *91* (6), 725–732.

(4) D'Hollander, W.; Roosens, L.; Covaci, A.; Cornelis, C.; Reynders, H.; Van Campenhout, K.; de Voogt, P.; Bervoets, L. Brominated Flame Retardants and Perfluorinated Compounds in Indoor Dust from Homes and Offices in Flanders, Belgium. *Chemosphere* **2010**, *81* (4), 478–487.

(5) Iyer, P. *The Global Soul: Jet Lag, Shopping Malls, and the Search for Home*; Vintage, 2011.

(6) Olsen, G. W.; Burris, J. M.; Mandel, J. H.; Zobel, L. R. Serum Perfluorooctane Sulfonate and Hepatic and Lipid Clinical Chemistry Tests in Fluorochemical Production Employees. *J. Occup. Environ. Med.* **1999**, *41* (9), 799–806.

(7) Giesy, J. P.; Kannan, K. Global Distribution of Perfluorooctane Sulfonate in Wildlife. *Environ. Sci. Technol.* **2001**, *35* (7), 1339–1342.

(8) Hekster, F. M.; Laane, R. W. P. M.; De Voogt, P. Environmental and Toxicity Effects of Perfluoroalkylated Substances. *Rev. Environ. Contam. Toxicol.* **2003**, 99–121.

(9) Lau, C.; Anitole, K.; Hodes, C.; Lai, D.; Pfahles-Hutchens, A.; Seed, J. Perfluoroalkyl Acids: A Review of Monitoring and Toxicological Findings. *Toxicol. Sci.* **2007**, *99* (2), 366–394.

(10) Steenland, K.; Fletcher, T.; Savitz, D. A. Epidemiologic Evidence on the Health Effects of Perfluorooctanoic Acid (PFOA). *Environ. Health Perspect.* **2010**, *118* (8), 1100–1108.

(11) Prevedouros, K.; Cousins, I. T.; Buck, R. C.; Korzeniowski, S. H. Sources, Fate and Transport of Perfluorocarboxylates. *Environ. Sci. Technol.* **2006**, *40* (1), 32–44.

(12) Ding, G.; Peijnenburg, W. J. G. M. Physicochemical Properties and Aquatic Toxicity of Poly-and Perfluorinated Compounds. *Crit. Rev. Environ. Sci. Technol.* **2013**, *43* (6), 598–678.

(13) Key, B. D.; Howell, R. D.; Criddle, C. S. Fluorinated Organics in the Biosphere. *Environ. Sci. Technol.* **1997**, *31* (9), 2445–2454.

(14) Huang, S.; Jaffé, P. R. Defluorination of Perfluorooctanoic Acid (PFOA) and Perfluorooctane Sulfonate (PFOS) by Acidimicrobium Sp. Strain A6. *Environ. Sci. Technol.* **2019**, *53* (19), 11410–11419.

(15) Santos, A.; Rodríguez, S.; Pardo, F.; Romero, A. Use of Fenton Reagent Combined with Humic Acids for the Removal of PFOA from Contaminated Water. *Sci. Total Environ.* **2016**, *563*, 657–663.

(16) Li, S.; Zhang, G.; Zhang, W.; Zheng, H.; Zhu, W.; Sun, N.; Zheng, Y.; Wang, P. Microwave Enhanced Fenton-like Process for Degradation of Perfluorooctanoic Acid (PFOA) Using Pb-BiFeO3/RGO as Heterogeneous Catalyst. *Chem. Eng. J.* **2017**, *326*, 756–764.

(17) Wang, Y.; Zhang, P. Photocatalytic Decomposition of Perfluorooctanoic Acid (PFOA) by TiO2 in the Presence of Oxalic Acid. *J. Hazard. Mater.* **2011**, *192* (3), 1869–1875.

(18) Zhao, B.; Zhang, P. Photocatalytic Decomposition of Perfluorooctanoic Acid with β-Ga2O3 Wide Bandgap Photocatalyst. *Catal. Commun.* **2009**, *10* (8), 1184–1187.

(19) Yamada, T.; Taylor, P. H.; Buck, R. C.; Kaiser, M. A.; Giraud, R. J. Thermal Degradation of Fluorotelomer Treated Articles and Related Materials. *Chemosphere* **2005**, *61* (7), 974–984.

(20) Merino, N.; Qu, Y.; Deeb, R. A.; Hawley, E. L.; Hoffmann, M. R.; Mahendra, S. Degradation and Removal Methods for Perfluoroalkyl and Polyfluoroalkyl Substances in Water. *Environ. Eng. Sci.* **2016**, *33* (9), 615–649.

(21) Trojanowicz, M.; Bojanowska-Czajka, A.; Bartosiewicz, I.; Kulisa, K. Advanced Oxidation/Reduction Processes Treatment for Aqueous Perfluorooctanoate (PFOA) and Perfluorooctanesulfonate (PFOS)–a Review of Recent Advances. *Chem. Eng. J.* **2018**, *336*, 170–199.

(22) Beach, V.; Beach, V. *Engineering Evaluation and Cost Analysis for Private Drinking Water*; 2020.

(23) Sheets-Johnstone, M. *The Corporeal Turn: An Interdisciplinary Reader*; Andrews UK Limited, 2015.

(24) De Corte, S.; Hennebel, T.; De Gusseme, B.; Verstraete, W.; Boon, N. Bio-palladium: From Metal Recovery to Catalytic Applications. *Microb. Biotechnol.* **2012**, *5* (1), 5–17.

(25) McGlone, T.; Briggs, N. E. B.; Clark, C. A.; Brown, C. J.; Sefcik, J.; Florence, A. J. Oscillatory Flow Reactors (OFRs) for Continuous Manufacturing and Crystallization. *Org. Process Res. Dev.* **2015**, *19* (9), 1186–1202.

(26) Hoque, M. E.; Philip, O. J. Biotechnological Recovery of Heavy Metals from Secondary Sources—An Overview. *Mater. Sci. Eng. C* **2011**, *31* (2), 57–66.

(27) Zhou, D.; Luo, Y. H.; Zheng, C. W.; Long, M.; Long, X.; Bi, Y.; Zheng, X.; Zhou, C.; Rittmann, B. E. H2-Based Membrane Catalyst-Film Reactor (H2-MCfR) Loaded with Palladium for Removing Oxidized Contaminants in Water. *Environ. Sci. Technol.* **2021**, *55* (10), 7082–7093. https://doi.org/10.1021/acs.est.1c01189.

(28) Cai, Y.; Long, X.; Luo, Y.-H.; Zhou, C.; Rittmann, B. E. Stable Dechlorination of Trichloroacetic Acid (TCAA) to Acetic Acid Catalyzed by Palladium Nanoparticles Deposited on H2-Transfer Membranes. *Water Res.* **2021**, *192* (15), 116841.

(29) Zhou, C.; Ontiveros-Valencia, A.; Nerenberg, R.; Tang, Y.; Friese, D.; Krajmalnik-Brown, R.; Rittmann, B. E. Hydrogenotrophic Microbial Reduction of Oxyanions with the Membrane Biofilm Reactor. *Front. Microbiol.* **2019**, *9*, 3268.

(30) Luo, Y.-H.; Chen, R.; Wen, L.-L.; Meng, F.; Zhang, Y.; Lai, C.-Y.; Rittmann, B. E.; Zhao, H.-P.; Zheng, P. Complete Perchlorate Reduction Using Methane as the Sole Electron

Donor and Carbon Source. *Environ. Sci. Technol.* **2015**, *49* (4). https://doi.org/10.1021/es504990m.

(31) Luo, Y.-H.; Long, X.; Wang, B.; Zhou, C.; Tang, Y.; Krajmalnik-Brown, R.; Rittmann, B. E. A Synergistic Platform for Continuous Co-Removal of 1, 1, 1-Trichloroethane, Trichloroethene, and 1, 4-Dioxane via Catalytic Dechlorination Followed by Biodegradation. *Environ. Sci. Technol.* **2021**.

(32) Shoemaker, J. A.; Grimmett, P. E. *Method-537-US EPA*; 2009.

(33) Zhou, C.; Wang, Z.; Ontiveros-Valencia, A.; Long, M.; Lai, C. yu; Zhao, H. ping; Xia, S.; Rittmann, B. E. Coupling of Pd Nanoparticles and Denitrifying Biofilm Promotes H2-Based Nitrate Removal with Greater Selectivity towards N2. *Appl. Catal. B Environ.* **2017**, *206*, 461–470. https://doi.org/10.1016/j.apcatb.2017.01.068.

(34) Kresse, G.; Furthmüller, J. Efficient Iterative Schemes for Ab Initio Total-Energy Calculations Using a Plane-Wave Basis Set. *Phys. Rev. B* **1996**, *54* (16), 11169.

(35) Kresse, G.; Furthmüller, J. Efficiency of Ab-Initio Total Energy Calculations for Metals and Semiconductors Using a Plane-Wave Basis Set. *Comput. Mater. Sci.* **1996**, *6* (1), 15–50.

(36) Mathew, K.; Sundararaman, R.; Letchworth-Weaver, K.; Arias, T. A.; Hennig, R. G. Implicit Solvation Model for Density-Functional Study of Nanocrystal Surfaces and Reaction Pathways. *J. Chem. Phys.* **2014**, *140* (8), 84106.

(37) Mathew, K.; Kolluru, V. S. C.; Mula, S.; Steinmann, S. N.; Hennig, R. G. Implicit Self-Consistent Electrolyte Model in Plane-Wave Density-Functional Theory. *J. Chem. Phys.* **2019**, *151* (23), 234101.

(38) Perdew, J. P.; Burke, K.; Ernzerhof, M. Generalized Gradient Approximation Made Simple. *Phys. Rev. Lett.* **1996**, *77* (18), 3865.

(39) Kresse, G.; Joubert, D. From Ultrasoft Pseudopotentials to the Projector Augmented-Wave Method. *Phys. Rev. b* **1999**, *59* (3), 1758.

(40) Monkhorst, H. J.; Pack, J. D. Special Points for Brillouin-Zone Integrations. *Phys. Rev. B* **1976**, *13* (12), 5188.

(41) Methfessel, M.; Paxton, A. T. High-Precision Sampling for Brillouin-Zone Integration in Metals. *Phys. Rev. B* **1989**, *40* (6), 3616.

(42) Grimme, S.; Antony, J.; Ehrlich, S.; Krieg, H. A Consistent and Accurate Ab Initio Parametrization of Density Functional Dispersion Correction (DFT-D) for the 94 Elements H-Pu. *J. Chem. Phys.* **2010**, *132* (15), 154104.

(43) Gauthier, J. A.; Ringe, S.; Dickens, C. F.; Garza, A. J.; Bell, A. T.; Head-Gordon, M.; Nørskov, J. K.; Chan, K. Challenges in Modeling Electrochemical Reaction Energetics with Polarizable Continuum Models. *ACS Catal.* **2018**, *9* (2), 920–931.

(44) Bhati, M.; Chen, Y.; Senftle, T. P. Density Functional Theory Modeling of Photo-Electrochemical Reactions on Semiconductors: H2 Evolution on 3C-SiC. *J. Phys. Chem. C* **2020**, *124* (49), 26625–26639.

(45) Bolger, A. M.; Lohse, M.; Usadel, B. Trimmomatic: A Flexible Trimmer for Illumina Sequence Data. *Bioinformatics* **2014**, *30* (15), 2114–2120.

(46) Parks, D. H.; Chuvochina, M.; Chaumeil, P.-A.; Rinke, C.; Mussig, A. J.; Hugenholtz, P. A Complete Domain-to-Species Taxonomy for Bacteria and Archaea. *Nat. Biotechnol.* **2020**, *38* (9), 1079–1086.

(47) Chaumeil, P.-A.; Mussig, A. J.; Hugenholtz, P.; Parks, D. H. GTDB-Tk: A Toolkit to Classify Genomes with the Genome Taxonomy Database. Oxford University Press 2020.

(48) Menzel, P.; Ng, K. L.; Krogh, A. Fast and Sensitive Taxonomic Classification for Metagenomics with Kaiju. *Nat. Commun.* **2016**, *7* (1), 1–9.

(49) Manzini, G. An Analysis of the Burrows—Wheeler Transform. *J. ACM* **2001**, *48* (3), 407–430.

(50) Meinicke, P. UProC: Tools for Ultra-Fast Protein Domain Classification. *Bioinformatics* **2015**, *31* (9), 1382–1388.

(51) Meinicke, J.; Thüm, T.; Schröter, R.; Benduhn, F.; Saake, G. An Overview on Analysis Tools for Software Product Lines; 2014; pp 94–101.

(52) Wagner, G. P.; Kin, K.; Lynch, V. J. Measurement of MRNA Abundance Using RNA-Seq Data: RPKM Measure Is Inconsistent among Samples. *Theory Biosci.* **2012**, *131* (4), 281–285.

(53) Luo, Y.-H.; Long, X.; Wang, B.; Zhou, C.; Tang, Y.; Krajmalnik-Brown, R.; Rittmann, B. E. A Synergistic Platform for Continuous Co-Removal of 1, 1, 1-Trichloroethane, Trichloroethene, and 1, 4-Dioxane via Catalytic Dechlorination Followed by Biodegradation. *Environ. Sci. Technol.* **2021**, *55* (9), 6363–6372.

(54) Saldan, I.; Semenyuk, Y.; Marchuk, I.; Reshetnyak, O. Chemical Synthesis and Application of Palladium Nanoparticles. *J. Mater. Sci.* **2015**, *50* (6), 2337–2354.

(55) Clark, C. A.; Reddy, C. P.; Xu, H.; Heck, K. N.; Luo, G.; Senftle, T. P.; Wong, M. S. Mechanistic Insights into PH-Controlled Nitrite Reduction to Ammonia and Hydrazine over Rhodium. *ACS Catal.* **2019**, *10* (1), 494–509.

(56) Chaplin, B. P.; Reinhard, M.; Schneider, W. F.; Schüth, C.; Shapley, J. R.; Strathmann, T. J.; Werth, C. J. Critical Review of Pd-Based Catalytic Treatment of Priority Contaminants in Water. *Environ. Sci. Technol.* **2012**, *46* (7), 3655–3670.

(57) Kopinke, F.-D.; Mackenzie, K.; Koehler, R.; Georgi, A. Alternative Sources of Hydrogen for Hydrodechlorination of Chlorinated Organic Compounds in Water on Pd Catalysts. *Appl. Catal. A Gen.* **2004**, *271* (1–2), 119–128.

(58) Park, J.; An, S.; Jho, E. H.; Bae, S.; Choi, Y.; Choe, J. K. Exploring Reductive Degradation of Fluorinated Pharmaceuticals Using Al2O3-Supported Pt-Group Metallic Catalysts: Catalytic Reactivity, Reaction Pathways, and Toxicity Assessment. *Water Res.* **2020**, *185*, 116242.

(59) Lee, Y.-C.; Chen, Y.-P.; Chen, M.-J.; Kuo, J.; Lo, S.-L. Reductive Defluorination of Perfluorooctanoic Acid by Titanium (III) Citrate with Vitamin B12 and Copper Nanoparticles. *J. Hazard. Mater.* **2017**, *340*, 336–343.

(60) Wu, Z.; Pan, T.; Chai, Y.; Ge, S.; Ju, Y.; Li, T.; Liu, K.; Lan, L.; Yip, A. C. K.; Zhang, M. Synthesis of Palladium Phosphides for Aqueous Phase Hydrodechlorination: Kinetic Study and Deactivation Resistance. *J. Catal.* **2018**, *366*, 80–90.

(61) Long, M.; Long, X.; Zheng, C.-W.; Luo, Y.-H.; Zhou, C.; Rittmann, B. E. Para-Chlorophenol (4-CP) Removal by a Palladium-Coated Biofilm: Coupling Catalytic Dechlorination and Microbial Mineralization via Denitrification. *Environ. Sci. Technol.* **2021**, *55* (9), 6309–6319.

(62) Luo, Y.-H.; Zhou, C.; Bi, Y.; Long, X.; Wang, B.; Tang, Y.; Krajmalnik-Brown, R.; Rittmann, B. E. Long-Term Continuous Co-Reduction of 1, 1, 1-Trichloroethane and Trichloroethene over Palladium Nanoparticles Spontaneously Deposited on H2-Transfer Membranes. *Environ. Sci. Technol.* **2021**, *55* (3), 2057–2066.

(63) Freitas, A. F.; Mendes, M. F.; Coelho, G. L. V. Thermodynamic Study of Fatty Acids Adsorption on Different Adsorbents. *J. Chem. Thermodyn.* **2007**, *39* (7), 1027–1037.

(64) Lefèvre, G.; Preočanin, T.; Lützenkirchen, J. *Attenuated Total Reflection-Infrared Spectroscopy Applied to the Study of Mineral-Aqueous Electrolyte Solution Interfaces: A General Overview and a Case Study*; IntechOpen, 2012; Vol. 1.

(65) Zalineeva, A.; Baranton, S.; Coutanceau, C. How Do Bi-Modified Palladium Nanoparticles Work towards Glycerol Electrooxidation? An in Situ FTIR Study. *Electrochim. Acta* **2015**, *176*, 705–717.

(66) Gao, X.; Chorover, J. Adsorption of Perfluorooctanoic Acid and Perfluorooctanesulfonic Acid to Iron Oxide Surfaces as Studied by Flow-through ATR-FTIR Spectroscopy. *Environ. Chem.* **2012**, *9* (2), 148–157.

(67) Long, M.; Donoso, J.; Bhati, M.; Elias, W. C.; Heck, K. N.; Luo, Y.-H.; Lai, Y. S.; Gu, H.; Senftle, T. P.; Zhou, C. Adsorption and Reductive Defluorination of Perfluorooctanoic Acid over Palladium Nanoparticles. *Environ. Sci. Technol.* **2021**, *55* (21), 14836–14843.

(68) Tang, Y.; Zhou, C.; Van Ginkel, S. W.; Ontiveros-Valencia, A.; Shin, J.; Rittmann, B. E. Hydrogen Permeability of the Hollow Fibers Used in H2-Based Membrane Biofilm Reactors. *J. Memb. Sci.* **2012**, *407*, 176–183.

(69) Qiao, W.; Miao, J.; Jiang, H.; Yang, Q. Degradation and Effect of 6: 2 Fluorotelomer Alcohol in Aerobic Composting of Sludge. *Biodegradation* **2021**, *32* (1), 99–112.

(70) Zhang, S.; Merino, N.; Wang, N.; Ruan, T.; Lu, X. Impact of 6: 2 Fluorotelomer Alcohol Aerobic Biotransformation on a Sediment Microbial Community. *Sci. Total Environ.* **2017**, *575*, 1361–1368.

(71) Dinglasan, M. J. A.; Ye, Y.; Edwards, E. A.; Mabury, S. A. Fluorotelomer Alcohol Biodegradation Yields Poly-and Perfluorinated Acids. *Environ. Sci. Technol.* **2004**, *38* (10), 2857–2864.

(72) Kertesz, M. A. Desulfonation of Aliphatic Sulfonates by Pseudomonas Aeruginosa PAO. *FEMS Microbiol. Lett.* **1996**, *137* (2–3), 221–225.

(73) Eichhorn, E.; van der Ploeg, J. R.; Leisinger, T. Characterization of a Two-Component Alkanesulfonate Monooxygenase from Escherichia Coli. *J. Biol. Chem.* **1999**, *274* (38), 26639–26646.

(74) García, R. A.; Chiaia-Hernández, A. C.; Lara-Martin, P. A.; Loos, M.; Hollender, J.; Oetjen, K.; Higgins, C. P.; Field, J. A. Suspect Screening of Hydrocarbon Surfactants in AFFFs and AFFF-Contaminated Groundwater by High-Resolution Mass Spectrometry. *Environ. Sci. Technol.* **2019**, *53* (14), 8068–8077.

(75) Field, J.; Sedlak, D.; Alvarez-Cohen, L. *Characterization of the Fate and Biotransformation of Fluorochemicals in AFFF-Contaminated Groundwater at Fire/Crash Testing Military Sites*; Oregon State University Corvallis United States, 2017.

(76) Zeng, C.; Atkinson, A.; Sharma, N.; Ashani, H.; Hjelmstad, A.; Venkatesh, K.; Westerhoff, P. Removing Per-and Polyfluoroalkyl Substances from Groundwaters Using Activated Carbon and Ion Exchange Resin Packed Columns. *AWWA Water Sci.* **2020**, *2* (1), e1172.

(77) Barzen-Hanson, K. A.; Roberts, S. C.; Choyke, S.; Oetjen, K.; McAlees, A.; Riddell, N.; McCrindle, R.; Ferguson, P. L.; Higgins, C. P.; Field, J. A. Discovery of 40 Classes of Per-and Polyfluoroalkyl Substances in Historical Aqueous Film-Forming Foams (AFFFs) and AFFF-Impacted Groundwater. *Environ. Sci. Technol.* **2017**, *51* (4), 2047–2057.

(78) Place, B. J.; Field, J. A. Identification of Novel Fluorochemicals in Aqueous Film-Forming Foams Used by the US Military. *Environ. Sci. Technol.* **2012**, *46* (13), 7120–7127.

(79) Leemann, A.; Loser, R. Analysis of Concrete in a Vertical Ventilation Shaft Exposed to Sulfate-Containing Groundwater for 45 Years. *Cem. Concr. Compos.* **2011**, *33* (1), 74–83.

(80) Miao, Z.; Brusseau, M. L.; Carroll, K. C.; Carreón-Diazconti, C.; Johnson, B. Sulfate Reduction in Groundwater: Characterization and Applications for Remediation. *Environ. Geochem. Health* **2012**, *34* (4), 539–550.

(81) Yong, Z. Y.; Kim, K. Y.; Oh, J.-E. The Occurrence and Distributions of Per-and Polyfluoroalkyl Substances (PFAS) in Groundwater after a PFAS Leakage Incident in 2018. *Environ. Pollut.* **2021**, *268*, 115395.

(82) Hepburn, E.; Madden, C.; Szabo, D.; Coggan, T. L.; Clarke, B.; Currell, M. Contamination of Groundwater with Per-and Polyfluoroalkyl Substances (PFAS) from Legacy Landfills in an Urban Re-Development Precinct. *Environ. Pollut.* **2019**, *248*, 101–113.

(83) Park, M.; Wu, S.; Lopez, I. J.; Chang, J. Y.; Karanfil, T.; Snyder, S. A. Adsorption of Perfluoroalkyl Substances (PFAS) in Groundwater by Granular Activated Carbons: Roles of Hydrophobicity of PFAS and Carbon Characteristics. *Water Res.* **2020**, *170*, 115364.

(84) Yuan, S.; Chen, M.; Mao, X.; Alshawabkeh, A. N. Effects of Reduced Sulfur Compounds on Pd-Catalytic Hydrodechlorination of Trichloroethylene in Groundwater by Cathodic H2 under Electrochemically Induced Oxidizing Conditions. *Environ. Sci. Technol.* **2013**, *47* (18), 10502–10509.